A Comprehensive Analysis of Differential Cellular Effects of B-domain-deleted and Full-length FVIII Expression in HEK293 Cells

Dissertation

zur

Erlangung des Doktorgrades (Dr. rer. nat.)

der

Mathematisch-Naturwissenschaftlichen Fakultät

der

Rheinischen Friedrich-Wilhelms-Universität Bonn

vorgelegt von

Rawya Al-Rifai

Aus

Hayzouk / Libanon

Bonn, April 2025

Angefertigt mit Genehmigung der Mathematisch-Naturwissenschaftlichen
Fakultät der Rheinischen Friedrich-Wilhelms-Universität Bonn

Gutachter/Betreuer: Priv. Doz. Dr. Osman El-Maarri

Gutachterin: Prof. Dr. Diana Imhof

Tag der Promotion: 25.09.2025

Erscheinungsjahr: 2025

As God told in *Quran,*

'Indeed, with the hardship comes ease.'

This reminder strengthens me in moments of doubt, reassuring me that persistence leads to not only success but also peace and growth through each trial.

My path toward earning my doctorate has taught me that every accomplishment has silent force behind it. Long after the difficulties have past, the road molds you in ways you never would have imagined and develops resilience, clarity, and strength to lead you forward. Since I know that every little step brings me one step closer to the breakthrough, the secret is not to figure out the simplest solution but in finding the courage to stay on when challenges grow.

Our greatest weakness lies in giving up. The most certain way to succeed is always to try just one more time.

Thomas Edison

Table of Contents

List of abbreviations

Abbreviation	Definition
%	Percent
*	p ≤ 0.05
**	p ≤ 0.01
***	p ≤ 0.001
****	p ≤ 0.0001
°C	Degree Celsius
µL	Microliter
µM	Micromolar (concentration)
Aa	Amino Acid
AAV	Adeno-associated virus
AAV5/6/3/Rh74/S3	AAV Serotypes (e.g., 5, 6, 3, Rh74, synthetic S3)
ABR	Annual Bleeding Rate
ADP	Adenosine Diphosphate
AGT	Angiotensinogen
Amp	Ampicillin
aPC	Activated Protein C
APCs	Antigen-Presenting Cells
APP	Amyloid Precursor Protein
ARL8B	ADP Ribosylation Factor-Like GTPase 8B
ATCC	American Type Culture Collection
ATP	Adenosine Triphosphate
BACH1	BTB and CNC Homology 1
BDD	B-domain-deleted
BDD-FVIII	B-domain-deleted Factor VIII
BFA	Brefeldin A
BiP	Binding Immunoglobulin Protein (also known as GRP78)
bp	Base Pair
BSA	Bovine Serum Albumin
CALR	Calreticulin
CNX	Calnexin

Abbreviation	Definition
Cas	CRISPR Associated
CD4	Cluster of Differentiation 4
CDKN1A	Cyclin Dependent Kinase Inhibitor 1A (also known as p21)
CDKN1A/2A	Cyclin Dependent Kinase Inhibitor 1A/2A
CDKN1A/CDKN2A	Cyclin Dependent Kinase Inhibitor 1A/2A
cDNA	Complementary DNA
CFTR	Cystic Fibrosis Transmembrane Conductance Regulator
CFU	Colony Forming Units
CI	Cell Index (RTCA readout)
CLEC4M	C-Type Lectin Domain Family 4 Member M
CNX	Calnexin
co	Codon-optimized
CO_2	Carbon Dioxide
COPI	Coat Protein Complex I
COPII	Coat Protein Complex II
CPT1B	Carnitine Palmitoyltransferase 1B
CQ	Chloroquine
CRISPR/Cas9	Clustered Regularly Interspaced Short Palindromic Repeats / CRISPR-associated protein 9
crRNA	CRISPR RNA
CT	Threshold Cycle (in qPCR)
C-terminus	Carboxy-Terminus
d, h, min, s	Day, Hour, Minute, Second
DAPI	4′,6-diamidino-2-phenylindole
ddNTP	Dideoxyribonucleotide Triphosphate
DEGs	Differentially Expressed Genes
DMD	Duchenne Muscular Dystrophy
DMEM	Dulbecco’s Modified Eagle Medium
DMSO	Dimethyl Sulfoxide
DNA	Deoxyribonucleic Acid

Abbreviation	Definition
dNTP	Deoxynucleotide Triphosphate
DSB	Double-Strand Break
dsDNA	Double-Stranded DNA
DTT	Dithiothreitol (if mentioned in buffer prep)
e.g.	Exempli Gratia (For Example)
ECAR	Extracellular Acidification Rate
EDTA	Ethylenediaminetetraacetic Acid
EGR1	Early Growth Response Protein 1
EMA	European Medicines Agency
ER	Endoplasmic Reticulum
ERAD	ER-Associated Degradation
ERGIC	ER-Golgi Intermediate Compartment
ESR2	Estrogen Receptor Beta
et al.	Et Altera (And Others)
*F5F8*D	Combined Deficiency of Factor V and Factor VIII
F8	Gene encoding Factor VIII
F9	Gene encoding Factor IX
FASTQ	File format for raw sequencing reads
FBS	Fetal Bovine Serum
FCCP	Carbonyl cyanide-4 (trifluoromethoxy) phenylhydrazone
FCGR2B	Fc Gamma Receptor IIb
FDA	Food and Drug Administration
FIX	Factor IX
FIXa	Activated Factor IX
FIX-Padua	Hyperactive FIX variant (R338L mutation)
FL	Full-length
FL-FVIII	Full-Length Factor VIII
FOXM1	Forkhead Box M1
FOXO1	Forkhead Box O1
FOXO1/3	Forkhead Box O1/O3
FOXO3	Forkhead Box O3
Furin	Proprotein Convertase Furin
FV	Factor V

Abbreviation	Definition
FVIII	Factor VIII
FVIIIa	Activated Factor VIII
g	Gram
GABARAP	Gamma-Aminobutyric Acid Receptor-Associated Protein
GABARAPL1	GABA Type A Receptor-Associated Protein Like 1
GM130	Golgi Matrix Protein 130
GnRH-A	Gonadotropin-Releasing Hormone Agonist
gRNA	Guide RNA
GTF	Gene Transfer Format (for genome annotation)
HA	Hemagglutinin (epitope tag)
HC	Hepatocytes
HCC	Hepatocellular Carcinoma
HEK293	Human Embryonic Kidney 293 cells
Hemgenix	Etranacogene Dezaparvovec
HIF1A	Hypoxia Inducible Factor 1 Subunit Alpha
HRP	Horseradish Peroxidase
i.e.	id est means "in other words."
INS	Insulin gene
INSR	Insulin Receptor
IPA	Ingenuity Pathway Analysis
iProof / Phusion	High-fidelity DNA polymerases
IRES	Internal Ribosome Entry Site
ITR	Inverted Terminal Repeat
IU/dL	International Units per Deciliter
JTH	Journal of Thrombosis and Haemostasis
kb	Kilobase
KO	Knockout
LAMP1	Lysosome-Associated Membrane Protein 1
LB	Luria-Bertani (broth/agar)
LC3B	Microtubule-Associated Protein 1A/1B-Light Chain 3
let-7	Family of microRNAs involved in cell differentiation and proliferation

Abbreviation	Definition
Leu	Leucine
LIN9	LIN-9 DREAM Complex Component
LMAN1	Lectin, Mannose Binding 1
LSEC	Liver Sinusoidal Endothelial Cells
LSECs	Liver Sinusoidal Endothelial Cells
Lys	Lysine
LYVE1	Lymphatic Vessel Endothelial Hyaluronan Receptor 1
MAP4K4	Mitogen-Activated Protein Kinase Kinase Kinase Kinase 4
MCFD2	Multiple Coagulation Factor Deficiency 2
MeRef	Methylation Reference Gene
MHC	Major Histocompatibility Complex
MISeq	High-throughput sequencing buffer system (custom in your case)
mRNA	Messenger RNA
MYC	Myelocytomatosis Oncogene
N6	A partially retained B-domain construct with 6 glycosylation sites
NAbs	Neutralizing Antibodies
ns	Not Significant ($p > 0.05$)
NucBlue™	DAPI-based nuclear stain (Thermo Fisher)
OCR	Oxygen Consumption Rate
PACE	Proprotein Convertase
PAGE	Polyacrylamide Gel Electrophoresis
PBS	Phosphate-Buffered Saline
PCA	Principal Component Analysis
PCC	Pearson Correlation Coefficient
PCR	Polymerase Chain Reaction
PDI	Protein Disulfide-Isomerase
PEI	Polyethylenimine
PenStrep	Penicillin-Streptomycin
PI3Kγ	Phosphoinositide 3-Kinase Gamma
pmol/min	Picomoles per minute (rate of OCR or ATP production)

Abbreviation	Definition
PPE	Personal Protective Equipment
Pro	Proline
PTC	Premature Termination Codon
PVDF	Polyvinylidene Fluoride (membrane)
QC	Quality Control
qPCR	Quantitative Polymerase Chain Reaction
R^2 / R2	Coefficient of Determination (Pearson's)
Rab	Ras-related proteins in brain (a family of small GTPases)
RAB11	Recycling Endosome Marker
RAB26	Rab GTPase 26
RAB5	Early Endosome Marker
RAB5/7/8a/11/26	Members of the RAB protein family (endocytic trafficking regulators)
RAB7	Late Endosome Marker
RAB8a	Vesicle Trafficking Regulator
RB1	Retinoblastoma Protein
RCF	Relative Centrifugal Force
RHQR	Protease recognition motif
RICTOR	Rapamycin-Insensitive Companion of mTOR
RIPA	Radioimmunoprecipitation Assay (buffer)
RNA	Ribonucleic Acid
RNA-seq	RNA sequencing
Roctavian	Valoctocogene Roxaparvovec
RT	Room Temperature / Reverse Transcription (context dependent)
RTCA	Real-Time Cell Analysis
RT-PCR	Reverse Transcription Polymerase Chain Reaction
SD	Space of Disse
SDS	Sodium Dodecyl Sulfate
SEM	Scanning Electron Microscopy
Ser	Serine
SIN LV	Self-Inactivating Lentiviral Vector

Abbreviation	Definition
siRNA	Small Interfering RNA
SIRT	Sirtuin (Signaling Pathway)
SOC	Super Optimal Broth (medium for E. coli recovery)
SP	Sieve Plates
SQ	Serine-Glutamine sequence (truncated B-domain linker)
STAB2	Stabilin-2
TAE	Tris-Acetate-EDTA
Taq	Thermus aquaticus (polymerase)
TaqMan	Brand of probe-based qPCR reagents
TaqPol	Taq Polymerase
TBS	Tris-buffered Saline
TEAD1	TEA Domain Transcription Factor 1
TF	Transcription Factor
TGFB1	Transforming Growth Factor Beta 1
TGN46	Trans-Golgi Network Protein 46
TLRs	Toll-Like Receptors
TMB	Tetramethylbenzidine
TP53	Tumor Protein p53
Tyr	Tyrosine
UPR	Unfolded Protein Response
UV	Ultraviolet
VAMP8	Vesicle-Associated Membrane Protein 8
vECs	Vascular Endothelial Cells
vg/kg	Vector Genomes per Kilogram
VIII	Factor VIII
VWD	von Willebrand Disease
VWF	von Willebrand Factor
WT	Wild-Type
xCELLigence	Real-time Cell Analysis System by Agilent
Z-score	Statistical measurement describing a value's relation to the mean
ΔF508	Deletion of Phenylalanine at Position 508

List of Figures

List of Tables

Abstract

Gene therapy has emerged as a promising approach for Hemophilia A and B, enabling sustained production of clotting factors and reducing reliance on frequent FVIII infusions. While Hemophilia B therapies targeting Factor IX show durable outcomes, Hemophilia A treatments using B-domain-deleted Factor VIII (BDD-FVIII), a truncated form adapted for adeno-associated virus delivery, often show reduced persistence. This study investigates cellular and molecular mechanisms underlying this disparity by comparing BDD-FVIII with full-length FVIII (FL-FVIII).

Using stably transfected HEK293 cells, we evaluated expression and secretion levels. BDD-FVIII showed improved expression, secretion and lower endoplasmic reticulum (ER) retention, likely due to its smaller size and reduced interaction with chaperones such as Calnexin and LMAN1.

We further conducted immunofluorescence co-localization studies, targeted chemical treatments, and gene knockouts of key trafficking regulators. These experiments revealed that FL-FVIII depends on classical ER-to-Golgi transport, while BDD-FVIII interacts less with early secretory pathway components. These findings demonstrate that FL- and BDD-FVIII engage distinct intracellular trafficking routes and quality control mechanisms.

Deletion of the FVIII B-domain significantly altered cellular behavior beyond secretion. BDD-FVIII-expressing cells showed reduced proliferation alongside activation of stress-related pathways, as confirmed by proliferation assays and RNA-seq analysis. Metabolic profiling showed that FL-FVIII imposes a greater folding and energetic burden due to its complex structure. FL-FVIII cells exhibited high mitochondrial ATP production but low residual ATP, indicating energy exhaustion. In contrast, BDD-FVIII cells maintained higher residual ATP with lower mitochondrial ATP, reflecting better energy efficiency.

Transcriptomic analysis revealed distinct gene expression profiles between FL-FVIII and BDD-FVIII, affecting pathways involved in cell cycle regulation, stress response, and metabolism. Notably, we identified a range of differentially regulated molecules between the two variants, including transcriptional regulators, kinases, enzymes, and chemical drugs. Among these, one compound previously used in gene therapy for Hemophilia A emerged as particularly interesting, as it has been shown to mitigate

therapy-induced stress. This raises the possibility that such compounds could contribute to stabilizing BDD-FVIII by promoting a transcriptional and functional shift toward the FL-FVIII profile. These findings highlight the potential for therapeutic modulation using small molecules or kinase inhibitors to target stress-adaptive pathways.

Taken together, our results show that although the FVIII B-domain is not essential for coagulation, it plays a broader role in regulating secretion, metabolic homeostasis, and long-term cell adaptation. This study provides insight into the differential cellular effects of BDD- and FL-FVIII and may support the development of more targeted and personalized gene therapy strategies for Hemophilia A.

Keywords: Hemophilia A, Gene therapy, Factor VIII (FVIII), B-domain deletion (BDD-FVIII), Intracellular trafficking, AAV vector, Endoplasmic reticulum stress, Metabolic adaptation, Cellular homeostasis, CRISPR/Cas9 knockout, Co-localization analysis, Energy profiling.

Zusammenfassung

Gentherapie stellt einen vielversprechenden Therapieansatz für Hämophilie A und B dar, da sie eine anhaltende Produktion von Gerinnungsfaktoren ermöglicht und die Abhängigkeit von häufigen Infusionen von FVIII-Konzentraten verringert. Während Therapien für Hämophilie B, die auf den Faktor IX (FIX) abzielen, langanhaltende und stabile Langzeitergebnisse zeigen, weisen Behandlungen für Hämophilie A, die auf dem B-Domänen-deletierten Faktor VIII (BDD-FVIII) basieren, einer verkürzten Form, die für die Verpackung in Adeno-assoziierte Viren (AAV) optimiert wurde, häufig eine reduzierte Persistenz auf. Ziel dieser Studie ist es, die zellulären und molekularen Mechanismen zu untersuchen, die zu dieser Diskrepanz beitragen, indem BDD-FVIII mit dem Faktor VIII in voller Länge (FL-FVIII) verglichen wird.

Durch die Verwendung stabil transfizierter HEK293-Zellen wurden Expressionsniveaus, intrazellulärer Transport, Sekretionseffizienz und zelluläre Stressreaktionen analysiert. BDD-FVIII zeigte eine verbesserte Sekretion und geringere Retention im endoplasmatischen Retikulum, vermutlich aufgrund einer reduzierten Interaktion mit Chaperonen wie Calnexin und LMAN1.

Des Weiteren haben wir Immunfluoreszenz-Kolokalisationsstudien, gezielte chemische Störungen und Gen-Knockouts von wichtigen Regulatoren für den Transport beim Menschen durchgeführt. Die Studien haben offenbart, dass FL-FVIII auf den traditionellen Transportweg vom ER zum Golgi angewiesen ist, während BDD-FVIII weniger mit den frühen Komponenten des sekretorischen Wegs in Wechselwirkung tritt. Die Resultate verdeutlichen, dass FL- und BDD-FVIII verschiedene interne Transportrouten und Qualitätskontrollmechanismen verwenden.

Die Entfernung der FVIII B-Domäne führte zu einer signifikanten Veränderung des zellulären Verhaltens, die über die Sekretion hinausging. Zellen, die BDD-FVIII exprimieren, wiesen eine verminderte Vermehrung und Aktivierung von stressbedingten Signalwegen auf, was mittels RNA-Seq und Proliferationstests nachgewiesen wurde und auf einen gesteigerten intrazellulären Stress hindeutet. Die Analyse des Stoffwechselprofils ergab, dass FL-FVIII aufgrund seiner komplizierten Struktur zu einer erhöhten Falt- und Energiebelastung führt. Die FL-FVIII-Zellen wiesen eine erhöhte Produktion von mitochondrialem ATP auf, jedoch einen geringen Rest-ATP-Spiegel, was auf einen Energiemangel hindeutet. Im Unterschied dazu

wiesen BDD-FVIII-Zellen trotz einer niedrigeren mitochondrialen Leistung ein höheres intrazelluläres ATP auf, was auf eine verbesserte Energieeffizienz hindeutet.

Die Analyse des Transkriptoms offenbarte verschiedene Genexpressionsmuster zwischen FL-FVIII und BDD-FVIII, die sich auf Signalwege beziehen, die die Regulation des Zellzyklus, die Stressreaktion und den Stoffwechsel beeinflussen. Auffällig war, dass wir diverse Moleküle mit unterschiedlichen Regulierungsmechanismen in beiden Varianten feststellten, wie zum Beispiel Transkriptionsregulatoren, Kinasen, Enzyme und chemische Substanzen. Eine herausragende Verbindung in diesem Zusammenhang war bereits in der Gentherapie für Hämophilie A verwendet worden, da sie nachweislich die durch die Therapie verursachten Stressreaktionen reduziert. Das könnte dazu führen, dass diese Verbindungen dazu beitragen, die Stabilität von BDD-FVIII zu verbessern, indem sie eine Veränderung in der Transkription und Funktion unterstützen, die zu einem FL-FVIII-Profil führt. Die Resultate zeigen, dass eine gezielte Beeinflussung stressadaptiver Signalwege durch kleine Moleküle oder Kinaseinhibitoren therapeutisch moduliert werden kann.

Insgesamt deuten unsere Resultate darauf hin, dass die FVIII-B-Domäne zwar nicht unverzichtbar für die Blutgerinnung ist, jedoch eine umfassendere Funktion bei der Kontrolle der Sekretion, der metabolischen Balance und der langfristigen Zellanpassung hat. Die Untersuchung bietet einen Überblick über die verschiedenen zellulären Auswirkungen von BDD- und FL-FVIII und könnte dazu beitragen, maßgeschneiderte Gentherapiestrategien für Hämophilie A zu entwickeln.

Schlüsselwörter: Hämophilie A, Gentherapie, Faktor VIII (FVIII), B-Domänen-deletierten (BDD-FVIII), intrazellulärer Transport, AAV-Vektor, endoplasmatischer Retikulum Stress, metabolische Anpassung, zelluläre Homöostase, CRISPR/Cas9-Knockout, Co-Lokalisationsanalyse, Energy profiling.

Introduction

Background

Blood coagulation relies on factor VIII (FVIII), which is regarded as an essential coagulation protein [1]. It assists in hemostasis process by facilitating thrombin production and the formation of fibrin clots. FVIII acts as a procofactor in the blood coagulation cascade, becoming activated (FVIIIa) at sites of vascular damage. In its active form, FVIIIa interacts with coagulation factor IX on the surface of activated platelets, amplifying the activation of factor X in the intrinsic coagulation pathway [2,3].

Disruptions in FVIII whether due to genetic mutations ,deficiency or cellular dysfunctions, which clinically considered a severe bleeding disorder called as Hemophilia A [4]. The production, regulation, and secretion of FVIII involve complex cellular mechanisms primarily carried out by specialized liver cells [5].

Liver sinusoidal endothelial cells (LSECs) are specialized endothelial cells that line the hepatic sinusoids, and they are different from other liver cell types because of their unique structural and functional characteristics[6]. Unlike conventional endothelial cells, LSECs possess fenestrations, tiny pores in their plasma membrane that facilitate the exchange of macromolecules between sinusoidal blood and liver parenchyma. Furthermore, they lack a traditional basement membrane, enhancing their ability to filter and absorb circulating substances. These unique structural features underscore their specialized role and essential contribution to liver function [7].

Beyond their role in molecular exchange, LSECs are now recognized as the primary producers of FVIII, emphasizing their importance in maintaining hemostasis. Their secretory capabilities enable them to efficiently synthesize and release FVIII into the bloodstream, ensuring sufficient levels for proper blood clotting. Additionally, LSECs contribute to the post-translational modifications of FVIII, which are crucial for its stability and functional activity[8].

The unique phenotype of LSECs, characterized by their fenestrations, absence of basement membrane and specialized intracellular pathways, enhances their ability to handle large glycoproteins such as FVIII **(Figure 1)**. Among these pathways, transcytosis plays a crucial role by facilitating the vesicular transport of FVIII across

the endothelium, enabling its effective exchange between the bloodstream and hepatocytes for clearance, regulation, or secretion [9,10].

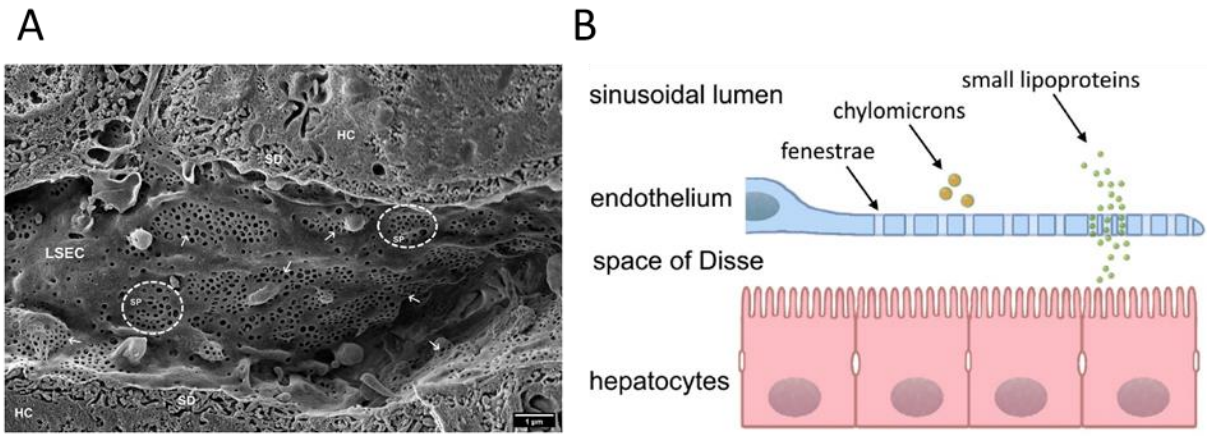

Figure 1. Ultrastructural and Schematic Representation of Hepatic Sinusoids in a C57BL6 Mouse.
A- SEM image of hepatic sinusoids of a C57BL6 mouse, approximately 4 months old. Liver Sinusoidal Endothelial Cells (LSECs) are covered in multiple fenestrations (arrows) arranged into sieve plates (SP, dotted line circles) distributed over the whole sinusoid. SD, space of Disse; HC, hepatocytes. **B-** Sinusoidal lumen illustartion13. *Reproduced from Szafranska K, Kruse LD, Holte CF, McCourt P, Zapotoczny B. The whole Story About Fenestrations in LSEC. Frontiers in physiology. 2021;12:735573.*

One of our previous studies demonstrated that LSECs express key genes and pathways critical for the production and secretion of Factor VIII (FVIII), highlighting their unique role in coagulation physiology. This distinct gene expression profile sets LSECs apart from other vascular endothelial cells (vECs), including those derived in vitro. For instance, CLEC4M, a gene involved in glycoprotein processing, and STAB2, a gene linked to endocytosis and secretion, both of which are essential for the effective synthesis and release of FVIII, were shown to be substantially overexpressed in LSECs. Furthermore, elevated levels of LYVE1 (a marker of lymphatic and liver endothelial cells) and FCGR2B (involved in immune regulation) were found to be part of a distinct gene expression signature in LSECs, underscoring their specific functional role in the liver and coagulation processes[8].

The production and secretion of FVIII are energy-intensive processes. Groundbreaking research by Kauffman et al. has emphasized the ATP requirement for FVIII release. ATP enables the disaggregation of FVIII within the endoplasmic reticulum (ER), a critical step that regulates the rate of its secretion [11]. In situations of

ATP depletion, the efficiency of FVIII secretion is significantly reduced, which can lead to intracellular accumulation and potential protein misfolding [12].

FVIII folding requires molecular chaperones, particularly BiP (immunoglobulin-binding protein). These chaperones attach to newly formed FVIII in the ER to aid in proper folding. In the ER, these chaperones bind nascent FVIII to promote proper folding [13]. The release of FVIII from BiP, which enables its progression through the secretory pathway, is an ATP-driven process. This energy-intensive mechanism ensures that only correctly folded proteins are secreted, preventing the accumulation of misfolded or aggregated FVIII [14].

Under cellular stress conditions, such as ATP depletion or protein folding dysfunction, the ER stress response is triggered. This response disrupts FVIII secretion, as energy-dependent folding mechanisms are compromised. Kauffman et al. demonstrated that these conditions worsen the aggregation of misfolded FVIII, further inhibiting its secretion and contributing to the pathology of Hemophilia A [15].

Conventional treatments for Hemophilia A, including FVIII replacement therapy, provide short-term relief but come with drawbacks such as the development of inhibitors, the need for frequent administration, and high treatment costs [16]. Since gene therapy addresses the underlying genetic issue, it is a novel method [17].

By providing functional copies of the *F8* gene to FVIII-producing cells, gene therapy aims to restore therapeutical FVIII levels. Adeno-associated viruses (AAVs) have been shown to be effective vectors for delivering the *F8* gene to these cells. Recent advances in AAV-based therapies have shown promising preclinical and clinical results and allow for long-term correction of FVIII deficiency [18–20].

Review

I- AAV Gene Therapy: Overview and Applications

Gene therapy aims to provide functional copies of the *F8* gene to FVIII-producing cells in order to restore therapeutical FVIII levels [21]. Because of its distinct biological properties, the adeno-associated virus (AAV) has become one of the most promising vectors for delivering therapeutic genes among the many others that are currently accessible.

AAV is a non-pathogenic, replication-deficient parvovirus that naturally infects humans and requires a helper virus, such as adenovirus or herpesvirus, for replication [22]. Without this co-infection, AAV integrates into a specific site on chromosome 19, establishing a latent infection. Initially overlooked for therapeutic applications, AAV gained prominence because of its low immunogenicity and ability to provide sustained gene expression with minimal adverse immune responses [23].

1. Key Features of AAV for Gene Therapy

1.1 Molecular Design for Therapeutic Applications

To adapt AAV for therapeutic use, its native viral sequences are replaced with therapeutic genes, while retaining the inverted terminal repeats (ITRs) necessary for packaging and initiating second-strand DNA synthesis [23]. Because of this innovation, AAV is a very adaptable vector that can produce long-lasting gene expression. Clinical research has demonstrated its efficacy in the treatment of diseases such as muscular dystrophies, Hemophilia B, and Leber congenital amaurc

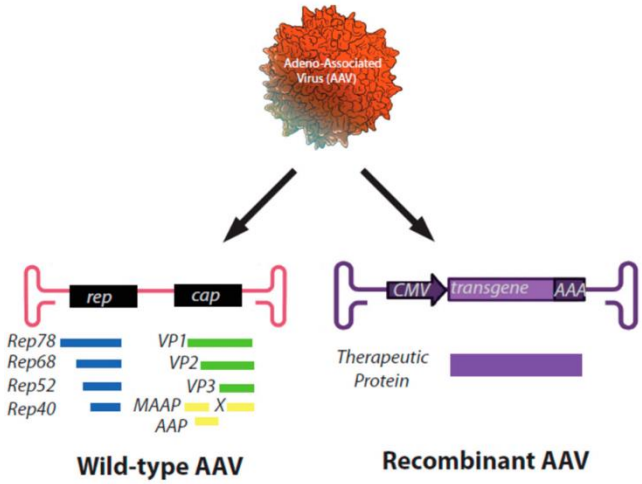

Figure 2. Schematic representation of genomes of a wild-type AAV virus (left) and a recombinant AAV particle (right).

Reproduced from Bower, J.J.; Song, L.; Bastola, P.; Hirsch, M.L. Harnessing the Natural Biology of Adeno-Associated Virus to Enhance the Efficacy of Cancer Gene Therapy. Viruses 2021, 13, 1205. https://doi.org/10.3390/v13071205.

1.2 Tissue Tropism and Safety

AAV's broad tissue tropism and excellent safety profile make it suitable for various diseases. Because it is non-pathogenic and non-replicative, the likelihood of insertional mutagenesis is greatly decreased. Additionally, its low immunogenicity compared to other viral vectors minimizes the likelihood of adverse immune reactions, even after systemic delivery [22].

1.3 Limitations and Packaging Capacity

AAV's modest packaging capacity (~4.7 kb) is a major drawback that makes it difficult to deliver big therapeutic genes [25]. To fit within the vector, for instance, genes encoding big proteins, like dystrophin for Duchenne muscular dystrophy (DMD), need to be shortened or altered [26,27]. Despite this limitations, creative approaches like gene

truncation, codon optimization, and mini-gene constructs development have expanded the therapeutic potential of AAV, allowing it to deliver a diverse array of treatments.

2. Gene Modifications for AAV Therapy

2.1 Truncated Gene Variants

To address the vector's size constraints, truncated versions of therapeutic genes have been developed. For example, in DMD therapy, the mini-dystrophin gene is a shortened version of the full dystrophin gene, one of the largest known genes, spans approximately 2.4 million base pairs (bp) and produces a messenger RNA (mRNA) of about 14 kb. This miniaturized version retains critical functional domains, such as those required for actin binding and interaction with the dystroglycan complex, which are necessary for preserving the stability and structural integrity [28,29]. Similar to this, the B-domain-deleted Factor VIII (BDD-FVIII) variation is frequently used in Hemophilia A gene therapy since it is compatible with AAV vectors. AAVs cannot include the 7 kb full-length FVIII gene in their packaging. The B-Domain, which comprises approximately 40% of the protein and is not required for its coagulation function, is effectively removed in order to reduce the size of the FVIII gene to fit inside the AAV vector [30–32].

2.2 Functional Enhancements

Beyond size reduction, additional modifications improve therapeutic protein activity. For example, the "FIX Padua" variant (R338L) is a breakthrough in Hemophilia B gene therapy. This single amino acid substitution increases the specific activity of FIX by approximately eightfold compared to wild-type FIX. It permits smaller dosages of the treatment vector while preserving clinical efficacy by increasing the clotting efficiency [33]. Codon optimization further enhances intracellular translation efficiency, allowing for greater therapeutic protein production [34].

3. Intracellular Impact of overexpressing a gene.

3.1 Effects of Overexpressing a Gene

Gene therapy faces multifaceted challenges that extend beyond the selection of suitable vectors, and the gene fragmentation or truncation. Furthermore, the overexpression of introduced genes in cells that do not naturally express them, can

lead to unintended cellular toxicity or dysregulation of native pathways. For example, hepatocytes do not naturally express FVIII; instead, FVIII is primarily produced by LSECs, which are responsible for its synthesis and release into the bloodstream. This distinction is critical for understanding the design of gene therapy vectors. Despite this, AAV-based gene therapy for Hemophilia A often targets hepatocytes rather than LSECs due to the difficulty in achieving efficient transduction of LSECs and the broader use of hepatocyte-specific promoters [35,36]. The limitations of AAV in targeting LSECs include their fenestrated structure, unique markers, the absence of specific LSEC-tropic capsids, and reduced transduction efficiency in non-hepatocyte liver cells [35,37].

Furthermore, Zhouji Chen, Roland W. Herzog, and Randal J. Kaufman's paper "Cellular stress and coagulation factor production: when more is not necessarily better" highlights a major obstacle in gene therapy: striking a balance between the risks of overexpressing therapeutic proteins and the effectiveness of treatment [38]. Excessive production of proteins, such as coagulation factors for Hemophilia, can overwhelm the protein-folding machinery in the ER, leading to ER stress. This stress activates the unfolded protein response (UPR), which disrupts cellular functions, induces inflammation, and can even trigger cell death [13,39,40]. Furthermore, overexpression raises the risk of immunological reactions since the body may mistake the plentiful therapeutic proteins for alien substances, which could result in inflammation and decreased therapeutic effectiveness. Protein misfolding or aggregation brought on by high expression levels can also impair function and put additional strain on the cell [41].

In addition to causing ER stress, the overproduction of therapeutic proteins, such as coagulation factors for Hemophilia, significantly burdens the cell's energy pathways, especially those that involve the synthesis and consumption of ATP. Large amounts of ATP are needed to power ribosomal translation, molecular chaperone action, and the correct folding of developing proteins inside the ER, making protein synthesis and folding energy-intensive processes [42]. When therapeutic protein overexpression occurs, the demand for ATP will increase. This increased demand can strain mitochondrial ATP production, the primary energy-generating pathway in most cells [13]. If ATP levels become insufficient, cellular processes like protein folding and secretion become inefficient, leading to protein misfolding, aggregation, and further ER stress [43].

By upsetting the fragile balance of gene expression and pathway connections, overexpression of any gene can affect a number of cellular pathways, including those

essential to energy metabolism [44]. Research has demonstrated that overexpression of certain genes can significantly disrupt cellular energy homeostasis. For instance, studies show that overexpression of AMP-related genes and transcription factors can alter energy-sensing pathways, thereby compromising energy balance [45].

3.2 Effects of Overexpressing a Modified Gene

Even little changes in amino acids can have a major impact on protein folding, stability, and intracellular trafficking in diseases such as cystic fibrosis, VWF disease, and neonatal diabetes. This can lead to decreased functionality and the advancement of the disease. For example, studies have demonstrated that altered codon usage can lead to mistranslation, impacting co-translational folding and resulting in cellular stress [46]. Similarly, truncated proteins lacking essential structural domains may destabilize the overall protein structure, making them more prone to degradation [47]. The truncation of genes, particularly those encoding multi-domain proteins, may result in the loss of domains critical for intracellular targeting and localization, cause lack of formation of disulfide bonds, suboptimal growth conditions, absence of posttranslational modifications, and the normally concerted action of multiple types of chaperones in vivo [48]. Proteins that fail to localize correctly within the cell may lose their functionality or accumulate in non-native compartments, causing potential cellular toxicity [48].

For example, the most common mutation in cystic fibrosis, CFTR's ΔF508 mutation, affects the structure of the CFTR protein by deleting a phenylalanine residue at position 508 and impairs its folding. This misfolded protein is retained in the ER, where it undergoes degradation, resulting in reduced chloride transport across epithelial cells and thick mucus accumulation, leading to chronic infections and organ dysfunction [49,50].

Von Willebrand Factor (VWF) disease arises from a range of genetic variations that can influence protein folding and stability, leading to intracellular retention and degradation. Specific missense mutations, such as p.Cys1060Tyr, p.Cys1130Phe, and p.Cys1149Arg, interfere with the formation of disulfide bonds at important cysteine residues within the D3 domain of the VWF protein. This improper folding could stop the protein from exiting the endoplasmic reticulum, reducing the quantity of functional VWF released into the bloodstream. Such molecular pathways are crucial when taking into account the quantitative VWF loss seen in Types 1 and 3 von Willebrand Disease

(VWD). Furthermore, these mutations underscore the complex connection between VWF biosynthesis and degradation vulnerability, highlighting the need for a more thorough comprehension of the molecular mechanisms underlying its synthesis, folding, and clearance. These findings, as discussed by Yadegari and Oldenburg [51], provide insights into the genotype-phenotype correlations in VWD and underline the critical role of specific amino acid residues in maintaining the structural integrity and function of VWF.

Similarly, in neonatal diabetes, mutations in the INS gene, such as C96Y and G32S, prevent the formation of disulfide bonds in proinsulin. These mutations prevent proper folding and trafficking of insulin, causing ER retention and activation of the UPR. Chronic UPR activation leads to beta-cell apoptosis, reducing insulin secretion and causing permanent diabetes [52,53]. These intracellular disruptions induce ER stress, oxidative damage, and inflammatory responses, further exacerbating disease pathology [54].

II- Case Study: Hemophilia A gene therapy

Hemophilia A, also known as classical Hemophilia, is a group of inherited bleeding disorders caused by a deficiency in clotting factor VIII, leading to excessive and prolonged bleeding, either spontaneously or after injury [55]. This condition is an X-linked recessive disorder. Around 50% of male offspring born to female carriers inherit the condition, while female carriers may have reduced factor VIII levels but typically do not exhibit symptoms [56,57]. Males with Hemophilia A cannot pass the condition to their sons but will transmit the gene to their daughters.

Gene therapy offers a transformative approach to treating Hemophilia A by targeting the root cause of the disorder[58]. This approach involves delivering a functional FVIII gene to the patient's cells, enabling sustained production of FVIII and reducing or eliminating the need for frequent infusions. AAV vectors are currently the most commonly used delivery system due to their ability to achieve long-term expression of the therapeutic gene with minimal immune response [59]. One key advancement in Hemophilia A gene therapy has been the use of bioengineered FVIII constructs. The natural FVIII protein contains multiple domains, including the A, B, and C domains, with the B-Domain being non-essential for clotting activity [60]. Truncated or B-domain-deleted (BDD) FVIII constructs are widely used in gene therapy as they offer a smaller

genetic payload, which is better suited for packaging into AAV vectors, while maintaining the protein's biological activity[61]. However, the removal of the B-Domain introduces certain challenges. While it enhances gene therapy efficiency by improving packaging and reducing the complexity of the construct, the absence of the B-Domain can impact FVIII folding, secretion efficiency, and stability. It may also alter glycosylation patterns, potentially affecting the protein's half-life and function [62]. Furthermore, modified constructs may expose cryptic epitopes, increasing the risk of immune responses. Although BDD constructs are promising, addressing these challenges is essential to ensure Hemophilia A gene therapy's long-term safety, stability, and efficacy.

1. Detailed Insights into FVIII and Its B-Domain

1.1 Structure and Processing of FVIII

The gene responsible for encoding FVIII is situated on the X chromosome at locus Xq28 [56], spanning roughly 186 kb of genomic DNA and comprising 26 exons (Figure 3A). During transcription, this gene produces a 9 kb messenger RNA (mRNA) that includes untranslated regions [63]. The coding DNA sequence (cDNA), which directs the synthesis of the FVIII protein, measures approximately 7 kb [64].

The functional FVIII protein exists as a heterodimer consisting of two chains. These chains contain three homologous A domains, a single B-Domain, and two homologous C domains [16]. The structural organization follows the sequence (A1-A2-B) as the heavy chain and (A3-C1-C2) as the light chain, extending from the amino terminus to the carboxyl terminus (Figure 3B).

These domains are critical for FVIII’s function, as they provide specific binding sites for various elements involved in the coagulation cascade like FIX that binds to A2 domain[16,65]. FVIII is inherently unstable and circulates in the plasma, where it binds to von Willebrand factor (vWF), which serves as a protective chaperone molecule. In adults, its half-life is around 12 hours, while in children, it is generally shorter. By associating with vWF, FVIII is shielded from proteolytic degradation and is directed to sites of vascular injury [66].

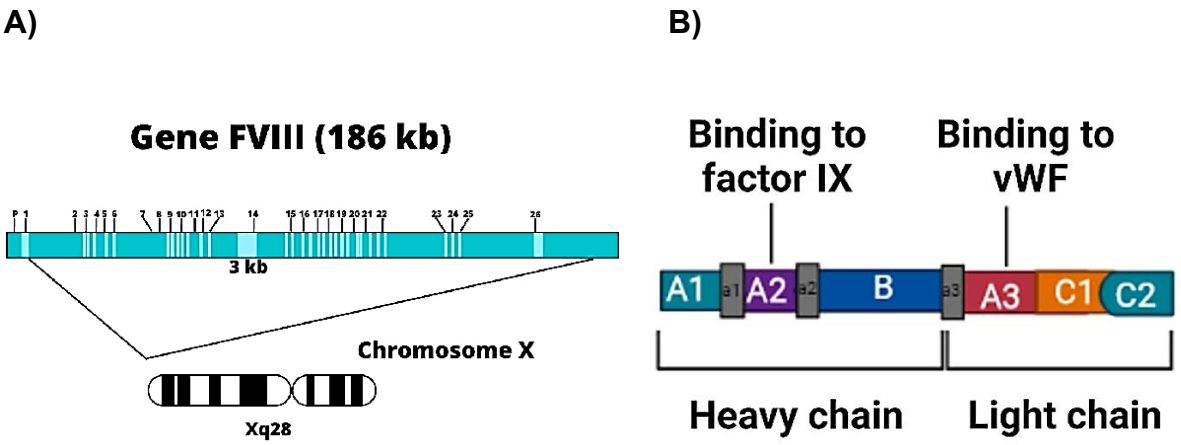

Figure 3. A- Structure of F8 gene, showing its location on the X chromosome (Xq28). B-Structure of FVIII protein.
After thrombin activation, FVIII becomes a heterodimer, consisting of a heavy chain (A1-A2-B) and a light chain (A3-C1-C2). *Reproduced from Sarmiento Doncel S, Díaz Mosquera GA, Cortes JM, Agudelo Rico C, Meza Cadavid FJ, Peláez RG. Hemophilia A: A Review of Clinical Manifestations, Treatment, Mutations, and the Development of Inhibitors. Hematology reports. 2023;15(1):130-150.*

1.2 Structure and Function of the B-Domain in FVIII

The B-Domain of FVIII is a highly glycosylated, non-enzymatic region located between the A2 and A3 domains (Figure 4). It spans approximately 980 amino acids and is characterized by its flexible structure. The B-Domain is intrinsically disordered and lacks a strict structural organization, in contrast to the A and C domains, which have distinct tertiary structures essential to FVIII's enzymatic action [67]. The B-Domain contains numerous O-linked and N-linked glycosylation sites, contributing to its dense glycosylation profile. These modifications are distributed throughout the domain and play a critical role in its structural characteristics by increasing hydrophilicity and solubility. This glycosylation also prevents aggregation during biosynthesis and stabilizes the protein as it progresses through the secretory pathway [68]. With a low level of sequence conservation between species, the B-Domain's sequence is noticeably different from the remainder of the FVIII molecule. This suggests that the domain plays ancillary roles rather than directly participating in the enzymatic action of FVIII [69]. Its flexible nature allows it to serve as a spacer between the functional A2 and A3 domains, providing structural support without interfering with the catalytic activity [70]. Despite being non-essential for FVIII's procoagulant activity [71], the B-Domain helps maintain the overall integrity and stability of the protein during its synthesis and secretion [72]. Its unique structural features make it an area of significant interest, especially when designing truncated FVIII constructs for therapeutic applications.

1.3 Role of the B-Domain and B-domain-deleted (BDD) FVIII

Although the B-Domain is not required for the coagulant function of FVIII, it is essential for its creation, secretion, and stability. However, B-domain-deleted (BDD) FVIII constructs have been developed for therapeutic purposes because they preserve functional activity while boosting expression yields and lowering immunogenicity. Studies into the structure of BDD-FVIII (Figure 4), including a bioengineered variant's (ET3i) high-resolution (3.2 Å) structure, have shed light on the domain design and metal-binding sites (Cu+, Zn2+, Ca2+). Conformational alterations in the C2 domain have also been discovered by these investigations, which could affect how FVIII interacts with phospholipid membranes, VWF, and FIXa.

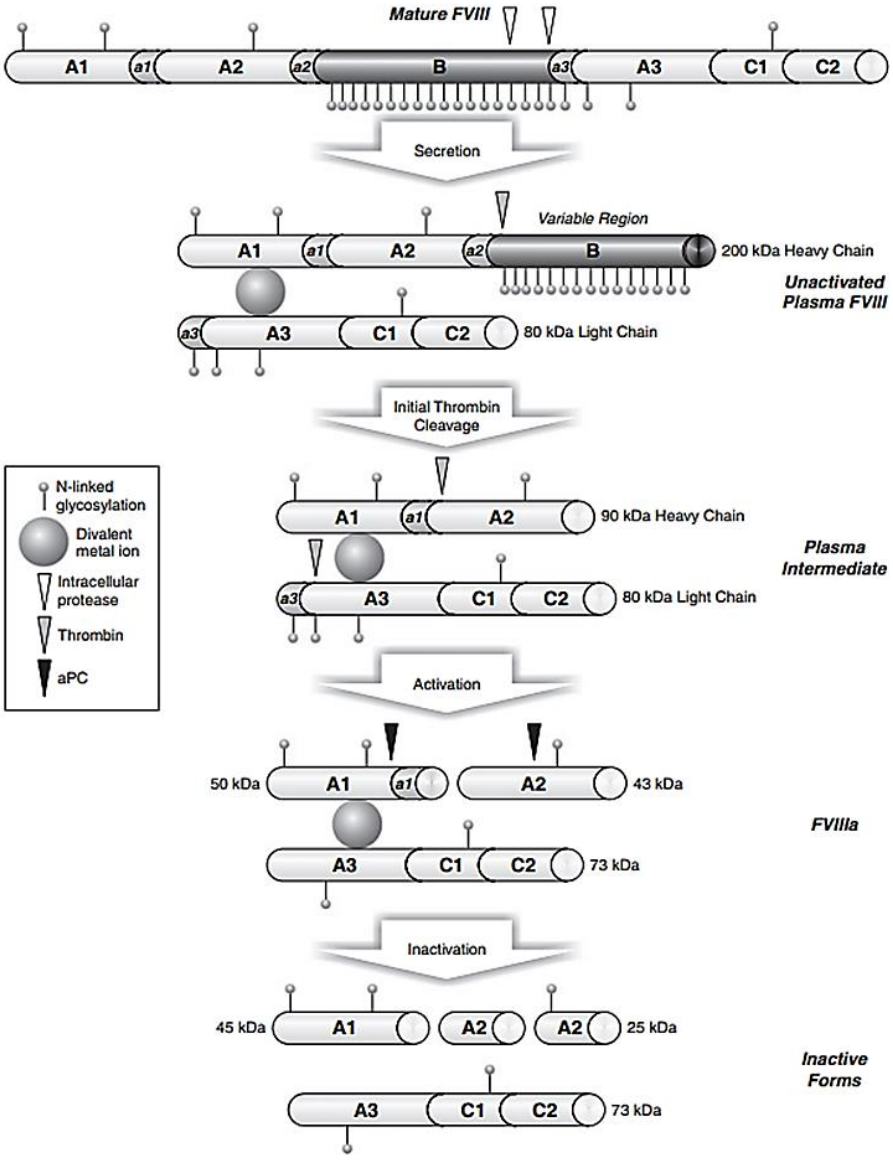

Figure 4. Schematic illustration of FVIII domains and its activation pathway.

This schematic illustration showing the transition from the full-length protein to its activated form (FVIIIa) and subsequent inactivation. The diagram highlights thrombin cleavage sites and key processing steps leading to FVIII activation and inactivation. Abbreviations: aPC (activated protein C), FVIII (Factor VIII), FVIIIa (activated Factor VIII). *Reproduced from Pipe SW. Functional roles of the factor VIII B-Domain.Hemophilia : the official journal of the World Federation of Hemophilia. 2009;15(6):1187-1196.*

1.4 Furin/PACE Cleavage Sites

Numerous Furin/proprotein convertase (PACE) cleavage sites, identified by the conserved R-X-X-R pattern, are present in the B-Domain of FVIII and are essential for the proteolytic processing and activation of FVIII. During the coagulation cascade, these sites allow the protein to be cleaved at particular residues, changing FVIII from its inactive to active form [73].

One of the key cleavage events occurs at Arg740, enabling further processing stages required for complete FVIII activation [74]. This sequential cleavage underscores the regulatory function of the B-Domain in controlling the activation of FVIII [75]. In the development of B-domain-deleted (BDD) FVIII constructs for gene therapy, the R-X-X-R cleavage motifs have been a focal point of optimization[76].

While the bulk of the B-Domain is removed to reduce the overall gene size and improve vector packaging efficiency, certain cleavage sites, such as those near Arg740, are often retained or engineered into BDD constructs. This ensures that the truncated FVIII maintains proper activation dynamics and mimics the functionality of the full-length protein. Studies have shown that maintaining these cleavage patterns in BDD constructs improves FVIII activation and secretion efficiency.

Furthermore, optimized R-X-X-R sequences contribute to improved post-translational processing, ensuring the therapeutic protein undergoes proper folding, glycosylation, and activation after secretion [77]. These modifications are particularly beneficial in the context of adeno-associated virus (AAV)-mediated gene therapy, where efficient protein expression and activation are critical for long-term therapeutic success.

1.5 Interactions with Molecular Chaperones

Molecular chaperones, such as BiP (Binding immunoglobulin Protein), calnexin, and calreticulin, play a crucial role in ensuring the proper folding, assembly, and quality

control of FVIII within the ER [78,79]. These chaperones interact with FVIII's B-Domain to promote folding and stop the release of misfolded or aggregated proteins [13,80].

The interactions are particularly important because of the complex structure of FVIII and the high risk of misfolding associated with its synthesis. Studies by Pipe et al. [80] and Dorner et al. [81] highlighted that one of the main factors fostering these interactions is N-linked glycosylation in the B-Domain, which gives molecular chaperones essential binding sites and ensures the proper conformational maturation of FVIII. Specifically, glycosylation not only enhances the solubility of FVIII but also creates structural motifs recognized by the calnexin/calreticulin chaperone system, which is necessary for ER-associated folding. BiP, an Hsp70 family chaperone, binds to hydrophobic regions of nascent FVIII polypeptides, shielding these regions from premature aggregation and directing them toward proper folding pathways [80,82]. However, as components of the glycoprotein quality control system, calnexin and calreticulin link to glycosylated residues in the B-Domain [83]. These connections allow only correctly folded FVIII molecules to go through the secretory system, whereas the ER-associated degradation (ERAD) pathway holds misfolded proteins in the ER for degradation [84,85]. Other unknown pathways could be also involved [86].

1.6 Interaction with the LMAN1/MCFD2 Cargo Receptor Complex

A crucial stage in the production and secretion of FVIII is its trafficking from the ER to the Golgi apparatus, which is mostly dependent on the LMAN1/MCFD2 cargo receptor complex. Properly folded FVIII is effectively transported along the secretory route thanks to this complex. Zhang et al. provided crucial insights into the interaction between FVIII's B-Domain and the LMAN1/MCFD2 complex, highlighting its role in mediating ER-to-Golgi transport [87] (Figure 5).

The B-Domain contains specific motifs that are recognized by LMAN1 (lectin, mannose-binding 1), a receptor that binds glycoproteins destined for secretion, and MCFD2 (multiple coagulation factor deficiency protein 2), which acts as a co-receptor to stabilize this interaction [88]. Mutations or disruptions in LMAN1 or MCFD2 impair the trafficking of FVIII, causing a condition known as combined deficiency of factor V and factor VIII (F5F8D) [89]. This autosomal recessive disorder is characterized by reduced levels of both coagulation factors, leading to a bleeding phenotype [90]. Nichols and Ginsburg were among the first to associate LMAN1 dysfunction with F5F8D [91], while

later studies by Zhang et al. confirmed the role of MCFD2 in forming a functional cargo receptor complex [92]. Since FVIII is difficult to transport due to its large size and complicated glycosylationprofile, its interaction with the LMAN1/MCFD2 complex is particularly important [93].The complex acts as a quality control checkpoint, ensuring only properly folded and glycosylated FVIII molecules proceed to the Golgi apparatus for further maturation [94].

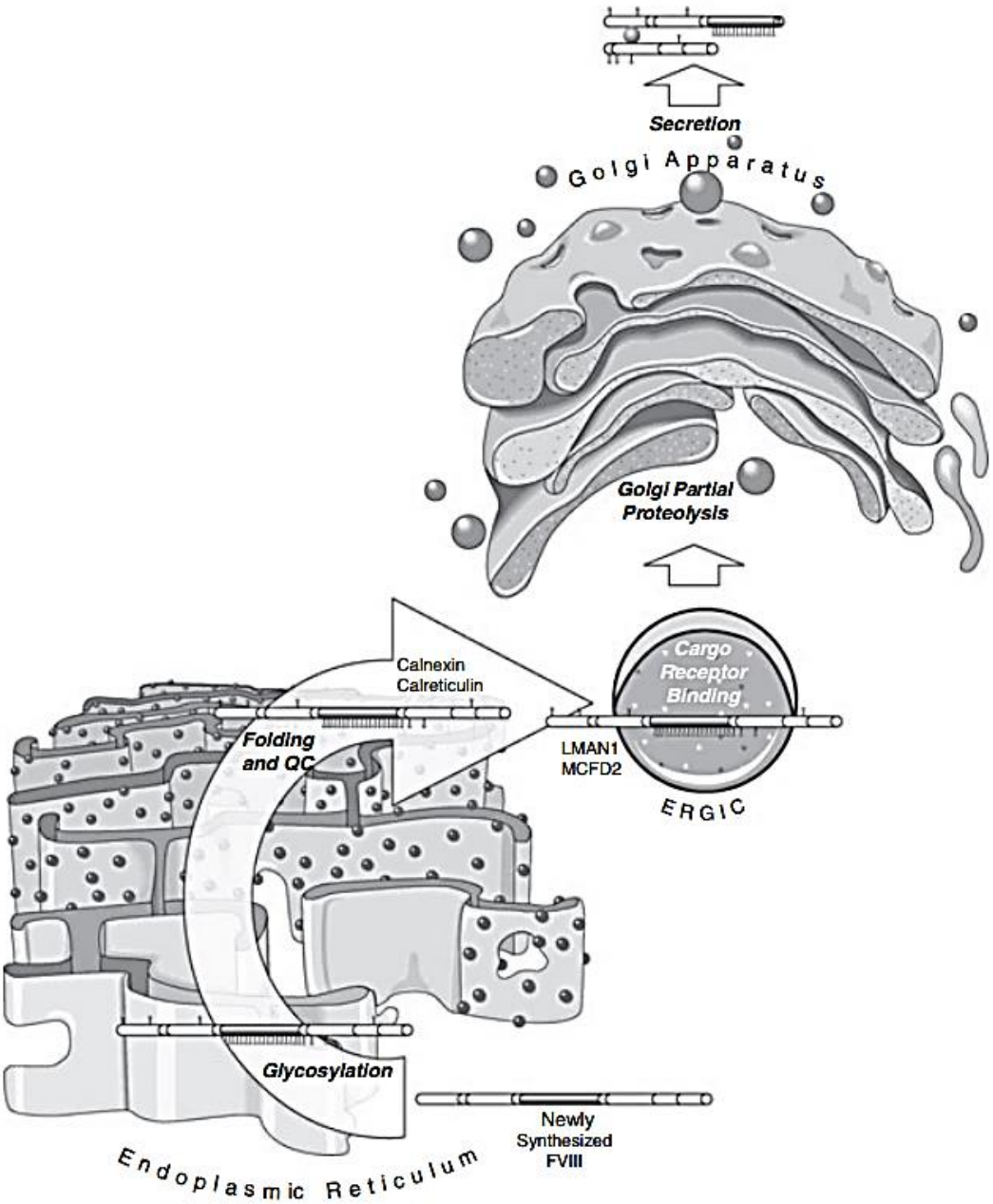

Figure 5. Schematic illustration of FVIII intracellular trafficking and secretion pathway.

This schematic depicts the intracellular journey of FVIII, from its synthesis to secretion. It highlights key processes such as glycosylation and folding in the ER, quality control by calnexin and calreticulin, transport through the ERGIC via LMAN1/MCFD2, proteolytic processing in the Golgi, and eventual secretion into the extracellular space. ERGIC (endoplasmic reticulum-Golgi intermediate compartment), LMAN1 (mannose-binding lectin 1), MCFD2 (multiple coagulation factor deficiency protein 2), QC (quality control). *Reproduced from Pipe SW. Functional roles of the factor VIII B-Domain.Hemophilia : the official journal of the World Federation of Hemophilia. 2009;15(6):1187-1196.*

1.7 Interactions with Rab Proteins

Rab GTPases have crucial roles in vesicle synthesis, motility, docking, and fusion, making them crucial regulators of intracellular vesicle trafficking. Through their interactions with effector molecules, these proteins facilitate the movement of cargo across cellular compartments and coordinate vesicular routes [95,96]. Although direct interactions between the FVIII as whole or its B-Domain and Rab proteins remain underexplored, their known involvement in similar vesicular trafficking systems provides insights into their potential roles in FVIII intracellular transport. Rab proteins, such as Rab1, Rab5, Rab7, and Rab11, are particularly relevant in the context of secretory and endocytic pathways. In order to sustain effective transport, Rab1 probably interacts indirectly with cargo molecules and controls ER-to-Golgi trafficking, a crucial stage in FVIII secretion [97]. Rab5 and Rab7, key regulators of early and late endosomes, respectively, have been shown to coordinate receptor-mediated endocytosis and degradation pathways [98,99]. For FVIII, this suggests that Rab5 and Rab7 might influence the recycling or degradation of improperly folded FVIII molecules retained in the ER or endosomal system. Rab11, known for its role in recycling vesicles back to the plasma membrane, could potentially support the exocytosis of FVIII-containing vesicles, ensuring efficient secretion[100]. Furthermore, Rab8a may indirectly support FVIII trafficking by altering intracellular signaling pathways necessary for secretion. Rab8a interacts with phosphoinositide 3-kinase γ (PI3Kγ) to control signaling and vesicle dynamics [101]. Rab26, in particular, plays a specialized role in pathways involving the transport of signaling molecules. It contributes to endosomal processes essential for cellular communication and the functioning of specific organelles [102]. This implies that Rab26 may influence vesicular systems and signaling pathways to modulate the transfer of FVIII or other coagulation factors. The autophagy pathway's connection to Rab26 might also aid in the breakdown or recycling of faulty FVIII molecules.

The absence of direct studies on the interactions between Rab proteins and FVIII represents a gap in our understanding of FVIII's intracellular transport. However, given the established role of Rab proteins in vesicular trafficking, it is plausible that these GTPases contribute to the coordination of FVIII's movement from the ER to the Golgi, as well as its subsequent secretion or recycling processes.

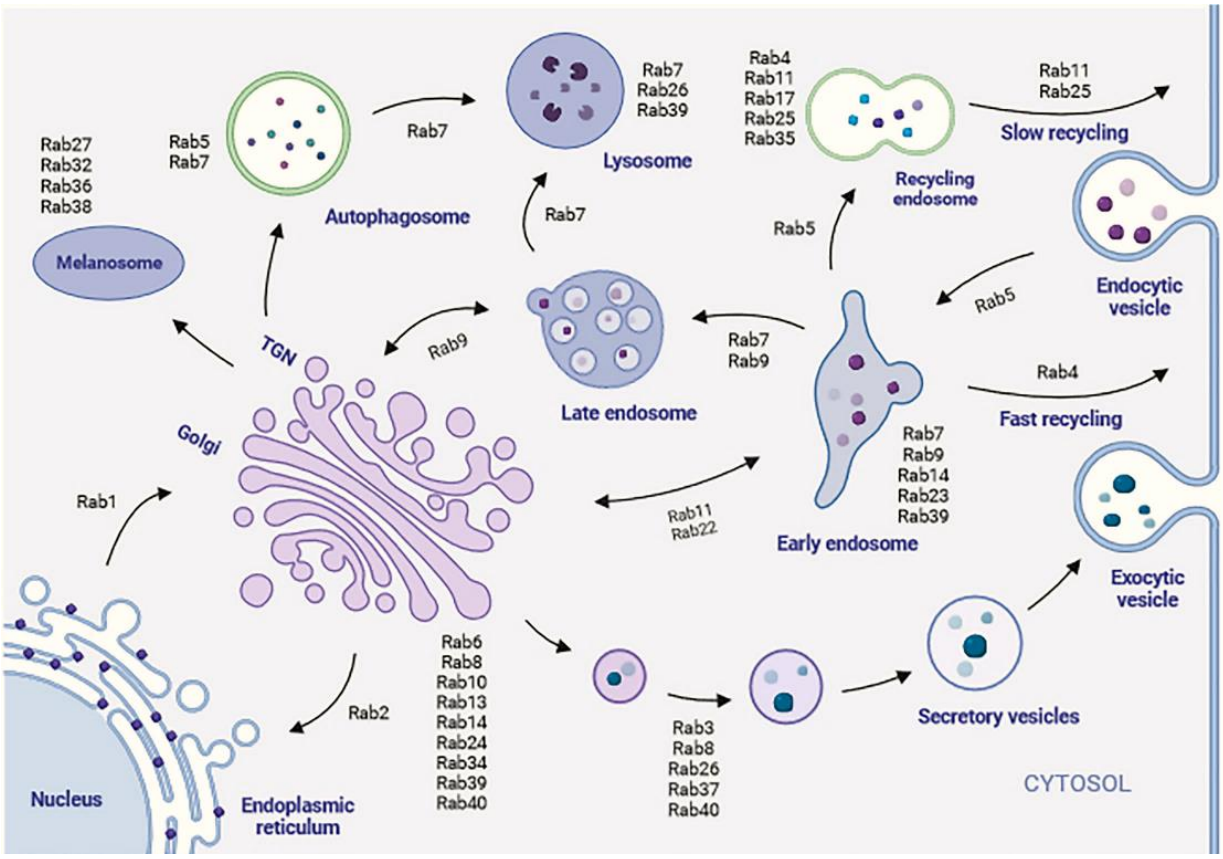

Figure 6. Rab GTPases and Their Roles in Intracellular Vesicle Trafficking. This figure illustrates how different Rab GTPases coordinate the movement of vesicles within cells. These proteins play key roles in directing intracellular transport, including the movement of vesicles between organelles, and in processes such as endocytosis (bringing materials into the cell) and exocytosis (releasing materials out of the cell). Each Rab protein is associated with specific routes and destinations, for example, some guide transport between the ER and Golgi, others regulate endosome maturation and recycling, and several control secretions to the cell surface. The overall coordination by Rab GTPases ensures that cellular cargo reaches the right place at the right time. *Reproduced from Xu, S., Cao, B., Xuan, G. et al. Function and regulation of Rab GTPases in cancers. Cell Biol Toxicol 40, 28 (2024). https://doi.org/10.1007/s10565-024-09866-5*

2. Variants in the B-Domain Influencing FVIII Trafficking and Secretion

2.1 Impact on Glycosylation and Intracellular Transport

Although the B-domain of FVIII is not comparable to any other known domain, the FV gene's B-domain retains its size and high level of N-linked glycosylation [103]. The N-

linked glycosylation sites play a crucial role for FVIII stabilization, folding, and export from the ER. These glycosylation sites, characterized by Asn-X-Ser/Thr motifs, serve as critical anchors for the binding of molecular chaperones such as calnexin and calreticulin. During biosynthesis, these interactions help FVIII fold correctly and stop aggregation [104]. Disruption of these glycosylation motifs through mutations or deletions significantly impairs FVIII's intracellular processing and functionality [105].

The recruitment of ER-resident chaperones is hampered by mutations that alter the glycosylation motifs in the B-Domain, which delays the folding and retention of FVIII in the ER [106]. This highlights the dual role of glycosylation in promoting FVIII secretion and protecting it from premature degradation [72]. Glycosylation also influences FVIII's membrane association, a critical step in its intracellular transport [107]. In order for FVIII to engage with the transport machinery needed for export to the Golgi apparatus, it must be properly glycosylated in order to be anchored to the ER membrane. This interaction emphasizes the significance of glycosylation for both preserving the structural integrity of FVIII and guaranteeing its effective trafficking across the secretory pathway.

Beyond intracellular trafficking, glycosylation plays a pivotal role in stabilizing FVIII in circulation. Glycan structures protect FVIII from proteolytic degradation and increase its half-life in the bloodstream[108]. Aberrant glycosylation can expose cryptic epitopes, leading to increased immunogenicity and the formation of inhibitory antibodies, which remain a significant challenge in FVIII replacement therapies [109].

2.2 Experimental and Clinical Findings on FVIII Variants

2.2.1 Effects of Partial B-Domain Retention or Alternative B-Domain Constructs

To improve the effectiveness of Factor VIII (FVIII) secretion and its therapeutic potential, constructs with partial B-domain retention or modified sequences have been produced [110]. The B-domain, though non-essential for clotting activity, plays a critical role in intracellular processing, folding, and secretion[111]. Modifications to this region have focused on retaining functional glycosylation sites while optimizing sequence length and structure for improved secretion. Notable engineered FVIII constructs include **(Figure 7)**:

- **SQ Variant**: The SQ name is derived from the initials of the retained sequence in the truncated B-Domain, Serine (S) and Glutamine (Q), which are part of the linker region. In order to support appropriate intracellular processing and secretion, this conserved sequence guarantees the preservation of crucial glycosylation sites and folding components. The full-length FVIII protein's amino acids 743–763 are equivalent to the SQ sequence.
  This region includes critical residues necessary for glycosylation and interaction with molecular chaperones. Specifically, this segment contains the Asn-X-Ser/Thr glycosylation motifs, which are recognized by ER-resident chaperones such as calnexin and calreticulin [112,113]. When compared to BDD-FVIII, the SQ FVIII variant showed a 2.0-fold increase in FVIII activity, while the SQ FVIII Fugu B variant showed a 2.33-fold increase. Furthermore, as compared to BDD-FVIII, the codon-optimized SQ FVIII (co) variation showed a 3.5-fold increase in FVIII activity, SQ FVIII Fugu B (co) attained a 5.5-fold increase, and SQ FVIII N6 (co) achieved a 4.2-fold increase.

- **N6 Variant**: In contrast to the SQ build, the N6 construct keeps more of the B-Domain, notably residues 746–1668, which contain more glycosylation sites and functional components. This extended sequence supports enhanced folding, chaperone interactions, and secretion and potentially reduces immunogenicity by maintaining native-like post-translational modifications [110,112]. In comparison to BDD-FVIII, the FVIII N6 variant displayed a 1.67-fold increase in FVIII activity. The codon-optimized SQ FVIII N6 (co) variant further improved FVIII activity to 4.2-fold compared to BDD-FVIII.

- **Fugu B**: Inspired by the pufferfish (Fugu) FVIII gene, this construct replaces the human B-Domain with sequences from the Fugu ortholog. The Fugu A1, A2, A3, C1, and C2 domains exhibit 46%, 43%, 47%, 52%, and 50% sequence identity to human orthologs, respectively, as well as FVIII cDNA sequences. The sequence identity between the Fugu factor VIII B-Domain and its human equivalent is only 6%. However, although there is no apparent sequence conservation between B-Domains, the Fugu B-Domain is also highly glycosylated with 10 asparagine (N)-linked glycosylation attachment sites across its 224 amino acid length. The Fugu B-Domain, being significantly shorter, enhances secretion

without compromising FVIII's procoagulant function [112]. The FVIII Fugu B variant showed a 1.33-fold increase in FVIII activity relative to BDD-FVIII. With codon optimization, SQ FVIII Fugu B (co) displayed the highest FVIII activity, reaching a 5.5-fold increase compared to BDD-FVIII.

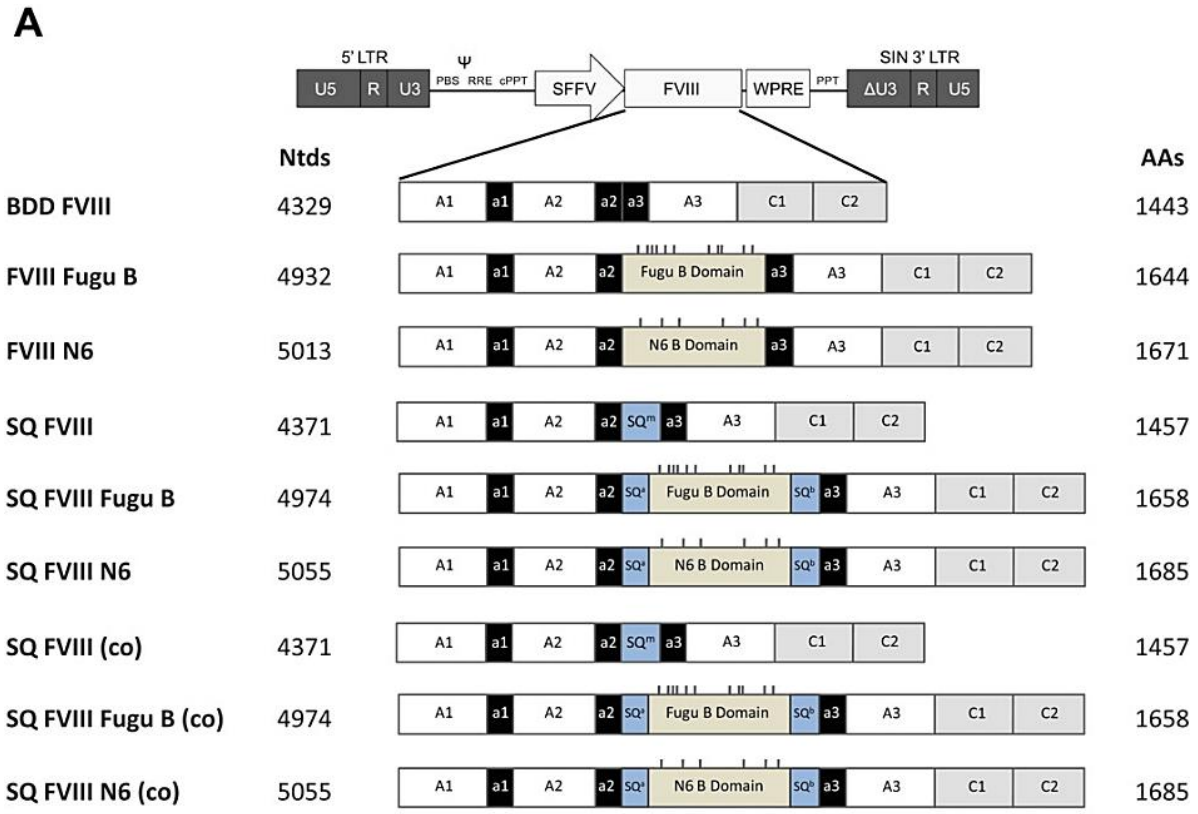

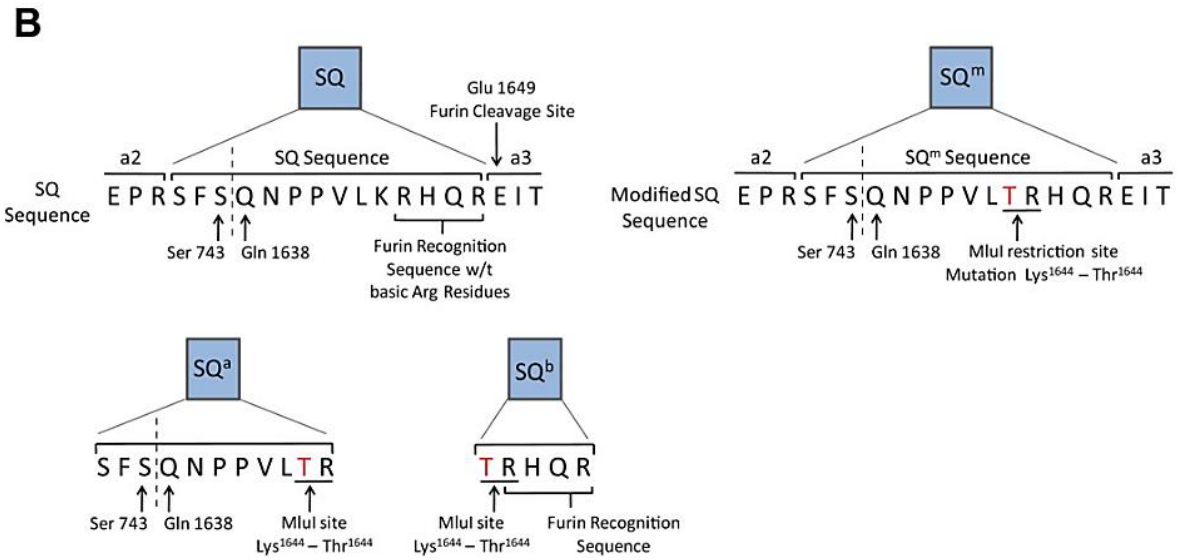

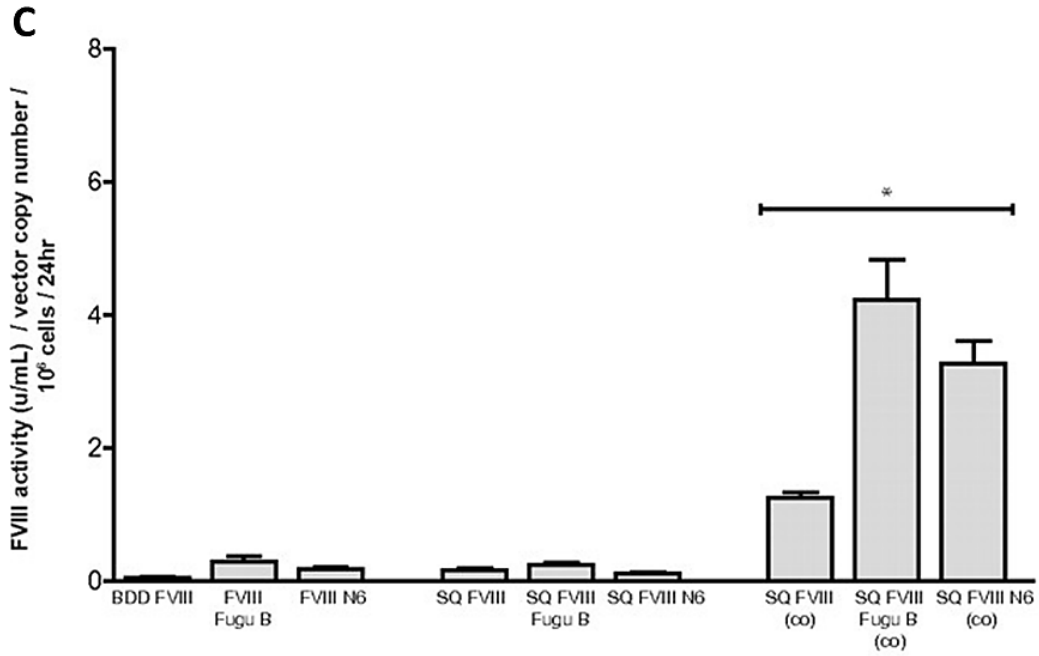

Figure 7. Overview of FVIII Variants and Their Modifications.
A- Nine different FVIII variants were designed and cloned into a self-inactivating lentiviral (SIN LV) backbone. These include BDD-FVIII (B-domain-deleted FVIII), FVIII Fugu B (BDD-FVIII with the Fugu B-Domain), FVIII N6 (BDD-FVIII with the human N6 B-Domain), and SQ FVIII (BDD-FVIII with a modified SQ amino acid sequence, SQm). Additional variants include SQ FVIII Fugu B and SQ FVIII N6, which incorporate the Fugu or N6 B-Domains, respectively, forming distinct SQa (N-terminal) and SQb (C-terminal) sequences. Codon-optimized variants (SQ FVIII (co), SQ FVIII Fugu B (co), and SQ FVIII N6 (co)) share the same amino acid structure as their non-optimized counterparts but use codon-optimized cDNA for enhanced expression. Dashes indicate asparagine (N)-linked glycosylation sites within the B-Domain.
B- The SQ sequence serves as a 14-amino acid linker between the a2 and a3 domains, containing a protease recognition site (RHQR) for efficient cleavage. A modified SQ sequence (SQm) includes a mutation (Lys1644 → Thr1644) introduced via an MluI restriction enzyme site for inserting the Fugu or N6 B-Domains. SQa and SQb are the N-terminal (11 amino acids) and C-terminal (5 amino acids) fragments created upon insertion of the Fugu or N6 B-Domains, with SQb retaining the RHQR cleavage site. MluI restriction sites are underlined, and the K to T mutation is highlighted in red.
C- Chromogenic assay measuring the relative FVIII activity of different FVIII constructs in vitro. **293T cells (1 × 10^5)** were transduced with 3 µL of each FVIII construct: BDD-FVIII, FVIII Fugu B, FVIII N6, SQ FVIII, SQ FVIII Fugu B, SQ FVIII N6, SQ FVIII (co), SQ FVIII Fugu B (co), or SQ FVIII N6 (co). After **48 hours**, the media was replaced with **500 µL serum-free media**, and FVIII activity was measured **24 hours later** using a chromogenic assay. *Reproduced from Ward NJ, Buckley SMK, Waddington SN, et al. Codon optimization of human factor VIII cDNAs leads to high-level expression. Blood. 2011;117(3):798-807.*

2.2.2 Tumorigenic Effects of FVIII Variants

Recent data raises the possibility that FVIII variations, especially those employed in gene therapy, could affect tumorigenicity. Cellular reactions and long-term safety

profiles may be impacted by variations in the design of FVIII constructs, such as B-domain-deleted vs alternative B-domain variants.

Hepatocellular Carcinoma (HCC) Risk with BDD-FVIII: Tumorigenic effects upon expressing FVIII variants with different B-Domain constructs was recently investigated [114]. The effects of two FVIII variants were investigated in mice: a complete B-Domain deletion (BDD) variant, and a short variant (N6) **(Figure 7A)** that retains 6 glycosylation sites (226 amino acids) with different folding efficiencies in the ER when expressed in hepatocytes and does not significantly aggregate or cause hepatocyte apoptosis. Remarkably, 100% of the mice that received the BDD vector developed hepatocellular carcinoma (HCC), compared to only 58% of mice that received N6 vector. No liver tumors were observed upon receiving empty vectors [114].

III- Performance of Current Gene Therapy for FVIII: Comparison to FIX

Gene therapy has revolutionized the treatment landscape for Hemophilia, providing a potential long-term or curative solution by delivering a functional copy of the defective gene. In the case of Hemophilia A (HA), caused by *f8* gene mutations leading to Factor VIII (FVIII) deficiency, several gene therapy candidates have progressed through clinical trials, showing promising but variable efficacy. When it comes to vector efficiency, expression durability, and immunological responses, gene therapy for FVIII has presented more difficulties than for Hemophilia B (HB), which is caused by mutations in the F9 gene that result in Factor IX (FIX) deficiency.

1. The principle of gene therapy approach in Hemophilia

Recombinant adeno-associated virus (AAV), a safe and non-replicating vector, is used in gene therapy for Hemophilia. A bioengineered gene cassette with tissue-specific promoters and regulatory elements is used in place of the viral DNA. Following intravenous delivery, the AAV is subjected to nuclear import and endocytosis, which releases episomal DNA that permits the expression of therapeutic genes, like FVIII or FIX, to generate the required clotting factors. However, pre-existing neutralizing antibodies, possible liver responses, temporary therapeutic effects, and the inability to re-administer treatment because of antibody formation are some of the drawbacks of AAV-based therapies. Unlike lentiviruses, AAV vectors do not integrate into the host genome, meaning Hemophilia can still be inherited despite treatment. A promising

alternative with potentially fewer side effects is the CRISPR/Cas9 system, which offers the ability to permanently correct gene mutations in a targeted manner. Hemophilia, a monogenic disorder, is particularly suited for gene therapy because even a small increase in clotting factor activity can significantly reduce bleeding risk. The compact size of FVIII and FIX genetic transcripts allows them to be efficiently packaged into AAV vectors. Treatment outcomes are easily monitored through measurable criteria such as clotting factor activity, bleeding episodes, and factor replacement needs. The aforementioned limiting factors, along with age-related comorbidities and geographic variations in AAV antibody prevalence, can significantly reduce the number of eligible patients. Hemophilia care is typically delivered in specialized multidisciplinary centers, ensuring comprehensive and coordinated treatment.

2. Gene Therapy for Hemophilia A: Current Performance and Challenges

To enable endogenous FVIII synthesis, the major method for FVIII gene therapy uses adeno-associated virus (AAV) vectors to transfer a B-domain-deleted *F8* transgene to hepatocytes. Through clinical studies, several biopharmaceutical companies have progressed gene therapy candidates, including:

2.1 BioMarin (Roctavian, valoctocogene roxaparvovec) – BDD-FVIII [115]:

BioMarin developed valoctocogene roxaparvovec (Roctavian), an AAV5-based gene therapy designed to deliver B-domain-deleted (BDD) FVIII, enabling it to fit within the AAV vector. The therapy employs a recombinant AAV5 vector featuring codon optimization and a liver-specific hybrid transcription promoter, with the B-Domain replaced by a 14-amino acid linker sequence to enhance intracellular cleavage [112]. The first study of this liver-directed gene therapy was reported in 2017 [19], and the Phase 3 GENEr8-1 trial (NCT03370913) involved administering a single intravenous dose (6×10^{13} vg/kg) to 134 adult males with severe Hemophilia A [116]. Results showed an average FVIII activity increase to 41.9 IU/dL at 49-52 weeks, accompanied by an 83.8% reduction in bleeding rate and a 98.6% decrease in FVIII infusion rate. Long-term follow-up revealed that FVIII levels dropped to 24.4 IU/dL after 2 years, with 18% of patients maintaining levels ≥40 IU/dL and 24% falling below 5 IU/dL [117]. A 7-year follow-up demonstrated a 96% reduction in the annual bleeding rate (ABR) [118]. Roctavian was approved by the EMA in 2022 and the FDA in 2023 for adults with severe Hemophilia A without inhibitors.

2.2 Spark Therapeutics / Roche (SPK-8011, SPK-8016) – BDD-FVIII:

Spark Therapeutics, acquired by Roche, developed SPK-8011, an AAV3-based gene therapy delivering BDD-FVIII. In the SPK-8011 trial (NCT03003533), 18 males received varying vector doses ($5 \times 10^{11} – 2 \times 10^{12}$ vg/kg), resulting in FVIII levels ranging from 12-30 IU/dL after 2 years and a 91.5% reduction in bleeding rates. However, two patients lost FVIII expression due to an immune reaction to the AAV capsid, which was unresponsive to corticosteroids, and the therapy is currently in Phase 3 development [119]. The SPK-8016 trial (NCT03734588) targets Hemophilia A patients without inhibitors or pre-existing AAV antibodies. In a preliminary study, four patients receiving 5×10^{11} vg/kg achieved FVIII levels of 6.2%-21.8% at 52 weeks, though seven bleeding events (six traumatic, one spontaneous) were reported, leading to the trial's suspension due to lower-than-expected impact [120].

2.3 Pfizer / Sangamo (giroctocogene fitelparvovec, PF-07055480) – BDD-FVIII:

Clinical trials have demonstrated promising FVIII levels, but durability remains a concern[121]. Pfizer and Sangamo are advancing giroctocogene fitelparvovec, an AAV6-based gene therapy using BDD-FVIII. In the NCT03061201 trial, 11 patients received doses ranging from 9×10^{11} to 3×10^{13} vg/kg, with the highest dose group achieving normal FVIII levels (mean: 61.5 IU/dL at 8 weeks). After 1-year, median FVIII levels were 50.2 IU/dL, though some patients experienced a gradual decline over 156 weeks. No bleeding occurred in year 1, but 0.9 bleeds per year were reported in year 2, including three bleeds (two traumatic, one joint-related) in two patients, with no patients resuming prophylaxis. This therapy is currently under Phase 3 evaluation[121].

3. Gene Therapy for Hemophilia B: Current Performance

To enable endogenous FIX synthesis, gene therapy for Hemophilia B typically employs adeno-associated virus (AAV) vectors to deliver the F9 gene directly to hepatocytes. This strategy benefits from the relatively small size of the F9 gene and the therapeutic potency of the FIX protein, which provides clinical benefit even at modest expression levels. Multiple biopharmaceutical companies have successfully advanced this approach into late-stage clinical trials and regulatory approvals:

3.1 CSL Behring (Hemgenix, etranacogene dezaparvovec) – FIX Padua variant:

CSL Behring's Hemgenix (etranacogene dezaparvovec) became the first gene therapy approved by both the EMA and FDA for Hemophilia B in 2022 and 2023, respectively[122]. The therapy uses an AAV5 vector carrying a codon-optimized F9 transgene encoding the high-activity FIX-Padua variant under the control of a liver-specific promoter. In the pivotal HOPE-B trial (NCT03569891), a single intravenous dose of 2×10^{13} vg/kg resulted in sustained FIX activity, with a mean FIX level of ~36.7% at 18 months and a 64% reduction in annual bleeding rates[123]. Most participants discontinued regular factor IX prophylaxis entirely.

3.2 Spark Therapeutics / Pfizer (SPK-9001, fidanacogene elaparvovec) – FIX Padua:

PrBEQVEZ™, scientifically known as fidanacogene elaparvovec, is an advanced gene therapy co-developed by Spark Therapeutics and Pfizer, aimed at providing a long-term treatment solution for Hemophilia B. This therapy uses a specially designed adeno-associated virus vector (AAVRh74) to deliver a high-functioning variant of the human Factor IX gene into liver cells. Once delivered, the gene enables the patient's own body to produce Factor IX naturally, reducing or potentially eliminating the need for regular factor replacement therapy.[124]. In December 2023, fidanacogene elaparvovec was approved for adults (≥18 years) with moderately severe to severe Hemophilia B (FIX activity ≤2%) who lack neutralizing antibodies to AAVRh74. This approval was based on the BENEGENE-2 Phase 3 trial, where 45 male participants received a single 5×10^{11} vg/kg dose after completing six months of FIX prophylaxis. The therapy led to a significant drop in annual bleeding rates and sustained therapeutic FIX levels. Patients are being monitored for up to 15 years, including through a long-term follow-up study (NCT05568719) [125].

3.3 Freeline Therapeutics – FLT180a (Verbrinacogene Setparvovec) – FIX Padua:

FLT180a, also known as c, is an investigational liver-targeted gene therapy developed by Freeline Therapeutics for Hemophilia B. It uses a synthetic AAVS3 capsid, engineered to efficiently transduce liver cells, and carries a gain-of-function Padua variant (R338L) of the F9 gene, which has approximately eight times the activity of

wild-type Factor IX. In the B-AMAZE clinical trial, ten patients with severe or moderately severe Hemophilia B received single intravenous doses ranging from 3.84×10^{11} to 1.28×10^{12} vg/kg. All patients demonstrated dose-dependent increases in Factor IX activity, with most achieving sustained therapeutic levels. At a median follow-up of 27.2 months, five patients had normal FIX activity (51–78%), three had moderate levels (23–43%), and one patient reached an unusually high level (260%). Only one participant resumed prophylaxis. Adverse events were generally manageable. Around 10% were attributed to the gene therapy, while 24% were linked to immunosuppressive treatment used to preserve gene expression. Elevated liver enzymes were the most common side effect, particularly in those on prolonged tacrolimus, immunosuppressive drug. One serious case of arteriovenous fistula thrombosis occurred in the patient with supratherapeutic FIX levels [126].

Table 1. Gene Therapy Trials for Hemophilia A and B

Aspect	Hemophilia A (FVIII)	Hemophilia B (FIX)
Gene Size	**Large gene size:** Requires B-domain deletion (BDD-FVIII) to fit within AAV vectors. - Potential impact on expression efficiency.	**Smaller gene size:** F9 gene fits easily within AAV vectors without modifications. - Higher expression efficiency.
Expression Levels	**Variable FVIII levels:** - **BMN 270 (Roctavian):** 41.9 IU/dL at 49-52 weeks, 24.4 IU/dL at 2 years. - **SPK-8011:** 12-30 IU/dL at 2 years. -**PF-07055480 (giroctocogene fitelparvovec):** 61.5 IU/dL at 8 weeks, 50.2 IU/dL at 1-year, gradual decline over 156 weeks.	**Stable FIX levels:** - **Hemgenix (etranacogene dezaparvovec):** Long-term FIX expression with near-normal clotting activity. - **SPK-9001 (fidanacogene elaparvovec):** Stable FIX production with significant reduction in annualized bleeding rates. - **BBM-H901:** Promising FIX expression with sustained activity.

Aspect	Hemophilia A (FVIII)	Hemophilia B (FIX)
Durability of Expression	**Decline over time:** - **Roctavian:** FVIII levels dropped from 41.9 IU/dL at 1-year to 24.4 IU/dL at 2 years. - **PF-07055480:** Gradual decline observed over 156 weeks.	**Long-term stability:** - **Hemgenix:** FIX expression remains stable over time. - **SPK-9001:** Fewer reports of declining FIX levels.
Bleeding Rate Reduction	**Significant reduction:** - **Roctavian:** 83.8% reduction in bleeding rate at 1-year, 96% reduction at 7 years. - **SPK-8011:** 91.5% reduction in bleeding rates at 2 years. - **PF-07055480:** No bleeding in year 1; 0.9 bleeds/year in year 2.	**Sustained reduction:** - **Hemgenix:** Near-normal clotting activity with significant reduction in annualized bleeding rates. - **SPK-9001:** Stable FIX production with sustained reduction in bleeding rates.
Immune Response	**Immune-mediated loss of expression:** - **SPK-8011:** Two patients lost *F8* expression due to immune reaction. - Corticosteroids often required to manage immune responses.	**Reduced immune response:** - Fewer immune-related complications compared to FVIII therapy. - Less reliance on corticosteroids.
Pre-existing AAV Antibodies	**Exclusion of patients:** Patients with pre-existing immunity to AAV vectors are ineligible for current gene therapy.	**Less restrictive:** Fewer issues with pre-existing AAV antibodies.
Therapeutic Advantages	**B-domain-deletion (BDD-FVIII):** Enhances intracellular cleavage and fits within AAV vectors.	**FIX-Padua variant:** Hyperactive FIX variant enhances clotting activity at lower expression levels.

Aspect	Hemophilia A (FVIII)	Hemophilia B (FIX)
	- **Codon optimization:** Improves FVIII expression.	- **Efficient packaging:** F9 gene fits easily within AAV vectors.
Challenges	**Gene size constraints:** Requires B-domain-deletion, potentially affecting expression efficiency. - **Sustained expression issues:** FVIII levels decline over time in some patients. - **Immune response variability:** Immune-mediated loss of expression in some patients.	**Fewer challenges:** smaller gene size, stable expression, and reduced immune response make FIX therapy more straightforward.
Key Trials Summary	- **BMN 270 (Roctavian):** - Phase 3 trial: FVIII levels of 41.9 IU/dL at 1-year, 24.4 IU/dL at 2 years. - 96% reduction in ABR at 7 years. - Approved by EMA (2022) and FDA (2023). - **SPK-8011:** - FVIII levels of 12-30 IU/dL at 2 years. - 91.5% reduction in bleeding rates. - Two patients lost FVIII expression due to immune reactions. - **PF-07055480 (giroctocogene fitelparvovec):** - FVIII levels of 61.5 IU/dL at 8	- **Hemgenix (etranacogene dezaparvovec):** - Long-term FIX expression with near-normal clotting activity. - 71% reduction in bleeding rate compared to baseline. - Approved by FDA (2022) and EMA (2023). - **SPK-9001 (fidanacogene elaparvovec):** - Stable FIX production with significant reduction in annualized bleeding rates. - FIX activity of 25% normal at 2 years. - **BBM-H901:** - Promising FIX expression with sustained activity.

Aspect	Hemophilia A (FVIII)	Hemophilia B (FIX)
	weeks, 50.2 IU/dL at 1-year, with gradual decline over 156 weeks. - No bleeding in year 1; 0.9 bleeds/year in year 2.	- Median annualized bleeding rate reduced from 12 to 0.

❖ **Problem statement**

Gene therapy has revolutionized the treatment of both Hemophilia A and B, with FIX gene therapy demonstrating greater stability, efficiency, and clinical success. The smaller F9 gene allows for more efficient vector delivery, minimizes immune reactions, and ensures long-lasting *f9* expression. In contrast, FVIII gene therapy faces challenges due to the large size of the *f8* gene, requiring modifications like B-domain deletion that can compromise expression efficiency. Immune-related variability and declining FVIII over time further hinder its sustained efficacy.

Several limitations persist in FVIII gene therapy:

- **Gene Size Constraints:** The *f8* gene is large, necessitating B-domain deletion to fit within AAV vectors, potentially affecting *f8* expression efficiency.
- **Immune Response and Variability:** Many patients exhibit variable FVIII levels post-treatment, and some experience immune-mediated loss of expression, requiring corticosteroid therapy.
- **Sustained Expression Issues:** Unlike FIX therapy, *f8* expression has shown variability over time, with some patients experiencing a decline.
- **Pre-existing AAV Antibodies:** Patients with pre-existing immunity to AAV vectors are ineligible for current gene therapy options.

This highlights the need for further exploration into the functional role of the deleted B-domain regions, which may help mitigate adverse cellular responses, such as ER stress and oncogenic signaling. Understanding the biological impact of these sequences could lead to safer and more effective FVIII constructs. Ongoing research is critical to improving FVIII gene therapy by refining vector design, managing immune responses, and enhancing long-term expression stability. These advancements aim to provide Hemophilia A patients with therapeutic benefits comparable to those achieved in Hemophilia B, ultimately improving clinical outcomes and quality of life.

Aim and objectives of study

Aim of study:

This doctoral thesis aims to perform a comprehensive investigation into the molecular and cellular differences between full-length FVIII (FL-FVIII) and B-domain-deleted FVIII (BDD-FVIII). By integrating experimental methodologies and advanced analytical techniques, this research seeks to provide an in-depth understanding of their intracellular processing, trafficking mechanisms, and their broader impacts on cellular homeostasis. These broader aims are detailed in 6 points below.

Objectives of study:

1. Explain Mechanisms of production and Secretion: Examine how full-length FVIII (FL-FVIII) and B-domain-deleted FVIII (BDD-FVIII) differ in terms of production and secretion efficiency.

2. Map Intracellular Trafficking Pathways: Examine FL-FVIII and BDD-FVIII's intracellular trafficking pathways, taking note of where they are found in important cellular compartments such the lysosomes, Golgi apparatus, and endoplasmic reticulum (ER).

3. Gene Knockout studies: To compare the intracellular dynamics of FL-FVIII and BDD-FVIII, carry conduct gene knockout studies that target important genes involved in FVIII trafficking.

4. Examine Vesicle Formation and Secretion Pathways: To comprehend regulatory processes, investigate the vesicle formation and secretion pathways of both FVIII types, paying particular attention to how they react to pharmacological inhibitors.

5. Analyze Impact on Cellular Homeostasis: Assess the impact of FL-FVIII and BDD-FVIII expression on cellular energy dynamics, mitochondrial function, and overall cellular health through ATP assays, Seahorse metabolic profiling, and cell proliferation studies.

6. Perform RNA-seq Analysis: Conduct RNA-seq analysis to provide a comprehensive transcriptomic perspective linking the experimental results to cellular transcriptomic.

In order to optimize FVIII-based treatments for Hemophilia A patients, these goals seek to offer a deep understanding of the molecular and cellular distinctions between FL-FVIII and BDD-FVIII.

Materials and Methods

Materials

Table 2. Cells.

Eukaryotic Cells	**Provider**
HEK293 Cells	ATCC
Competent Cells	**Provider**
One Shot TOP10 Chemically Competent E. coli	ThermoFisher

Table 3. Vectors.

Vectors	***Provider***
pCi-**FVIII**-IRES-Puro vector (for full-length FVIII)	Addgene
pCi-**FVIII**-Del-IRES-Puro vector (for BDD-FVIII)	Addgene
CRISPR CD4 Nuclease Vector	ThermoFisher
Calnexin (CNX) (NM_001746) Human Tagged ORF Clone	OriGene
Calreticulin (CALR) (NM_004343) Human Tagged ORF Clone	OriGene
LMAN1 (NM_005570) Human Tagged ORF Clone	OriGene
MCFD2 (NM_139279) Human Tagged ORF Clone	OriGene
pRP[Exp]-EGFP-CMV>h**GABARAP**[NM_007278.2]	VectorBuilder

Table 4. siRNA.

siRNA Name	**Sequence (5‘-3‘)**	**Provider**
Hs_**CNX_1**_FlexiTube siRNA	SI00027636	QIAGEN
Hs_**CNX_6_**FlexiTube siRNA	SI02663367	QIAGEN
Hs_**CNX_7**_FlexiTube siRNA	SI02757300	QIAGEN
Hs_**CALR_1**_FlexiTube siRNA	SI00062874	QIAGEN
Hs_**CALR_8**_FlexiTube siRNA	SI02654589	QIAGEN
Hs_**CALR_9**_FlexiTube siRNA	SI02777096	QIAGEN

siRNA Name	Sequence (5‘-3‘)	Provider
Hs_**LMAN1_4**_FlexiTube siRNA	SI00078988	QIAGEN
Hs_**LMAN1_7**_FlexiTube siRNA	SI04933334	QIAGEN
Hs_**MCFD2_5**_FlexiTube siRNA	SI03135496	QIAGEN
Hs_**MCFD2_6**_FlexiTube siRNA	SI04243764	QIAGEN
Hs_**MCFD2_7**_FlexiTube siRNA	SI04257225	QIAGEN
Hs_**GABARAP_1**_FlexiTube siRNA	SI00096194	QIAGEN
Hs_**GABARAP_4**_FlexiTube siRNA	SI00096215	QIAGEN
Hs_**GABARAP_5**_FlexiTube siRNA	SI03105795	QIAGEN
AllStars **Neg. Control**	SI03650318	QIAGEN

Table 5. gRNA.

Targeted Gene	Targeted Exon	Sequence of gRNA
CNX-KO	2	GCTTGGAACTGCTATTGTTG
CALR-KO	2	GCTGGATCGAATCCAAACAC
LMAN1-KO	1	TCACTCGGTCGCTTCGTCCG
MCFD2-KO	3	TTCTCCCAACCCGGCAGCATG
GABA-KO	1	GTTCGAGAAGCGCCGCTCTG

Table 6. PCR primers (colony PCR & Sequencing PCR).

Primer Name	Sequence (5‘-3‘)	Provider
U6-Forward	GAGGGCCTATTTCCCATGATTC	Eurofins
CNX_forward1	ATGGAAGGGAAGTGGTTGCTG	Eurofins
CNX _forward2	GACAAGACCCCTTATACGATT	Eurofins
CNX _forward3	GTACCTGATCCAGACGCAGAG	Eurofins
CNX _forward4	TTCCTGGTTATCCTCTTCTGC	Eurofins
CNX-Reverse1	GGAATAGATTCAAAGACCATTT	Eurofins

Primer Name	Sequence (5‘-3‘)	Provider
CALR_forward1	ATGCTGCTATCCGTGCCGCTG	Eurofins
CALR_forward2	GATGAGTTTACACACCTGTAC	Eurofins
CALR_forward3	CTGGACCTCTGGCAGGTCAAG	Eurofins
CALR_Reverse1	CTCGAAACTGGCCGACGAAGC	Eurofins
LMAN1_forward1	CAG CTG CTC CTG GCC GTG	Eurofins
LMAN1_forward2	GCT CTG CCA ATC AGC GAG	Eurofins
LMAN1_Reverse1	ACA GCG CAT ATG GTG TGC	Eurofins
LMAN1_Reverse2	CAG GGT AGC CGC GGA TGA	Eurofins
MCFD2_forward1	TGA CAA GCT CTC TTC CTA	Eurofins
MCFD2_forward2	ACAAATGTGACCCGTGATAA	Eurofins
MCFD2_ Reverse1	ATA CCT GAC TTA TAG GTG	Eurofins
MCFD2_Reverse2	GAGTGATGGCTGTGGAGAG	Eurofins
GABARAP_forward1	AGCGTTAGCGCCGCTGAGGT	Eurofins
GABARAP_forward2	CTTAAAGTTTCATAATAGCC	Eurofins
GABARAP_forward3	CCACCAAGCTGAACTGAATT	Eurofins
GABARAP_Reverse1	TCAACCCCACATCCACCACT	Eurofins
FVIII-forward1	ATGCAAATAGAGCTCTCCACC	Eurofins
FVIII-forward2	ACTGTGCCTTACCTACTCAT	Eurofins
FVIII-forward3	AGTAGACAGCTGTCCAGAGG	Eurofins
FVIII-forward4	AGTGACTGTAGAAGATGGGC	Eurofins
FVIII-forward5	TCAGACTTTCGGAACAGAGG	Eurofins
FVIII-forward6	ACAACTGCAGCAACAGAGTTG	Eurofins
FVIII-forward7	GAATAGTCCATCAGTCTGGC	Eurofins
FVIII-forward8	CCTCAGATACATACAGTGAC	Eurofins

Primer Name	Sequence (5‘-3‘)	Provider
FVIII-forward9	AGATCTCCATTACCCATTGC	Eurofins
FVIII-forward10	AAGCTATTGGATCCTCTTGC	Eurofins
FVIII-forward11	TGTCCCTCAGTTCAAGAAAG	Eurofins
FVIII-forward12	TCCCTGCAATATCCAGATGG	Eurofins
FVIII-forward13	GAAGTTCTCCAGCCTCTACA	Eurofins
FVIII-forward14	AGGAGTTCCTCATCTCCAGC	Eurofins
FVIII-end-F	ACCAATATGTTTGCCACCTG	Eurofins
HA-tag-R	GTAATCTGGAACATCGTATG	Eurofins
alfa-tag-R	GTCAGCCTCCTCCTCAGCTC	Eurofins

Table 7. Antibodies.

Antibodies	Company	Reference Number
FVIII	Affinity Biologicals	SAF8C-AP
Calnexin (E-10)	Santa Cruz	sc-46669
Calreticulin (H-170)	Santa Cruz	sc-11398
PDI (C81H6)	CST	3501
ERGIC-53 (B-9)	Santa Cruz	sc-271517
MCFD2 (F-3)	Santa Cruz	sc-390463
COPI	Santa Cruz	sc-393615
COPII (Sec31a)	CST	D1G71
COPII	Santa Cruz	sc-376587
GM130	BD transduction laboratories	610823
GM130	CST	D6B1
TGN46	SIGMA ALDRICH	T7576
Furin	abcam	ab3467
Rab8a	CST	D22D8

Antibodies	Company	Reference Number
Rab11	CST	D4F5
Rab5	CST	C8B1
Rab7	CST	D95F2
Rab7	Santa Cruz	sc- 376362
LAMP1	CST	D2D11
ARL8B	Proteintech	13049-1-AP
VAMP8	CST	13060
VAMP8	Santa Cruz	sc-166820
LC3B	abcam	51520
Rab26	Proteintech	14284-1-AP
GABARAP	Novus Biologicals	MAB8574
GABARAPL1	Proteintech	11010-1-AP
Alfa-Tag Antibody	NanoTag Biotech	N1581
Alfa-Tag Antibody	NanoTag Biotech	N1582
HA-Tag Antibody	Biozol	ABA-AB00828-7.1
Donkey anti-sheep Alexa Fluor 594	ThermoFisher scientific	A-11016
Donkey anti-rabbit Alexa Fluor 488	ThermoFisher	A-11008
Goat anti-rabbit Alexa Fluor 594	ThermoFisher	N-11012
Donkey anti-rat Alexa Fluor 488	ThermoFisher	A-21208
Donkey anti-mouse Alexa Fluor 488	ThermoFisher	A-21202
Goat anti-mouse Alexa Fluor 555	ThermoFisher	A-21422

Table 8. Media and Ready Buffers.

Media/Ready Buffers	Provider
Bovine Serum Albumin Solution 10%	Sigma
DMEM high glucose, pyruvate 10 x 500 mL	Gibco
DMEM/F-12, GlutaMAX Supplement 1x	Gibco
DPBS, no calcium, no magnesium	Gibco
Fetal Bovine Serum, qualified, heat inactivated	ThermoFisher
Fetal Bovine Serum, qualified, high Value	ThermoFisher
Laemelli Buffer 2x, 4x	biorad
NP40 Cell Lysis Buffer II (100ml)	ThermoFisher
Opti-MEM	Gibco
RIPA Lysis Buffer	Sigma-Aldrich
Seahorse XF Assay DMEM Medium	Agilent Technologies
S.O.C medium	ThermoFisher
Tris glycin running buffer	biorad
Tris Trycin running buffer	ThermoFisher
Westernblot 2x, 4x Laemmli Sample Buffer	Biorad
Westernblot Tris/Glycine/SDS 1L 10x	Biorad

Table 9. Buffers.

Buffer	***Preparation***
miSeq Buffer	0.12 g Tris was dissolved in 50 ml aqua dest and vortexed until homogeneous. The pH was adjusted to 7.5 using acid or base. Subsequently, 0.010 g $CaCl_2$, 0.0028 g $MgCl_2$, 200 µl of 0.2 M EDTA, and 1 ml Triton X-100 were added. The

Buffer	*Preparation*
	final volume was adjusted to 100 ml with aqua dest.
Western Blot Blocking Buffer (1% BSA in PBS)	1 g BSA dissolved in 100 mL PBS.
Transfer Buffer	25 mM Tris, 192 mM Glycine, 20% Methanol (diluted in water).
TBS-T (Tris-Buffered Saline with Tween 20)	20 mM Tris, 150 mM NaCl, 0.05% Tween 20 in 1 L of water, adjust to pH 7.4.
TAE Buffer	40 mM Tris, 20 mM Acetic acid, 1 mM EDTA in 1 L of water.
Stripping Buffer	7.5 g Glycine, 0.5 g SDS, 5 mL Tween-20, adjust pH to 2.2, heat at 30°C.
Gelatine Coating Buffer	Dissolve 0.1% Gelatine in PBS, sterilize by autoclaving.
4% Paraformaldehyde (PFA)	40 g Paraformaldehyde in 800 mL 1x PBS, heat to dissolve, adjust pH to 7.4.
Immunostaining Blocking Buffer	10% FBS, 0.1% Triton-X, 90% PBS.
Immunostaining Antibody Dilution Buffer	1% FBS, 0.1% Triton-X, 99% PBS.

Table 10. Chemicals and reagents.

Chemicals/Reagents	**Provider**
Agarose	Biozym
Agar	Sigma-Aldrich
Ampicillin	Sigma-Aldrich
BB2	Thermo Fisher Scientific
Beta-mercaptoethanol	PAN Biotech
Bovine Serum Albumin, ≥98%, 1x50G	Sigma-Aldrich
Brefeldin A (BFA)	Cayman Chemical
Calcium chloride (CaCl2)	Merck
Chloroquine	Cayman Chemical
CID Rab7 Inhibitor	Sigma-Aldrich
Complete ULTRA Tablets, Mini, EDTA-free	Roche

Chemicals/Reagents	Provider
DMSO (Dimethyl sulfoxide)	AppliChem
DNA Ladder (100 bp, 1 kb)	ThermoFisher
DNA loading dye	ThermoFisher
dNTP Mix (10 mM each), 1 mL	ThermoFisher
DPN1 500U	ThermoFisher
DpnI restriction enzyme	Bio-Rad
DreamTaq DNA Polymerase 200 Units	ThermoFisher
EDTA Ethylenediaminetetraacetic acid	Sigma-Aldrich
Formamide	Sigma-Aldrich
Gelatin	Sigma-Aldrich
Glycerol	Merck
Glycin min. 99 %, zur Synthese	Carl Roth
HOT FIREPol® DNA Polymerase	Solis BioDyne
HPLC-Wasser	Sigma-Merck
Immersol (Immersion oil)	Carl Zeiss Microscopy
Immobilon HRP Substrate	Millipore Sigma
Isopropanol	CARL Roth
iProof HF Fidelity DNA Polymerase	Bio-Rad
LB Broth	Sigma-Aldrich
Lipofectamine 2000	ThermoFisher
Loading Dye (6X)	ThermoFisher
Methanol	Merck
Magnesium chloride $MgCl_2$ 25 mM	ThermoFisher
MIDORI Green Advance	Nippon Genetics Europe
Mycoplasma-Off, 5 L	Minerva Biolabs
N-2 Supplement (100X), 5 mL	ThermoFisher
PageRulerTM Plus Prestained Protein Ladder	ThermoFisher
Penicillin-Streptomycin (10,000 U/mL)	ThermoFisher
PFA (paraformaldehyde)	Sigma-Aldrich
Phusion High-Fidelity DNA Polymerase (2 U/µL)	ThermoFisher
Precision Plus Protein Dual Color Standards	Bio-Rad
ProLong Glass Antifade Mountant with NucBlue Stain	ThermoFisher
Proteanase K	ThermoFisher

Chemicals/Reagents	Provider
Protease Inhibitor Complete, Mini-EDTA-free	Roche
Puromycin	ThermoFisher
RNase Inhibitor 2000 U	ThermoFisher
S Solution	ThermoFisher
Sodium-n-dodecyl sulfate (SDS)	Carl Roth
Skim milk	Millipore
Sodium acetate	Sigma-Aldrich
Sodium chloride	Carl Roth
Tris-(hydroxymethyl)-aminomethane (Tris)	Carl Roth
Triton X-100	Sigma-Aldrich
Tween-20	Sigma-Aldrich
Westernblot Mini-PROTEAN 16% Tricine Gel	ThermoFisher
Westernblot Mini-PROTEAN 4–15% TGX Stain-Free	Bio-Rad
Westernblot Mini-PROTEAN 7.5% MP TGX Gel	Bio-Rad
Westernblot Mini-PROTEAN Any kD MP TGX Gel	Bio-Rad
Westernblot Prec.Plus Protein Dual Color Standards	Bio-Rad

Table 11. Kits.

Kits	Provider
AgPath-ID One-Step RT-PCR Reagents	ThermoFisher
BigDye Terminator v1.1 Cycle Sequencing	ThermoFisher
Capturem™ IP & Co-IP Kit	Takara
Chromogenix Coamatic® Factor VIII Kit	coachrom
DNeasy Blood & Tissue Kit (50)	Qiagen
GeneArt Genomic Cleavage Assay Detection Kit	ThermoFisher
GeneArt™ CRISPR Nuclease Vector with	ThermoFisher
CD4 Enrichment Kit	
iProof PCR Kit, 50 U High	ThermoFisher
Luminescent ATP Detection Assay Kit	Abcam
Midiprep Kit 50x PureLink HiPure Plasmid	ThermoFisher
Miniprep Kit 100x PureLink HiPure Plasmid	ThermoFisher
MycoStrip kit	InvivoGen
PureLink Genomic DNA Mini Kit	ThermoFisher

Kits	Provider
PureLink RNA Mini Kit-250 preps	ThermoFisher
qBiomarker Copy Number Assay	Qiagen
QIAquick Gel Extraction Kit (50)	Qiagen
Seahorse XF Cell Mito Stress Test Kit	Agilent
Trans-Blot Turbo RTA Mini 0.45 µm PVDF Transfer Kit	biorad
VisuLize™ FVIII Antigen Kit	Affinity Biologicals

Table 12. Labware.

Labware	*Company Provider*
0.2µM filter	vWR
1 mL syringe	Braun
Aerosol resistant pipet tips	StarLab
Aluminium foil	Roth
cell Culture Plates (6, 12, 24, 96-well)	Sarstedt
Cell strainer, 70 µm and 40 µm, nylon	Falcon™ BD
coverslips	Marienfeld
Cryotubes with screw cap	Greiner Bio One
Cryovials	Corning
Filter system with bottle, 0.22 µm	Corning
Filter tips, graduated / bevelled (10 µL, 20 µL, 200 µL, 1000 µL)	Star Lab, TipOne
Filter unit 0.22 µM Stericup & Steritop	Millipore
freezing container	ThermoFisher
MicroAmp Optical 8-Cap Strips	ThermoFisher
MicroAmp Optical 8-Tube Strip, 0.2 mL	ThermoFisher
Microcentrifuge Tubes (1.5 mL, 2 mL)	Eppendorf
microPipettes and Pipette Tips	Eppendorf
Neubaeur	Marienfeld
Omnifix-syringe (1 mL, 2 mL, 3 mL, 5 mL, 10 mL)	Braun
Opaque 96-well Plate	ThermoFisher
Paper Towels & Paper Dispensers	Fuhrmann
parafilm	bemis company inc.

Table 13. Laboratory Equipment.

Instrument	***Manufacturer***
Nucleofector 4D system	Lonza
PCR Machine (Thermal Cycler)	Bio-Rad Laboratories
Gel Electrophoresis System	Bio-Rad Laboratories
7500 Fast Real-Time PCR Machine	Life Technologies, Applied Biosystems
96-Well Plate Reader (Synergy 2)	BioTek
Automated cell counter NucleoCounter® NC-202™	Chemometec
Cell Culture Incubator	Eppendorf
Centrifuge (3-16PK)	Sigma Laborzentrifugen GmbH
Centrifuge (5430R-X)	Eppendorf
Cell culture incubator Hera cell 24	ThermoFisher
Chemi Doc (Gel Doc XR+)	Bio-Rad
CO_2 Incubator	Eppendorf
Consort EV 243, 261 or 265 power supplies	Biotech Fisher
Electroporation Device	Lonza
Gel Electrophoresis System	Bio-Rad
Genome Analyzer II	Illumina Inc.
Ice machine AF30	Scotsman
Incubator Shaker	Eppendorf
Laminar Flow Hood	Eppendorf
Microcentrifuge	Eppendorf
Microscope	Carl Zeiss Microscopy
Mini Rocker	Peqlab Biotechnologie
Nucleofector 4D system	Lonza
PCR Machine (Thermal Cycler)	Bio-Rad
Power Supply	Biometra, GE healthcare
Seahorse XF Analyzer	Agilent Technologies
Spectrophotometer/Nanodrop (Nano-Drop ND 1000)	Peqlab Biotechnologie GmbH

Instrument	*Manufacturer*
Thermocycler (MJ Research)	Bio-Rad
Thermomixer	Eppendorf
Trans-Blot Turbo Transfer System	Bio-Rad
Vortexer	Janke & Kunkel IKA
Water Bath (Thermostat 2761)	Eppendorf
Western Blot Transfer Apparatus	Bio-Rad
xCELLigence RTCA DP Instrument	Agilent
Vacuum Pump PC 2002 VARIO	Vacuubrand

Table 14. Software.

	Software/Database
Cell counting	NC-view
Dissertation preparation	Microsoft Office
	Citavi 6
	BioRender
Nucleotide Sequence Databases	NCBI GenBank
	Ensembl
	UCSC Genome Browser
Protein Sequence Databases	UniProt
Seahorse Assay	Seahorse Wave
Sequence search	BLAST
	BLAT
Sequence analysis	Geneious
	Benchling
Statistical analysis	GraphPad Prism
Primer design	Oligo Calc
	Eurofins
	Primer-BLAST (NCBI)
gRNA Design Tools	Benchling
	IDT
Image Analysis Software	ZEN Blue 2.6 Pro Software
	ImageJ Software

Methods

I- Cell Culture

1. Cell Handling and Maintenance Techniques

1.1 Aseptic Techniques of HEK293 Cells

To provide a sterile and clean environment, all cell culture activities was carried out within a biosafety cabinet. Before being used, reagents and equipment were disinfected by autoclaving or filtering. Before and after every session, the inside of the biosafety cabinet was cleaned with 70% ethanol, and personal protective equipment (PPE) such lab coats and gloves were always used. Care was taken while handling pipettes, flasks, and other instruments to prevent contamination from surfaces or the air. To lower the possibility of contamination, 70% ethanol was sprayed on all goods entering the biosafety cabinet.

1.2 Maintenance

HEK293 cells, a widely used human embryonic kidney cell line, are maintained under standard culture conditions in a sterile, humidified incubator at 37°C with 5% CO_2 to support optimal growth and viability. These cells are cultured in Dulbecco's Modified Eagle Medium (DMEM, High Glucose), supplemented with 10% fetal bovine serum (FBS) to provide essential nutrients, and 1% Penicillin-Streptomycin (PenStrep) to prevent bacterial contamination. The medium is replaced every 2–3 days to maintain the appropriate pH and nutrient levels. Cells are passaged when they reach 70–90% confluence to prevent overgrowth and maintain their proliferation potential. For passaging, the culture medium is first aspirated, and the cells are rinsed gently with pre-warmed phosphate-buffered saline (PBS) to remove residual medium and serum that can inhibit enzymatic detachment. A sufficient volume of Trypsin-EDTA solution is then added to cover the cell monolayer, and the plate is incubated at 37°C for 2–3 minutes to detach the cells. Detachment is confirmed under a microscope, and complete medium (DMEM + 10% FBS + 1% PenStrep) is added to neutralize the trypsin. The cell suspension is transferred to a sterile centrifuge tube and spun at 1200 × g for 2 minutes. The supernatant is discarded, and the cell pellet is resuspended in fresh medium for further culture or experimental use.

1.3 Thawing and Preparing Cells for Culture

HEK293 cells were thawed and seeded into the desired culture plates based on experimental requirements. Prepared DMEM medium was pre-warmed to 37°C before thawing. Cryovials were thawed by immersing them in a 37°C water bath for 1-2 minutes until only a small amount of ice remained. The outside of the cryovial was disinfected with Bacillol, and then transferred into a sterile biosafety cabinet. The thawed cells were carefully transferred into a 15 mL sterile conical tube, and 6 mL of pre-warmed DMEM was slowly added to dilute the DMSO. The cell suspension was centrifuged at 1200 × g for 2 minutes. After centrifugation, the supernatant was aspirated, and the cell pellet was resuspended in fresh media. The resuspended cell suspension was then seeded into the appropriate culture plate, depending on the experimental design. The cells were incubated at 37°C in a 5% CO2 incubator.

1.4 Seeding Protocol

The seeding process begins with the detachment of cells using Trypsin-EDTA for 2 minutes at room temperature. The goal of this procedure is to ensure that cells are evenly dispersed as single cells and seeded at the desired density into culture plates. After detachment, the cells are centrifuged at the appropriate speed, and the resulting pellet is resuspended in a fresh, pre-warmed culture medium. The cells are then counted using an automated cell counter to determine the concentration required for accurate seeding. Depending on the experimental requirements, the cells are transferred either to gelatin-coated plates (for applications such as immunofluorescence staining) or to uncoated plates (for routine maintenance or other applications where coating is unnecessary). Cell seeding is performed at a density specific to the experiment. Once seeded, the plates are incubated in a humidified incubator at 37°C with 5% CO_2 to promote proper cell attachment and growth. Cell attachment is generally verified after 4-6 hours.

1.5 Cell Counting Using NucleoCounter® NC-202™

Cells were counted using the NucleoCounter® NC-202™ automated cell counter (ChemoMetec) for precise determination of cell concentration and viability.

A homogeneous cell suspension was prepared by gently pipetting to prevent clumping. Approximately 60 µL of the suspension was drawn into a Via1-Cassette™, containing acridine orange (to stain all cells) and DAPI (to stain non-viable cells). The filled cassette was inserted into the device, and the pre-set protocol was selected to analyze the sample. The system provided data on total cell count, viability, and cell concentration. Results were documented and used to adjust seeding densities as required. The cassette was disposed of in biohazard waste after analysis.

1.6 Preparation of Gelatin-Coated Culture Dishes

To prepare gelatin-coated plates, a 1% gelatin solution is made by dissolving 1 gram of gelatin in 100 mL of sterile distilled water. The solution is heated to 37°C while being continuously stirred to ensure complete dissolution. Once the gelatin has dissolved, the solution is sterilized by either filtration through a 0.22 µm filter or autoclaving. After sterilization, the solution is cooled to room temperature and is ready for use. For coating, sufficient 1% gelatin solution is added to cover the surface of the culture dish or flask. Typically, 5 mL is used for a 10-cm dish, and 1 mL is used for each well in a 6-well plate. The plate or dish is gently rocked to ensure even coverage of the surface and then incubated overnight at 4°C. After incubation, the gelatin solution is aspirated, and the plate is either used immediately for cell seeding or stored at 4°C for up to one week.

1.7 Passaging Protocol

HEK293 cells were routinely passaged when they reached 70–80% confluence to maintain their proliferation potential and prevent overgrowth. The process began by aspirating the spent medium and gently rinsing the cells with pre-warmed phosphate-buffered saline (PBS) to remove residual serum, which could inhibit enzymatic detachment. After rinsing, an appropriate volume of Trypsin-EDTA solution was added to cover the cell monolayer, and the plate was incubated at 37°C for 2–3 minutes to facilitate detachment. The detachment process was monitored under a microscope to ensure that all cells were detached without excessive incubation, which could damage the cells. Once the cells were detached, an equal volume of complete growth medium (DMEM, High Glucose supplemented with 10% fetal bovine serum and 1% Penicillin-Streptomycin) was

added to neutralize the Trypsin-EDTA. The cell suspension was transferred to a sterile centrifuge tube and centrifuged at 1200 × g for 2 minutes. The supernatant was discarded, and the pellet was gently resuspended in fresh, pre-warmed growth medium. Unlike seeding for specific experimental applications, cell counting was not performed during routine passaging. Instead, the cell suspension was diluted based on experimental requirements or the desired cell density for maintenance. A standard dilution ratio, such as 1:3 or 1:5, was typically used depending on the growth rate of the cells and the availability of culture vessels. The resuspended cells were then transferred to new culture plates containing fresh growth medium and distributed evenly to ensure uniform cell density across the plate. Plates were returned to a humidified incubator set to 37°C with 5% CO_2 to allow the cells to adhere and proliferate. The medium was replaced every 2–3 days, and the cells were monitored regularly for confluence and morphology to ensure optimal growth conditions.

1.8 Cryopreservation

HEK293 Cells were first detached using the appropriate method as described in the passaging protocol. After detachment, the cells were then resuspended in freezing medium, consisting of 90% of their respective culture media ((DMEM + 10% FBS + 1% PenStrep) and 10% DMSO. The cells were aliquoted then into sterile cryovials. To ensure a controlled freezing process, all cryovials were placed in an isopropanol-filled freezing container, allowing for a slow and constant reduction of temperature. The cells were stored at -80°C overnight to achieve complete freezing. After overnight storage, the cryovials were transferred to a liquid nitrogen tank (-196°C) for long-term preservation.

1.9 Mycoplasma Antigen Test

Mycoplasmas are extremely small, lack a cell wall, and are not visible under a microscope, routine testing is essential to maintain culture integrity. The MycoStrip® protocol was used as a rapid and sensitive method to detect mycoplasma contamination in cell culture supernatants. This assay is based on isothermal PCR amplification targeting the conserved 16S rRNA gene found in common mycoplasma species. For the procedure, 100 µL of culture supernatant was collected from each sample and centrifuged. The resulting pellet was resuspended in PBS and mixed with pre-aliquoted reaction reagents provided in

the MycoStrip® kit. The mixture was then incubated at 65°C for 40 minutes to allow DNA amplification. Following incubation, the reaction product was applied to the lateral flow detection strip. Results were interpreted within 2–5 minutes: a single band indicated a negative result, while two bands confirmed the presence of mycoplasma. The assay is highly specific and sensitive, capable of detecting as few as 10–100 colony-forming units per millilitre (CFU/mL).

2. Generation of HEK293 Cells stably Expressing FVIII Variants

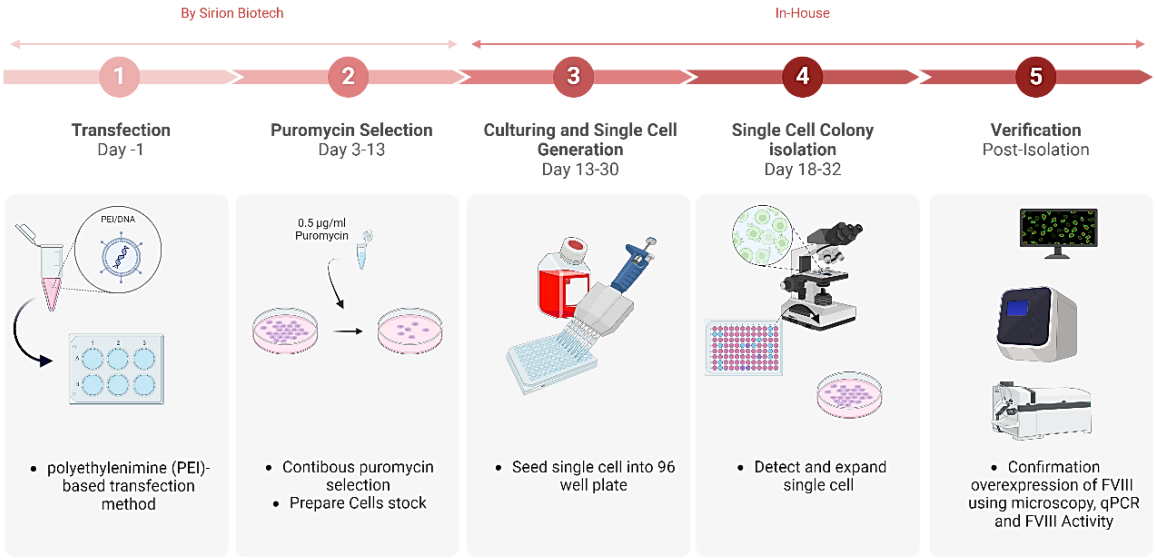

Figure 8. Generation of HEK293 cells stably expressing FVIII variants. Generation of cells was achieved using a PEI-based transfection method, followed by puromycin selection, single-cell isolation, and verification of FVIII expression through microscopy, qPCR, and functional activity assays. *Created with BioRender.com.*

2.1 Transfection and Selection Process: *The genetic modification of HEK293 cells to stably express either full-length Factor VIII (FL-FVIII) or B-domain-deleted Factor VIII (BDD-FVIII) was carried out by Sirion Biotech*. After 72 hours, the transfected cells were subjected to puromycin selection at a concentration of 0.5 µg/mL to eliminate non-transfected cells. Puromycin selection was maintained for 10 days, ensuring that only cells stably integrated with the FVIII-expressing vectors survived.

2.2 Generation of monoclonal cell lines: Before isolating single-cell clones, the transfected HEK293 cells were thawed and cultured according to the thawing protocol. Once stable populations were established in culture, single-cell clones

were isolated through serial dilution, a technique used to separate individual cells into distinct wells of a 96-well plate. The serial dilution was performed by counting the cells and then diluting them to a concentration of 1 cell per 50 µL. The wells were then checked under the microscope to identify wells containing single cells. These single cells were allowed to grow for 2 weeks, after which colonies were picked and expanded. The expanded clones were screened for FVIII secretion levels. Five clones from each group, FL-FVIII and BDD-FVIII, were selected based on their robust expression of the FVIII variants and their secretion profiles, as determined by assays measuring FVIII activity and protein levels in the culture supernatant. These assays are described in **Section X**.

II- Vectors construction

In this study, various vectors were prepared to clone sequences of interest, including gRNA and tags, using a standardized cloning protocol. This method allowed for precise insertion of the desired sequences across different vector backbones, ensuring consistency in the cloning approach. The subsequent table 15 provides an overview of the vectors utilized in this work, along with the corresponding inserts that were incorporated according to experimental requirements.

Table 15. Vectors Overview: Amplification Primers (contain designed gRNA and tags sequences).

Vectors	Inserts	Primers Sequences
CRISPR CD4 Nuclease Vector +	gRNA- CNX-F	TAT ATA TCT TGT GGA AAG GAC GAA ACA CCG **GCTTGGAACTGCTATTGTTG**
	gRNA- CNX-R	ATT TTA ACT TGC TAT TTC TAG CTC TAA AAC **CAACAATAGCAGTTCCAAGC**
	gRNA- CALR-F	TAT ATA TCT TGT GGA AAG GAC GAA ACA CCG **GCTGGATCGAATCCAAACAC**
	gRNA- CALR-R	ATT TTA ACT TGC TAT TTC TAG CTC TAA AAC **GTGTTTGGATTCGATCCA**
	gRNA- LMAN1-F	TAT ATA TCT TGT GGA AAG GAC GAA ACA CCG **TCACTCGGTCGCTTCGTCCG**

Vectors	Inserts	Primers Sequences
	gRNA- LMAN1-R	ATT TTA ACT TGC TAT TTC TAG CTC TAA AAC **CGGACGAAGCGACCGAGTGA**
	gRNA- MCFD2-F	TAT ATA TCT TGT GGA AAG GAC GAA ACA CCG **TTCTCCCAACCCGGCAGCATG**
	gRNA- MCFD2-R	ATT TTA ACT TGC TAT TTC TAG CTC TAA AAC **CATGCTGCCGGGTTGGGAGAA**
	gRNA- GABARAP-F	TAT ATA TCT TGT GGA AAG GAC GAA ACA CCG **GTTCGAGAAGCGCCGCTCTG**
	gRNA- GABARAP-R	ATT TTA ACT TGC TAT TTC TAG CTC TAA AAC **CAGAGCGGCGCTTCTCGAAC**
pCi-FVIII-IRES-Puro vector *	HA tag-F	ATG GAG GTT CTG GGC TGC GAG GCA CAG GAC CTC TAC GGG AGC GGA GGA GGT TCC GGT GGA GGT GGT TCT GGA **TAC CCA TAC GAT GTT CCA GAT TAC GCT**
	HA tag-R	TGA CGG CAG TGG CAG GTG CTG CAG TGG CCA CCC TCA **AGC GTA ATC TGG AAC ATC GTA TGG GTA** TCC AGA ACC ACC TCC ACC GGA ACC TCC TCC GCT CCC
pCi-FVIII-Del-IRES-Puro vector *	Alfa tag-F	ATG GAG GTT CTG GGC TGC GAG GCA CAG GAC CTC TAC GGG AGC GGA GGA GGT TCC GGT GGA GGT GGT TCT GGA CCC **AGC AGG CTG GAG GAG GAG CTG AGG AGG AGG CTG ACC GAG**
	Alfa tag-R	TGA CGG CAG TGG CAG GTG CTG CAG TGG CCA CCC TCA **CTC GGT CAG CCT CCT CCT CAG CTC CTC CTC CAG CCT GCT** GGG TCC AGA ACC ACC TCC ACC GGA ACC TCC TCC GCT CCC

+: Selection and Design of Guide RNA: Guide RNAs (gRNAs) were designed to target the exon region of the gene of interest using an online tool, such as E-CRISP or

CRISPR Design Tool. The gRNAs were selected based on their proximity to the gene's start codon, minimizing off-target effects. The designed oligonucleotides were synthesized by a commercial supplier.

The primers were designed with overlapping sequences that aligned the CRISPR CD4 Nuclease Vector with the desired gRNA:

- gRNA Target Sequence **(in bold)** – This is the specific sequence that guides CRISPR to the target gene.
- Overhangs (Plasmid Insertion Sites) – These are the additional sequences required for insertion into the CRISPR CD4 Nuclease Vector.

***:** The primers were designed with overlapping sequences that aligned the FVIII gene with the desired tags (HA or Alfa):

- The **5' primers** contained 36 base pairs from the FVIII coding sequence near the stop codon, followed by a Glycine (Gly) linker, and then the 39 bp HA or Alfa tag sequence **(in bold)**.
- The **3' primers** contained 36 base pairs of the vector sequence after the FVIII stop codon, a Glycine linker, and the complementary tag sequence to the 5' primer.

1. **PCR Amplification with iProof High-Fidelity DNA Polymerase**

   The first step involved amplifying the target regions using iProof high-fidelity DNA polymerase to ensure high accuracy and a low error rate. The reaction was prepared using iProof DNA polymerase, 5X iProof HF Buffer, dNTP mix, forward and reverse primers, template DNA, and nuclease-free water to make up a total volume of 50 µL.

   The PCR cycling conditions included an initial denaturation at 98°C for 30 seconds, followed by 30 cycles of denaturation at 98°C for 10 seconds, annealing at an optimized temperature for 30 seconds, and extension at 72°C for 2 minutes. A final extension step was performed at 72°C for 5 minutes before holding at 4°C indefinitely.

2. **Gel Extraction of PCR Products:** After amplification, agarose gel electrophoresis was performed to separate PCR products by size. The correct

DNA bands were visualized using UV light, excised from the gel, and purified using a gel extraction kit. The purified DNA fragments, serving as megaprimers, were quantified and prepared for fusion PCR.

3. **Fusion PCR Setup:** Fusion PCR was used to integrate the prepared megaprimers into the desired vector. The reaction was set up using Thermo Scientific™ Phusion™ High-Fidelity DNA Polymerase, 5X Phusion HF Buffer, dNTPs, forward and reverse primers, the desired DNA template, and DMSO (optional). The total reaction volume was 50 µL. The PCR cycling conditions included an initial denaturation at 98°C for 30 seconds, followed by 35 cycles of denaturation at 98°C for 10 seconds, annealing at an optimized temperature for 30 seconds, and extension at 72°C for 2 minutes. A final extension step at 72°C for 5 minutes was performed, followed by an indefinite hold at 4°C. After the reaction, DpnI digestion was performed to remove the methylated template plasmid, followed by transformation into E. coli competent cells.

4. **Transformation into E. coli Competent Cells:** 5 µL of the PCR product was transformed into competent E. coli cells. The mixture was incubated on ice for 30 minutes, heat shocked at 42°C for 30 seconds, and then allowed to recover in SOC or LB medium at 37°C for 1 hour. The cells were plated on LB agar containing 75 µg/mL ampicillin and incubated overnight at 37°C.

5. **Colony PCR:** Colony PCR was performed to confirm the presence of the correct insert. The forward primer was designed to anneal to the inserted tag, while the reverse primer annealed to the vector sequence. Positive colonies displayed a PCR band, while negative colonies showed no amplification. The reaction was set up using $MgCl_2$, 10X buffer, dNTPs, chromatography water, forward and reverse primers, formamide, and HotFire Polymerase. The PCR program included an initial denaturation at 95°C for 3 minutes, followed by 35 cycles of denaturation at 95°C for 30 seconds, annealing at 60°C for 30 seconds, and extension at 72°C for 2 minutes and 30 seconds. A final extension step at 72°C for 7 minutes was performed, followed by an indefinite hold at 4°C.

6. **Miniprep and Midi prep Methods for Plasmid DNA Isolation:** For **miniprep**, positive clones obtained from cloning were grown overnight in 5 mL LB medium containing ampicillin (50-100 µg/mL). The cultures were pelleted by centrifugation

at 4,000 rpm for 20 minutes at room temperature (RT), and the pellet was resuspended in 250 µL of resuspension solution containing RNase. The cells were then lysed with 250 µL of lysis solution by gently inverting the tube 4-6 times, incubating at RT for 5 minutes. To stop the lysis, 350 µL of neutralization solution was added, followed by thorough mixing and centrifugation at 13,000 rpm for 5 minutes at RT to pellet the debris and chromosomal DNA. The supernatant was transferred to a GeneJET spin column and centrifuged for 1 minute at 13,000 rpm. After discarding the flow-through, 500 µL of wash solution was added, followed by centrifugation for 1 minute; this washing step was repeated. The GeneJET spin column was then transferred to a clean 1.5 mL microcentrifuge tube, and 50 µL of nuclease-free water (H_2O) was added to the column membrane and incubated for 2 minutes. The tube was centrifuged for 2 minutes to elute the plasmid DNA, which was then measured using a Nanodrop spectrophotometer and stored at -20°C. For **midiprep**, the same steps of resuspension, lysis, neutralization, and washing were followed, but using a larger bacterial pellet from 50-100 mL of overnight LB culture. The midiprep plasmid isolation kit (Qiagen) was used, allowing for the extraction of higher concentrations of plasmid DNA for downstream applications.

7. **Sequencing Verification:** Extracted plasmids were verified by sequencing to confirm the correct integration of the HA or Alfa tag into the FVIII gene. The sequencing PCR reaction was prepared using 10X PCR buffer (5 µL), $MgCl_2$ (25 mM, 1.5 µL), dNTPs (2 mM, 1 µL), forward primer (10 pmol, 1 µL), reverse primer (10 pmol, 1 µL), DNA template (100 ng, 0.5 µL), DNA polymerase (0.5 µL), and nuclease-free water to adjust the final volume to 50 µL. The PCR cycling conditions included an initial denaturation at 98°C for 30 seconds, followed by 35 cycles of denaturation at 98°C for 10 seconds, annealing at 62°C for 30 seconds, and extension at 72°C for 2 minutes. The reaction concluded with a final extension at 72°C for 5 minutes, followed by an indefinite hold at 4°C. After amplification, sequencing analysis was conducted using Geneious and Benchling to confirm the expected sequence of the FVIII gene with the integrated HA or Alfa tag. The sequence was checked for accuracy, ensuring correct integration without mutations or unwanted modifications.

III- Transfection

Cell Seeding and Transfection: For transient transfection, HEK293 cells were used due to their high transfection efficiency and ease of handling. Cells were seeded onto gelatin-coated coverslips placed in 12-well plates to enhance cell attachment and allow for easy immunofluorescence processing.

1. **Cell Seeding**: Cells were seeded at an optimal density (1.0 x 10^5 cells per well) to ensure they reached approximately 70-80% confluence by the time of transfection.
2. **Transfection Procedure:** The transfection was performed using Lipofectamine 2000, a widely used transfection reagent suitable for HEK293 cells.

Transfection Steps:

a) **Preparation of DNA-Lipofectamine Complex**:

- In separate tubes, mix the following for each well:
  - **Tube 1**: Dilute 2 µg of plasmid DNA in 50 µL Opti-MEM (serum-free medium).
  - **Tube 2**: Dilute 2.5 µL of Lipofectamine 2000 in 50 µL Opti-MEM. Incubate for 5 minutes at room temperature.
- Combine Tube 1 and Tube 2, and allow the complex to form for 20 minutes at room temperature.

b) **Transfection**:

- Add the DNA-Lipofectamine mixture dropwise to each well containing HEK293 cells in 500 µL of growth in the absence of fetal bovine serum (FBS) and antibiotics, which were added 4 hours post-transfection to maintain cell health and growth.
- Gently swirl the plate to distribute the mixture evenly and incubate the cells at 37°C in a humidified 5% CO_2 incubator.
- Transfection duration: 48-72 hours for optimal expression of the overexpressed protein.

IV- Generation of Knockout Cell Lines Using CRISPR/Cas9

Generation of gene knockout HEK293 cell lines expressing either full-length FVIII or B-domain-deleted FVIII was performed using CRISPR-Cas9 genome editing. *Three of the full-length FVIII knockout cell lines, CNX-KO, LMAN1-KO, and GABARAP-KO had been previously generated by Dr. Heike Singer. The remaining full-length knockouts (CALR-KO and MCFD2-KO), along with all BDD-expressing KO lines, were generated by the author during the course of this study.*

1. **Cloning of gRNA into CRISPR/Cas9 Vector:** The synthesized gRNA oligos were annealed and cloned into a CRISPR/Cas9 plasmid vector containing the Cas9 nuclease gene and a selectable marker according to the cloning method in **section III**.

2. **Transfection:** The two target cell lines were cultured under standard conditions (37°C, 5% CO_2) in their respective growth media. Cells were seeded in 6-well plates and transfected with the CRISPR/Cas9 plasmid using a Lipofectamine 2000 transfection reagent according to the cloning method in **section IV 1.2**.

3. **Validation of CRISPR Activity/ Cleavage Assay**

   3.1 Cell Lysis: 72 hours after transfection cells were collected and pelleted by centrifugation at 1,200 rpm for 2 minutes. The supernatant was carefully removed, and the cells were lysed using the GeneArt® Genomic Cleavage Detection Kit (Catalog A24372). A mixture of 2 µL of protein degrader and 50 µL of cell lysis buffer was prepared. The entire volume (50 µL) was added to the cell pellet, ensuring proper resuspension. The cell suspension was transferred to PCR strips and placed in a thermocycler for lysis. The lysis PCR program included incubation at 68°C for 15 minutes, followed by 95°C for 10 minutes, and then holding at 4°C.

   3.2 PCR Amplification: Following lysis, the cell lysate was briefly vortexed and used for PCR amplification. The reaction was set up using: 2 µL of cell lysate (for the sample), 1 µL of 10 µM forward/reverse primer mix, AmpliTaq Gold® 360 Master Mix (25 µL) and Nuclease-free water to adjust the final volume to 50 µL. For the control reaction, 1 µL of control template and primers were

used instead of the cell lysate. The PCR cycling conditions consisted of enzyme activation at 95°C for 10 minutes, followed by 40 cycles of denaturation at 95°C for 30 seconds, annealing at 68°C for 30 seconds, and elongation at 72°C for 30 seconds. A final elongation at 72°C for 7 minutes was performed before holding at 4°C.

3.3 Agarose Gel Electrophoresis: To verify the success of the PCR, 3 µL of the PCR product was diluted with 10 µL of nuclease-free water and mixed with 2 µL of loading dye (1:40 dilution). The mixture was loaded onto a 1% agarose gel, alongside a 100 bp molecular weight ladder loaded in the first lane. The gel was run at 100 volts for approximately 40 minutes. A successful PCR was indicated by a clean product band of the expected size without significant non-specific amplification.

3.4 Re-Annealing of PCR Products: To form heteroduplex DNA containing indels, a re-annealing reaction was set up in sterile PCR strips. The reaction mixture consisted of 2 µL of PCR product, 1 µL of 10X detection buffer, and nuclease-free water up to a total volume of 9 µL. The mixture was briefly vortexed and centrifuged before being subjected to a controlled re-annealing program. The re-annealing PCR program involved an initial incubation at 95°C for 5 minutes, followed by a gradual temperature decrease from 95°C to 85°C at a rate of -2°C/second, and then further cooling from 85°C to 25°C at a rate of -0.1°C/second. The reaction was then held at 4°C indefinitely. This process facilitated the random annealing of PCR fragments containing indels and wild-type DNA, leading to the formation of mismatched heteroduplexes for subsequent analysis.

3.5 Gel-Based Detection of Cleavage Products: The heteroduplex DNA, containing mismatched DNA or indels, was then treated with Detection Enzyme (or Surveyor Nuclease), which cleaves mismatched DNA. This enzyme allows for quantification of gene modification by cleaving DNA at the indel sites. 0.5 µL of Detection Enzyme was added to each reaction (both sample and control). The mixture was briefly centrifuged and incubated at 37°C for 1 hour. After incubation, 10 µL of each reaction was loaded onto a 2% agarose gel alongside a DNA ladder and loading dye. The gel was run at 100 volts for 40 minutes. Successful cleavage was indicated

by the appearance of shorter DNA fragments (compared to the original uncut product) when visualized under UV light.

4. Single-Cell Cloning

To generate clonal knockout cell lines, transfected cells were diluted and plated into 96-well plates to isolate single colonies. Each well was microscopically monitored over a period of two weeks to ensure clonal expansion from a single cell. Only wells where a single cell was initially observed and subsequently began to proliferate into a visible colony were selected and labeled as clonal. Wells with no growth, multiple initial cells, or ambiguous origins were excluded to ensure clonal purity. This careful selection process was critical to confirm that the resulting knockout cell lines were derived from a single edited cell.

5. Verification of Knockout

5.1 Genomic DNA Extraction and PCR Screening: For this step, we used a self-made ‘miSeq’ buffer. A 100 ml miseq buffer is made by mixing 0.12 g tris with 50 ml aqua dest, we vortexed until the solution became homogenous. Next, we equilibrated the pH by addition of acid or base solution to reach 7.5 PH. 0.010g CaCl2, 0.0028 g MgCl2, 200 µl 0.2 M EDTA and 1 ml triton x100 were added. Then, the whole volume was filled up to 100 ml with aqua dest. The miSeq buffer was diluted 1:2 by addition 10 ml of the prepared buffer to 10 ml water. Before using miSeq buffer, 100 µl Proteinase K (0.2 mg/mL) would be added. We took the 96 well plate. We removed old medium and 90 µl of the prepared miSeq buffer was put in each well, and the plate was then placed directly on ice. Done with transferring the lysate to PCR tubes and performed a miSeq PCR for 3 times. The MiSeq PCR program consists of the following steps:

1. The initial denaturation is performed at 65°C for 10 minutes.
2. This is followed by a denaturation step at 95°C for 15 minutes.
3. Finally, the reaction is held at 4°C indefinitely.

For CRISPR amplification, the region flanking the CRISPR target site was amplified by PCR using gene-specific primers that were previously used in the cleavage assay. The same PCR program from the cleavage assay was followed. The PCR reaction mix was prepared with the following components: 16.0 µl of H_2O, 2.5 µl of 10x Reaction Buffer B (Mg^{2+} free) containing 0.8 M Tris-HCl, 0.2 M $(NH_4)_2SO_4$, and 0.2% w/v Tween-20, 2.5 µl of $MgCl_2$ (25 mM), 2.5 µl of dNTPs (2.5 mM), and 2.5 µl of 10x Solution S, which is an additive for difficult templates such as GC-rich DNA. Additionally, 0.5 µl each of forward and reverse primers, 0.7 µl of Hot-Fire Taq polymerase, and 2.0 µl of DNA isolation lysate were included in the reaction. The DNA lysate was added to a 24 µl master mix to complete the reaction setup. To verify the presence of PCR product, 5 µl of the PCR product were running with 2 µl of 1:40 loading Dye, and 2.5 µl of 100 bp ladder into 1% gel for 25 mins at 150 V.

5.2 Sequencing for Indel Confirmation:

PCR products from the target region were sequenced to confirm the presence of indels (insertions or deletions) at the gRNA target site, indicating successful gene knockout according to **section III 7.**

5.3 Mutation annotation and Nomenclature of the Knockouts:

To accurately describe the CRISPR/Cas9-induced mutations in knockout (KO) cell lines, mutation nomenclature was performed in accordance with the guidelines of the Human Genome Variation Society (HGVS). Both coding DNA (c.) and protein-level (p.) changes were annotated for each edited gene. All nucleotide and protein changes were described relative to the reference transcript sequence, where c.1 corresponds to the A of the ATG translation initiation codon. For each cell line, the genetic modifications were confirmed by Sanger sequencing. Resulting chromatograms were analyzed using sequence alignment tools (SnapGene or Benchling), and mutations were identified on both alleles. When biallelic editing occurred, the variants were reported using bracketed notation to indicate both alleles, e.g., c.[49_54delATTGT]; [49_54delATTGT].

The following conventions and abbreviations were used:

c. = coding DNA reference sequence

p. = protein-level effect

del = deletion of one or more nucleotides or amino acids

ins = insertion of one or more nucleotides

dup = duplication

fs = frameshift mutation

Ter or X = premature termination codon (stop codon)

Xn = number of amino acids following the frameshift before the stop codon

_ = indicates a range or span of nucleotides or amino acids

; = separates the two alleles in a diploid organism (biallelic or compound mutations)

Protein-level changes were written using the standard three-letter amino acid codes. Frameshift mutations were designated by the first affected amino acid, followed by “fs” and the number of altered residues before the new stop codon (e.g., p.Arg39LeufsX4 indicates a frameshift at arginine 39 with a premature stop after 4 altered amino acids). Deletions spanning more than one residue were denoted with an underscore (e.g., p.Arg40_Pro42delfsTer).

5.4 Western Blot:

To confirm the loss of protein expression, Western blot analysis was performed using specific antibodies against the target protein. Cells were lysed using RIPA buffer containing SDS and sodium deoxycholate, which effectively disrupts nuclear membranes. To prevent protease activity, complete ULTRA Tablets, Mini, EDTA-free inhibitors were added during lysis, with one tablet per 10 ml of RIPA buffer. Cells were incubated in this solution on ice for 10 minutes, followed by centrifugation at 8,000 × g for 5 minutes to pellet debris. The supernatant was collected and stored at -80°C. For sample preparation, lysates were thawed and mixed 1:1 with a buffer containing 2X Laemmli buffer and mercaptoethanol as a reducing agent. After vortexing, samples were heated to 95°C for 5 minutes and cooled on ice before a short centrifugation. Samples were loaded onto a 10% SDS-PAGE gel along with a molecular weight marker, and electrophoresis was run at 150 V for 30 minutes. Proteins were transferred from the gel to a PVDF

membrane, pre-soaked in methanol and transfer buffer, using a constant current of 250 mA for 1 hour. After transfer, the membrane was blocked overnight at 4°C in blocking solution (TBS, dry milk, Tween 20) to prevent non-specific binding.

The membrane was then incubated with the primary antibody targeting the desired gene (refer to Antibodies **Table 7** for details on the primary antibody used) for 2-3 hours at room temperature, washed, and incubated with the corresponding secondary antibody as listed in **Table 7**. For detection, the membrane was treated with a luminol/oxidizing reagent mixture, and protein bands were visualized using a chemiluminescence imaging system.

V- Molecular Analyses

1. Relative FVIII Copy Number Determination

1.1 DNA extraction: DNeasy Blood and Tissue Kit was used for DNA extraction from collected cell pellets. Fresh lysis buffer was prepared according to the kit's instructions. On ice, 600 µL of Cell Lysis Buffer was added to each pellet, and the samples were vortexed until the cell pellets were fully dispersed and lysed. After vortexing, 20 µL of Proteinase K solution was added to each sample, and the mixture was incubated at 55°C for 10 minutes to ensure complete cell lysis. The samples were briefly vortexed again after the incubation to mix the contents. Next, 200 µL of ethanol (96-100%) was added to the lysate, and the samples were vortexed briefly. The mixture was transferred to a spin cartridge inserted into a collection tube. The samples were centrifuged at 12,000 rcf for 1 minute to bind the DNA to the spin column, after which the flow-through was discarded, and the spin cartridge was placed back into the collection tube. The following washing steps were performed: 500 µL of Wash Buffer 1 was added to the cartridge, and the sample was centrifuged at 12,000 rcf for 1 minute. The flow-through was discarded. Then, 500 µL of Wash Buffer 2 was added, and centrifugation was repeated under the same conditions. This step was performed twice to ensure complete washing of the DNA. After washing, the spin cartridge was centrifuged for an additional 2 minutes at 12,000 rcf to dry the membrane. The spin cartridge was then placed into a clean recovery tube, and 100 µL of Elution Buffer was added directly to the center of the

membrane. The sample was incubated at room temperature for 1 minute, followed by centrifugation at 12,000 rcf for 2 minutes to elute the purified DNA into the recovery tube. DNA concentration was measured using a NanoDrop spectrophotometer. The purified DNA was stored at -20°C for subsequent downstream applications, such as PCR.

1.2 q-PCR: Two hundred nanograms of DNA was used to perform a qBiomarker Copy Number assay from Qiagen, designed in unique regions of the genome (Exon 12 of the FVIII gene) to interpret relative copy number changes for the FVIII gene in each clone. The qBiomarker SYBR Green Mastermix was used for the assay, and DNA was amplified using the Applied Biosystems 7500 system. The copy number profile of each sample was determined using the ΔΔCT method, comparing the target gene CT with the reference assay CT between the test sample genome and the reference genome. The reaction mixture for a single sample was prepared using 12.5 µL of qBiomarker SYBR Mastermix, 1.25 µL of the qBiomarker Copy Number PCR Assay either targeting FVIII or MeRef, and 7.0 µL of nuclease-free water, bringing the total volume per well to 23.0 µL For each reaction, 23 µL of this master mix was dispensed into the well, followed by the addition of 2 µL of DNA at a concentration of 2 ng/µL, resulting in a final reaction volume of 25 µL per well. The copy number assay used was the qBiomarker CNV PCR Assay for the human chromosome X tile 784337 VPH10X-0784337A, corresponding to the FVIII gene ENSG00000185010, with a genomic region spanning from position 154194701 to 154194962. The PCR conditions were as follows: The initial incubation step was performed at 50°C for 2 minutes. This was followed by an initial denaturation at 95°C for 10 minutes. The main cycling stage consisted of 40 cycles of denaturation at 95°C for 15 seconds. The final step involved annealing and extension at 60°C for 30 seconds.

2. *F8* Expression Determination

2.1 RNA Extraction: The PureLink RNA Mini Kit (ThermoFisher Scientific) was used for RNA extraction from the collected cell lysates. Fresh lysis buffer was prepared by adding 10 µL of 2-mercaptoethanol to each 1 mL of Lysis

Buffer. On ice, 600 µL of the fresh lysis buffer was added to each pellet, and the samples were vortexed until the cell pellets were dispersed and the cells appeared lysed. Next, 600 µL of 70% ethanol was added to each sample, which was then transferred to the spin cartridge and centrifuged at 12,000 rcf for 15 seconds. The flow-through was discarded, and the washing steps were performed with 700 µL of Washing Buffer 1, followed by 500 µL of Washing Buffer 2 (repeated twice) under the same centrifugation conditions.

The cartridge was then centrifuged at 12,000 rcf for 2 minutes to dry the membrane with bound RNA. The collection tube was discarded, and the spin cartridge was placed into a recovery tube. For the elution step, 50 µL of RNase-free water was added to the center of the spin cartridge, incubated for 1 minute, and then centrifuged for 2 minutes at 12,000 rcf to elute the RNA into the recovery tube. RNA concentration was measured using a NanoDrop spectrophotometer. The purified RNA was stored at -80°C for subsequent Real-Time PCR analysis.

2.2 Quantitative Real-Time PCR (RT-PCR): Quantitative TaqMan Real-Time PCR was performed using the Applied Biosystems® 7500 Real-Time PCR System and 7500 Software v2.0.6 on a 96-well plate. The AgPath-ID™ One-Step RT-PCR Reagents kit (Thermo Fisher Scientific, Catalog # 4387424) was used, which includes the 25X RT-PCR Enzyme Mix (containing ArrayScript™ Reverse Transcriptase and AmpliTaq Gold® DNA Polymerase), 2X RT-PCR Buffer (including ROX™ passive reference dye for fluorescent signal normalization), and nuclease-free water. For result normalization, the ß-actin gene was used as a housekeeping gene. Each sample was assessed with both the FVIII primer/probe mixture for measuring FVIII expression and the ß-actin primer/probe mixture for normalizing the results. The sequences of the primers and probes used for both genes are listed in **Table 16.**

Table 16. Primers and probes sequences for FVIII and ß-actin used in RT-PCR.

Primer/Probe Name	***Primer/Probe Sequence (5' → 3')***
FVIII RT-PCR Forward primer	5'GGACATGTGTTCACTGTACGA3'
FVIII RT-PCR Reverse primer	5'TGTAGATGCTCGCCAATAAGG3'
FVIII TaqMan Probe	5'TCTATCCAGGTGTTTTTGAGACA3'

Primer/Probe Name	*Primer/Probe Sequence (5' → 3')*
ß-Actin RT-PCR Forward primer	5'ACCTTCTACAATGAGCTGCG3'
ß-Actin RT-PCR Reverse primer	5'CCTGGATAGCAACGTACATGG3'
ß-Actin TaqMan Probe	5'ATCTGGGTCATCTTCTCGCGGTTG3'

On ice, a primer-probe master mix was prepared for each gene by mixing 18 µL of the corresponding forward and reverse primers, 5 µL of the TaqMan probe specific for each gene, and 59 µL of nuclease-free water. Two RT-PCR master mixes (for each gene) were then prepared on ice, mixing the components with 5-10% extra volume for each reaction. The RT-PCR thermal cycling conditions were as follows: The process began with a reverse transcription step at 45°C for 10 minutes to synthesize complementary DNA. This was followed by RT inactivation and initial denaturation at 95°C for 10 minutes to ensure complete enzyme inactivation and template denaturation. The amplification phase consisted of 40 cycles, each including a denaturation step at 95°C for 15 seconds, followed by annealing and extension at 60°C for 45 seconds to enable precise target amplification. Quantification of gene expression is carried out using the 2–ΔΔCt method. The Ct values for FVIII are normalized against ß-actin, and fold changes in gene expression are calculated relative to a reference control sample.

VI- Cellular Assays

1. Cell Proliferation Assay:

Real-time cell proliferation was assessed using the xCELLigence RTCA DP instrument, which allows continuous monitoring of cell growth and behavior without the need for labels or dyes. Cells were seeded into specialized xCELLigence microplates (RTCA E-plate 16) at a density of 50,000 cells per well to enable real-time growth rate comparison across different conditions.

The E-plate contains gold microelectrodes integrated into the bottom of each well, which detect changes in electrical impedance as cells adhere to and proliferate on the surface. This impedance correlates with the number, size, and shape of cells. The xCELLigence RTCA DP instrument was placed inside a standard cell culture incubator, maintaining physiological conditions of 37°C and 5% CO_2.

The system automatically recorded impedance measurements every 30 minutes over the course of a 96-hour experiment.

These impedance readings were translated into Cell Index (CI) values, which provide a quantitative assessment of cell number and health. CI values at each time point were calculated using the formula (Rn - Rb) / 15, where Rn is the impedance measured in the presence of cells, and Rb is the background impedance in wells containing only media.

The growth dynamics of the cells were further analyzed by calculating growth slopes, which represent the rate of change in cell proliferation over time. This analysis was performed using Roche RTA software, which is specifically designed to process and interpret real-time impedance data.

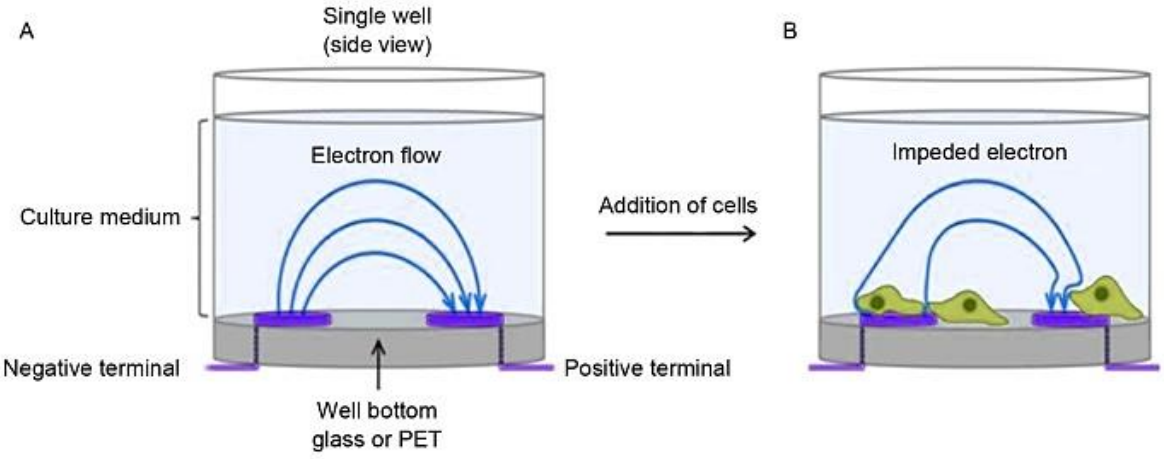

Figure 9. Overview of the xCELLigence Real-Time Cell Analysis (RTCA) System. A- Schematic representation of a single well before cell addition, showing the gold electrodes (in violet color) embedded in the glass or PET well bottom. Electron flow between the electrodes is largely unimpeded in the absence of cells, resulting in minimal impedance. **B-** After cell addition, the cells adhere to the electrode surface, impeding electron flow and increasing impedance [127] . *Reproduced from https://www.agilent.com/en/technology/cellular-impedance*

2. Residual ATP Content Measurement:

Residual ATP content in HEK cells was measured using the **Luminescent ATP Detection Assay Kit**, which provides a highly sensitive and quantitative method for determining intracellular ATP levels.

The assay was performed in an opaque white 96-well culture plate to minimize background signal from light reflection. A total of 30,000 HEK cells were seeded into each well, with 6 replicates per experimental condition to ensure statistical

significance and reproducibility. To generate a reference for ATP quantification, an ATP standard dilution series was prepared. This allowed for the creation of a standard curve against which the luminescent signals from experimental samples could be compared. To initiate the assay, 50 µL of lysis detergent were added to each well. The detergent not only lysed the cells but also stabilized the released ATP, ensuring accurate downstream measurements. Following lysis, 50 µL of substrate solution, containing D-Luciferin and firefly luciferase, was added to each well.

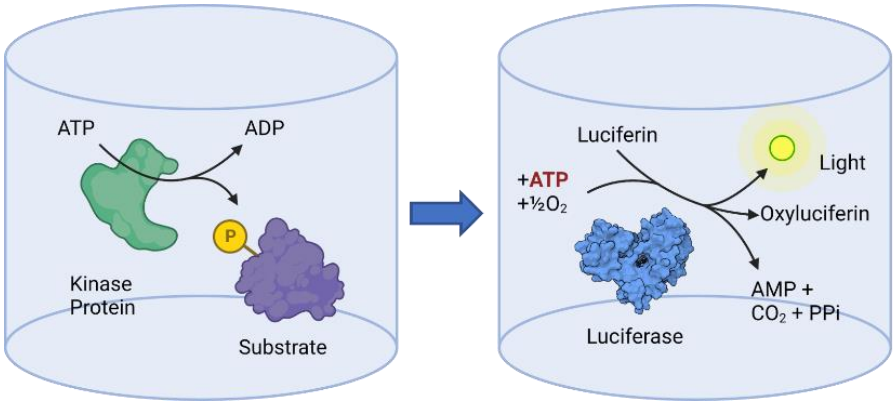

Figure 10. Principle of Luminescent ATP Detection Assay.
In the assays, a purified active kinase phosphorylates a substrate, a process in which ATP molecules are converted to ADP. The available ATP in the well is then measured by the ATP-dependent conversion of luciferin into oxyluciferin by the luciferase enzyme, producing a luminescent signal. Thus, the signal readout is inversely proportional to the kinase activity, as higher kinase activity results in lower ATP availability. *Reproduced from https://bpsbioscience.com/product-types/biochemical-assay-kits-by-format-type/luminescent?p=7*

The firefly luciferase enzyme catalyzes the reaction between ATP and luciferin, producing light in direct proportion to the ATP concentration present. After adding the substrate, the plate was incubated in the dark at room temperature for 10 minutes to allow the luminescent reaction to reach equilibrium. This dark incubation step was crucial to avoid interference from ambient light, which could affect the luminescent signal. After the incubation period, the luminescence produced by each well was measured using a microplate reader designed to detect and quantify low levels of light. To ensure accurate measurement of ATP levels, a standard curve was plotted based on the known ATP concentrations from the standard dilution series. The luminescent units recorded from each

sample were interpolated against this curve to determine the absolute ATP concentration in each well, expressed in micromolar (µM).

A blank control containing only the substrate solution and culture medium (without cells) was included in the assay to account for any background luminescence. This blank value was subtracted from the luminescent readings of the experimental wells to obtain corrected luminescence values corresponding solely to ATP content.

3. **Mitochondrial Stress and Bio-Function Measurements (Seahorse Experiment):**

To assess cellular energy function, including glycolytic and mitochondrial activity, the Agilent Seahorse XF Cell Mito Stress Test was used. A day prior to the assay, 5 × 10^5 cells were seeded into specialized Seahorse XF cell culture microplates in standard culture medium to allow proper attachment and acclimatization. Sensor cartridges used for the assay were hydrated overnight in Seahorse XF Calibrant at 37°C in a non-CO_2 incubator to ensure accurate oxygen consumption and extracellular acidification measurements. On the day of the assay, the normal culture medium was replaced with Seahorse XF Assay DMEM medium, pH 7.4, supplemented with glucose, pyruvate, and glutamine to support cellular metabolism. The microplates were incubated in a CO_2-free incubator for 30 minutes to equilibrate the cells to the assay environment. This medium change was essential for accurate measurements of oxygen consumption rate (OCR) and extracellular acidification rate (ECAR), which represent mitochondrial respiration and glycolysis, respectively.

To evaluate mitochondrial function under stress, cells were exposed to a series of metabolic inhibitors introduced sequentially during the assay:

- Oligomycin (1 µM) was added to inhibit ATP synthase (complex V), reducing mitochondrial ATP production and allowing the measurement of ATP-linked respiration.
- **FCCP (4 µM)**, a mitochondrial oxidative phosphorylation uncoupler, was added to disrupt the proton gradient across the inner mitochondrial membrane, thereby driving maximal oxygen consumption and allowing the measurement of the maximal respiration capacity.

A combination of **Rotenone (500 nM)**, a **complex I inhibitor**, and **Antimycin A (500 nM)**, a **complex III inhibitor**, was used to completely shut down mitochondrial respiration, enabling the determination of non-mitochondrial oxygen consumption. The **oxygen consumption rate (OCR)**, which reflects mitochondrial activity, was measured in real-time using the **Seahorse XF Pro Extracellular Flux Analyzer** (Agilent, Santa Clara, CA). The stepwise addition of inhibitors allowed for the calculation of key mitochondrial parameters, including:

- **Basal respiration**: The starting rate of oxygen consumption before inhibitor treatment, reflecting normal mitochondrial activity.
- **ATP production**: Determined after oligomycin treatment by measuring the drop in OCR.
- **Maximal respiration**: Determined after FCCP treatment, reflecting the maximal capacity of the electron transport chain.
- **Spare respiratory capacity**: Calculated as the difference between basal and maximal respiration, indicating the potential of the cell to respond to increased energy demands.
- **Non-mitochondrial respiration**: Determined after treatment with rotenone and antimycin A, representing oxygen consumption that is not linked to mitochondrial activity.

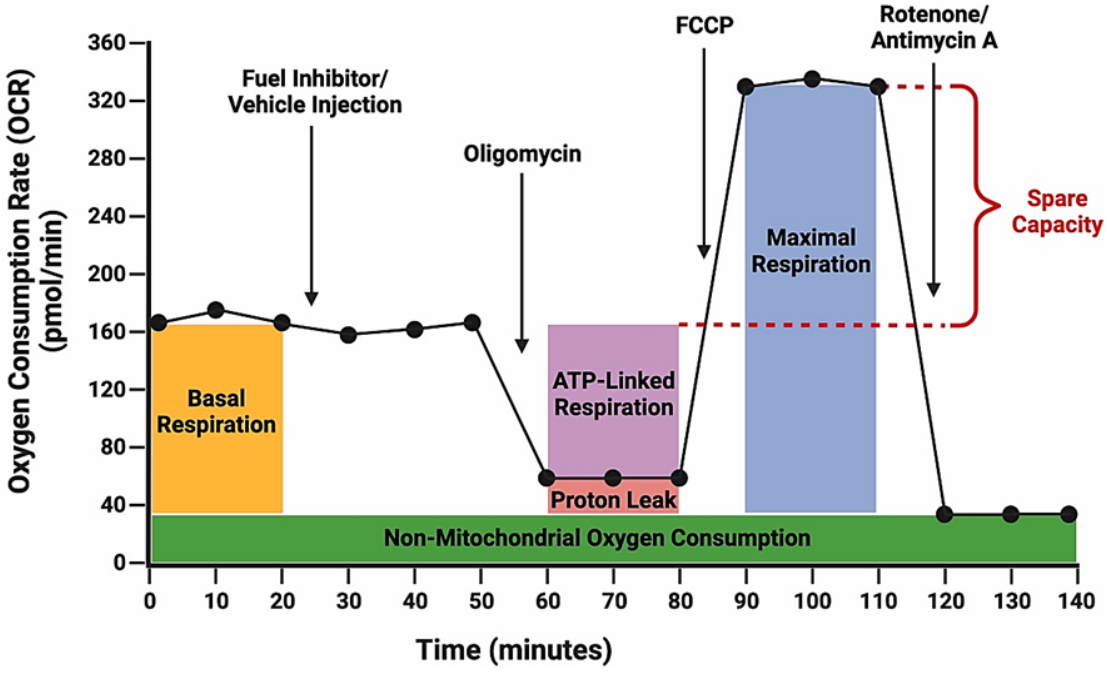

Figure 11. Key components of mitochondrial respiration in the Seahorse XF Cell Mito Stress Test.
Reproduced from https://doi.org/10.1016/j.xpro.2024.102971

VII- Immunofluorescence Staining

Immunofluorescence Staining was carried out to visualize protein localization and co-localization within the cells of interest. Cells were seeded onto 18 mm glass round cover slips coated with 0.1% gelatine derived from porcine skin in 12-well plates. The gelatine coating ensured proper adherence and spreading of cells on the glass surface, facilitating optimal staining conditions. Once the cells reached the desired confluence, they were fixed with 4% paraformaldehyde for 5-10 minutes at room temperature to preserve cell structure and immobilize the proteins in place.

After fixation, the cells were stored in PBS (phosphate-buffered saline) at 4°C until ready for use in further staining procedures. Blocking was performed to prevent non-specific antibody binding, using 1% BSA (bovine serum albumin) solution at room temperature for 30 minutes. This step ensures that the antibodies bind specifically to their target antigens without interference from other cellular proteins.

After blocking, the cells were incubated overnight with the primary antibodies diluted in 1% BSA solution at 4°C. The extended incubation at low temperature allows for optimal binding of the primary antibodies to their specific antigens within the fixed cells. On the following day, the cells were washed thoroughly with PBS to remove any unbound primary antibodies. Another blocking step with 1% BSA solution was conducted for 30 minutes at room temperature to further minimize non-specific interactions. The cells were then incubated with the appropriate fluorophore-conjugated secondary antibodies for 1 hour at room temperature in the dark. Protecting the cells from light during this step was critical to preserve the fluorescence of the secondary antibodies. The fluorophore-conjugated secondary antibodies were chosen based on their compatibility with the primary antibodies and the desired fluorescence channels. After incubation with the secondary antibodies, the cover slips were washed extensively to remove excess secondary antibodies.

The cover slips were then mounted onto glass slides using ProLong™ mounting medium containing NucBlue™ (DAPI) to stain cell nuclei. This mounting medium not only preserves the fluorescence signal but also provides clear visualization of the cell nucleus for structural reference during imaging. Imaging was performed using the ApoTome.2 microscope from Carl Zeiss, a specialized instrument that utilizes structured illumination to produce high-resolution, high-contrast images. The ApoTome.2 system eliminates out-of-focus light, providing sharp and clear images of the stained cellular structures. The resulting fluorescence images were used for

co-localization analysis to determine the spatial relationship between different proteins within the cells. To quantify the degree of co-localization between the proteins of interest, the Pearson's Correlation Coefficient was calculated using Zen Blue 2.6 pro software. This coefficient measures the correlation between the fluorescence signals of two channels, providing an objective assessment of how closely the two proteins co-localize in the cells. A coefficient closer to 1 indicates a high degree of co-localization, while values closer to 0 suggest little to no co-localization.

VIII- Cell Culture treatments

HEK293 cells were treated with various chemical agents to assess their impact on FVIII secretion. Cells were seeded at a density of 0.2 x 10^5 cells per well in 24-well plates in DMEM supplemented with 10% hiFBS and 1% penicillin/streptomycin. Treatments included:

- **Cycloheximide (5 µg/ml)** for 2-4 hours to inhibit protein synthesis.
- **Chloroquine (10 µM)** for 12 hours to increase lysosomal pH.
- **Glucose deprivation** for 12 hours using glucose-free DMEM.
- **Brefeldin A (0.1-0.3 µg/ml)** to disrupt Golgi function.
- **Rab7 inhibitor** for specific durations to block late endosome to lysosome trafficking.

After treatment, media were collected, and FVIII activity was measured using chromogenic assays.

IX- Functional Characterization of FVIII

1. Chromogenic Activity Assay for FVIII:

The chromogenic activity of FVIII in the media was measured using the Chromogenix Coamatic® Factor VIII kit, commonly used in both clinical and research settings to quantify the procoagulant function of FVIII. HEK293 cells expressing FVIII variants were seeded into 6-well plates at a density of 1×10^6 cells and cultured for 24, 48, and 72 hours. This time-course design allowed media samples to be collected at multiple time points to track changes in FVIII activity over time. The media were harvested at each time point and stored at -80°C until analysis. To ensure accuracy, samples were collected in triplicate. Before running the assay, the media samples were diluted in the buffer working solution provided in the kit to bring the FVIII levels within the dynamic

range of the chromogenic assay. The assay reaction involved the use of a chromogenic substrate (S-2765), a synthetic thrombin inhibitor, and a factor reagent containing bovine coagulation factors IXa, X, and thrombin, colyophilized with calcium chloride ($CaCl_2$) and phospholipids. In the presence of functional FVIII, factor IXa activates factor X to Xa, which subsequently hydrolyzes the chromogenic substrate, releasing para-nitroaniline (pNA), a yellow-colored compound. After the reaction components were incubated, the absorbance of the yellow color was measured spectrophotometrically at 405 nm. The intensity of the color is directly proportional to the amount of functional FVIII in the sample, as more FVIII leads to more factor Xa, which in turn increases the hydrolysis of the substrate. Absorbance readings were calibrated using a standard curve generated from known concentrations of FVIII provided by the kit's reference standards. Data were plotted to evaluate FVIII activity at each time point, allowing for the comparison of FVIII variants or different experimental conditions. Results were expressed in international units (IU) of FVIII activity per millilitre, enabling a clear comparison of activity levels over time.

2. FVIII Antigen Quantification:

To complement the chromogenic activity measurements, the VisuLize™ FVIII Antigen kit was used to quantify the total amount of FVIII protein present in the media and cell lysates, regardless of its functional state. This provided insights into both FVIII expression levels and secretion patterns. Cell culture media and lysates were collected for the assay. Lysates were prepared by lysing the cells in a lysis buffer, followed by centrifugation to remove cell debris. The resulting supernatants were then used for analysis. The wells in the assay plates, pre-coated with sheep polyclonal antibody specific to human FVIII (as provided in the kit), were ready to bind FVIII present in both cell lysates and media samples. Diluted samples were added to the wells and incubated for 1 hour at room temperature, allowing FVIII to bind to the antibody-coated plates. After incubation, the wells were washed to remove any unbound components. A second antibody, conjugated to horseradish peroxidase (HRP), was then applied. This peroxidase-labeled detecting antibody binds specifically to the FVIII already captured by the first antibody. The plates were incubated for 45 minutes at room temperature, after which they were washed again to remove unbound detecting antibody. Following the final wash, the HRP substrate tetramethylbenzidine (TMB) was added. The enzyme-substrate reaction produced a blue color, which turned yellow

when the reaction was stopped by adding sulfuric acid. The color intensity, proportional to the amount of FVIII antigen bound in the well, was measured at 450 nm using a microplate reader. To ensure accurate quantification, the assay was calibrated using a series of known FVIII concentrations provided by the kit's calibrator plasma. This allowed for the generation of a standard curve, which was used to calculate FVIII concentrations in the samples. Both positive and negative controls were included to verify the specificity and sensitivity of the assay. Results were expressed as the concentration of FVIII antigen (ng/mL) in both cell lysates and media samples.

X- RNA Sequencing and Data Analysis

RNA was extracted from HEK293 cell pellets using the PureLink™ RNA Mini Kit (Invitrogen, Cat. No. 12183018A) following the manufacturer's instructions. The concentration and purity of the extracted RNA were measured using a NanoDrop One spectrophotometer at 260 nm.

RNA samples from various cell clones were sequenced by the Core Facility for Next Generation Sequencing at the University Hospital Bonn (UKB) using the Illumina Hi-Seq 5000 platform, generating raw reads in FASTQ format. The quality of the sequencing reads was assessed using FastQC, and adapters were trimmed using Cutadapt to remove Illumina universal adapter sequences.

The downstream bioinformatics analysis was performed by Dr. Mohammad Ahmer Jamil.

The miARma-seq pipeline was employed for transcriptomic processing. Sequence alignment was performed using Tophat2 with the Bowtie algorithm, using the human genome (HG38 build from Ensembl) as the reference, along with its corresponding GTF annotation file. Gene-level read counts were generated within the miARma-seq pipeline, and data were subsequently processed using Qlucore Omics Explorer (versions 3.5 and 3.6). To normalize for library size differences, Trimmed Mean of M-values (TMM) normalization was performed using the same GTF file for gene annotation. Genes with fewer than five read counts per sample and those not expressed in both replicates of a sample were excluded. After filtering, 16,976 genes remained for further analysis. Differential expression analysis was conducted in R using the linear model (lm) function to identify significantly differentially expressed genes, enabling insights into the transcriptional differences between the cell clones under investigation. In addition to statistical modeling, Qlucore Omics Explorer was

also utilized for interactive visualization and exploratory transcriptomic analysis, including principal component analysis (PCA), hierarchical clustering, volcano plots, and heatmaps. Normalization, filtering, and dimension reduction were performed within Qlucore using either default or optimized statistical thresholds. This facilitated clear visual discrimination between experimental groups and the identification of biologically meaningful gene expression patterns. Furthermore, pathway and upstream regulator analysis was carried out using Ingenuity Pathway Analysis (IPA, QIAGEN). Pathways were considered significantly enriched when the $-\log_{10}$(p-value) exceeded 1.3, and predicted activation or inhibition was assessed using Z-scores of ≥ ±2.

XI- Statistical Analysis

All statistical analyses were performed using GraphPad Prism v9.0, R v4.1.0, and Qlucore Omics Explorer v3.8. Data are presented as mean ± standard deviation (SD) or standard error of the mean (SEM), as stated. A result was considered statistically significant when the two-tailed P-value was less than 0.05.

For multiple comparisons, the Benjamini-Hochberg false discovery rate (FDR) correction was applied, with significance defined as adjusted P (q-value) < 0.05. Both paired and unpaired two-tailed t-tests were used, depending on the experimental design: paired tests were applied when comparing matched or repeated measurements from the same biological sample, while unpaired tests were used for comparisons between independent groups. P-values are reported explicitly in figures and legends, using the following notation: **ns**, P > 0.05; *, P ≤ 0.05; **, P ≤ 0.01; ***, P ≤ 0.001; ****, P ≤ 0.0001.

Outlier detection was performed using GraphPad Prism's ROUT method (Q = 1%) or built-in outlier detection tools. Outliers were excluded only when supported by clear technical or quality control justification.

For imaging-based quantification, including co-localization analysis, data were collected from multiple fields, with a minimum of 40 cells per condition, to ensure statistical robustness. Co-localization was assessed using Pearson's correlation coefficient. All experiments included at least three independent biological replicates, and statistical tests were selected based on the type, structure, and distribution of the data.

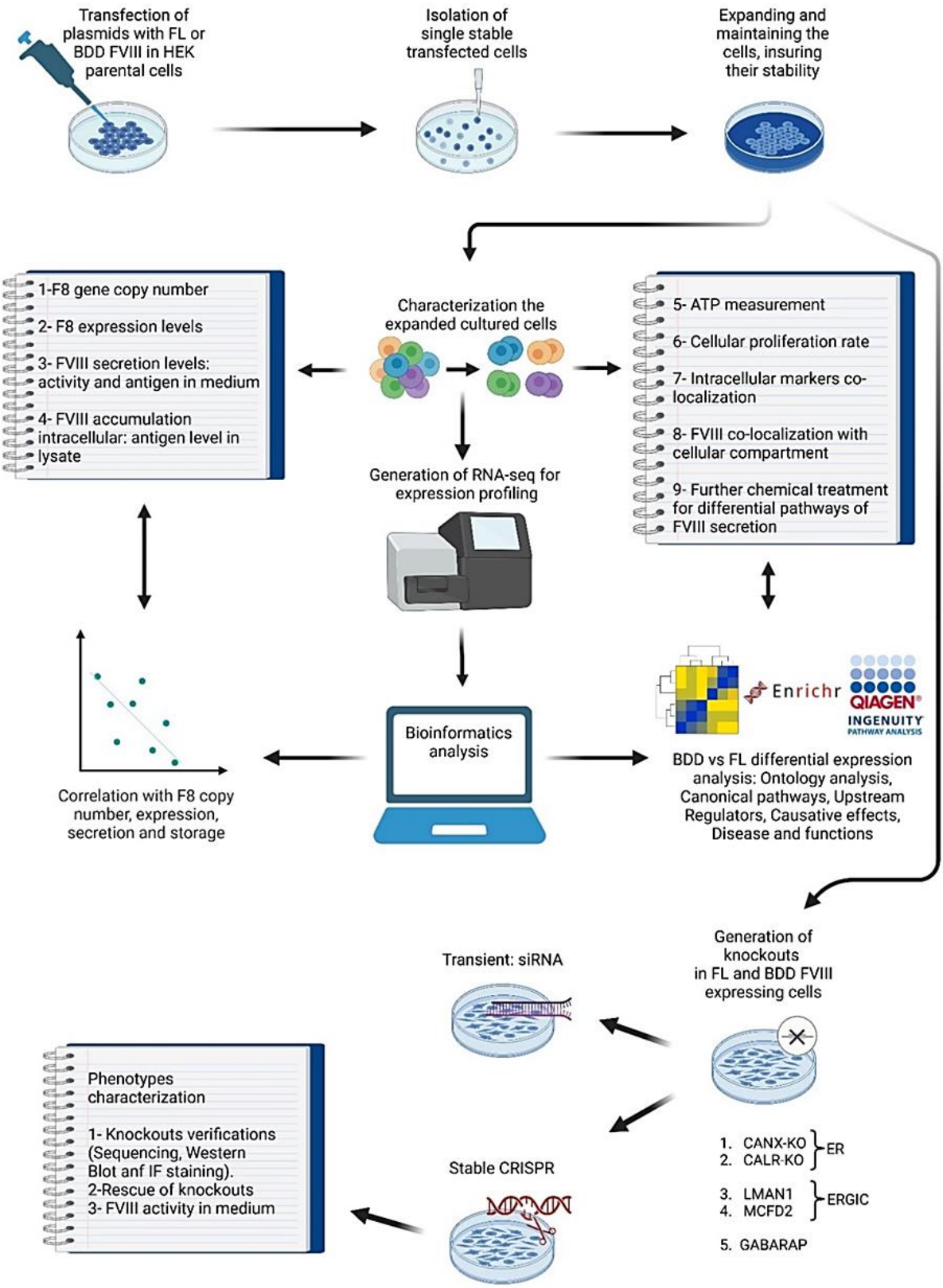

Figure 12. Overview of Experimental Workflow.

Created with BioRender.com

Results

I- Isolation of single cell HEK293 clones secreting FL- or BDD-FVIII reveal higher stability for the former

In order to study the differential intracellular distribution between FL- and BDD-FVIII we isolated single cells stably secreting either FL- or BDD-FVIII. Higher mortality, inconsistency in proliferation rates, slower growth and less stability of FVIII activity was observed for BDD-FVIII secreting cells. The isolated clones were initially characterized for their FVIII secretion ability by measuring relative FVIII activities and antigen in media after 48 hours **(Table 17)**. We note that the isolated clones secreting FL-FVIII exhibited more consistent FVIII activity levels, ranging from 10% to 27%. In contrast, BDD-FVIII clones showed greater variability, with FVIII activity ranging from 2% to 42%. Additionally, antigen levels in the cellular lysate were an order of magnitude higher in the FL-FVIII clones compared to the BDD-FVIII clones.

Table 17. The obtained FVIII Chromogenic activity (%) and FVIII antigen (IU/mL) values from FL- and BDD- clones after 48 hours in culture.

		HEK28	FL4	FL7	FL9	FL10	bdd1	bdd7	bdd12	bdd13	bdd27	oldbdd2
Medium	Activity	26,5	14,84	11,24	10,3	14,52	41,89	2,42	43,14	0	28,18	22,06
	Antigen	1,02	0,659	0,416	0,49	0,588	0,208	0,079	0,275	0,071	0,164	0,125
Lysate	Antigen	2,247	1,805	1,329	1,625	1,788	0,096	0,114	0,196	0,093	0,14	0,113

II- BDD-FVIII show relative higher expression/secretion and lower intracellular accumulation when compared to FL-FVIII

The variance in secretion among BDD- and FL-FVIII secreting clones are primarily attributed to differences in copy number integration and epigenetic status of integration sites. We determined relative *F8* copy number, expression levels, and secretion potentials (as derived from measured activity in the media) **(Figure 13).**

We observed a high positive correlation between copy number and the level of expression for both FL- (Pear R^2=0.90) and BDD-FVIII secreting clones (Pear R^2=0.69) (**Figure 13A)**. Notably, the linear curve slope was higher for BDD-FVIII (Y=7.71X-8.85) in comparison to FL-FVIII (Y=1.0X-0.16), suggesting divergence in expression levels per unit of copy number. This is supported by the difference in expression to copy number ratios between BDD-FVIII and FL-FVIII clones (Av. BDD=0.98; Av. FL=0.88;

p=0.079; **Figure 13A left panel**) which clearly indicate a higher expression per copy number for *BDD-F8* in comparison to *FL-F8.* The latter observation could be due to higher expression of shorter transcript corresponding to BDD-FVIII.

Furthermore, we investigated the correlation between *F8* expression and activity in the culture media. Both BDD-FVIII (Y=10.82X+41.98; R^2=0.91) and FL-FVIII clones (Y=7.72X+14.33; R^2=0.79) exhibited strong positive correlation between expression and activity **(Figure 13B)**. The ratio of activity to expression was more variable for BDD-FVIII clones and in general higher in values **(Figure 13B left panel)**. The latter indicates that per one expression unit more FVIII activity is observed in the media, which implies that both protein translation and production of BDD-FVIII mRNA is relatively higher than the FL-FVIII mRNA.

The correlation between FVIII activity and antigen levels in the medium was strong for both FL-FVIII (R^2 = 0.9604) and BDD-FVIII (R^2 = 0.9037) clones, indicating that both constructs produce consistent and reliable results **(Figure 13C)**. Although the correlation coefficient for BDD-FVIII is slightly lower than for FL-FVIII, the positive correlation remains robust. This suggests that the antigen levels in the medium are a reliable indicator of FVIII activity for both constructs. The difference in correlation strength may be due to the differential ability of the antibody used in the antigen detection assay to recognize FL-FVIII and BDD-FVIII differently. Despite this minor variation, the results for BDD-FVIII are still highly reliable and demonstrate that the antigen assay provides accurate insights into FVIII activity in the medium. This highlights the suitability of both constructs for comparative studies and confirms that antigen measurements can be confidently used to estimate FVIII activity, even with the observed differences in recognition efficiency.

Lastly, a linear positive correlation was observed between FVIII antigen levels in the lysates and FVIII antigen levels in the media for FL-FVIII clones (Y=1.37X+0.89; R^2=0.93) and to a good extent for BDD-FVIII clones (Y=0.35X+0.07; R^2=0.53**) (Figure 13D)**. However, FL-FVIII possesses a higher intracellular presence (ratio of lysate antigen/medium antigen **(Figure 13D left)** compared to BDD-FVIII, implying that FL-FVIII may have a greater capacity for intracellular accumulation and “storage”. Differences in ratios of lysate-antigen / medium-antigen for FL-FVIII clones (Av. =2.95) and BDD-FVIII clones (Av. =0.95) was highly significant (p=2.29E-05) **(Figure 13D left).** This finding also suggests that BDD-FVIII is more steadily secreted upon

expression, with the majority of intracellularly produced BDD-FVIII being released from the cell, while FL-FVIII shows comparatively a lower or less secretion compared to the total amount of the protein produced intracellularly. These results shed the light on the distinct expression and secretion characteristics of FL-FVIII and BDD-FVIII clones, highlighting the potential advantages and limitations for the use or production of each variant.

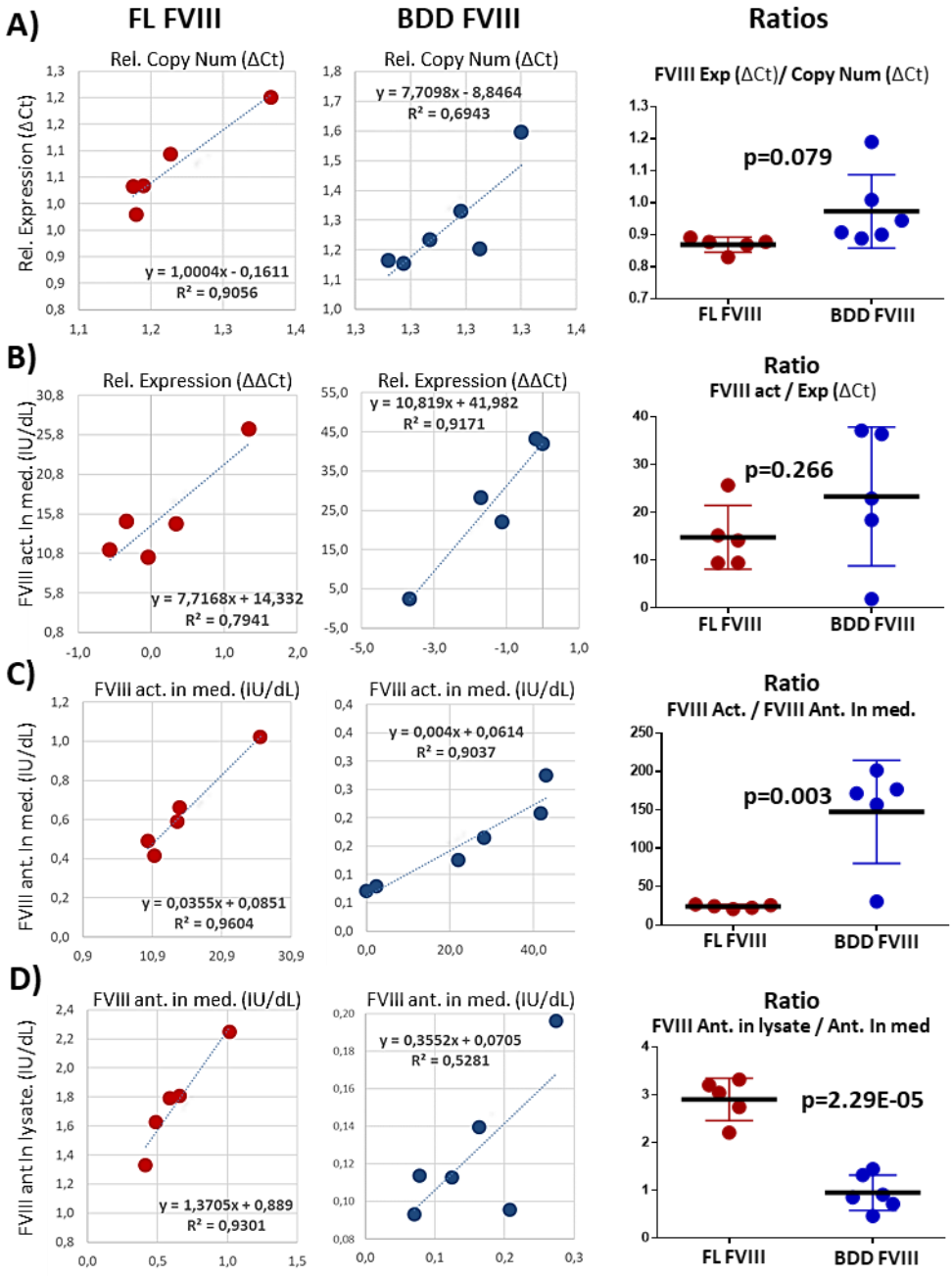

Figure 13. Copy Number, Expression, and Secretion (Antigen and Activity) of FL-FVIII and BDD-FVIII Secreting Clones.

A- The correlation between relative *F8* copy number and expression levels indicates that expression is directly proportional to copy number. However, the steeper slope for BDD-FVIII suggests higher relative expression per unit of copy number compared to FL-FVIII. **B-** The correlation between relative expression and activity in the medium demonstrates a stronger correlation for BDD-FVIII than FL-FVIII, indicating that BDD-FVIII clones exhibit higher relative expression and secretion. **C-** The correlation between activity and antigen levels in the medium reveals a slightly better positive correlation for FL-FVIII clones. This may be due to differential recognition of FL-FVIII and BDD-FVIII by the antibody used in the antigen assay. **D-** The correlation between antigen levels in the medium and in lysates is linear and strong for both FL-FVIII and BDD-FVIII clones. However, the ratio of intracellular FVIII to extracellular FVIII is approximately three times higher for FL-FVIII compared to BDD-FVIII, suggesting FL-FVIII has a greater intracellular "storage" capacity. The linear equation and Pearson correlation coefficient (R^2) are shown for each correlation, alongside the ratios of the parameters and the p-values from t-tests in the right column.

III- FL- and BDD-FVIII show differences in intracellular distribution

The lower intracellular presence of BDD-FVIII when compared to FL-FVIII **(Figure 13D)** clearly suggests that we expect differences in their intracellular distribution. To elucidate this, we measured co-localization between FVIII (FL and BDD) and 20 intracellular markers **(Figure 14).** This included markers in endoplasmic reticulum (CNX and PDI), ER to Golgi intermediate compartment (LMAN1, MCFD2, COPI and COPII), Golgi (GM130, TGN46, Furin), Ras-assosiated binding proteins (RABs) involved in endocytic trafficking (RAB8a, RAB11, RAB5 and RAB7), Lysosome (LAMP1 and ARL8B), and autophagosome markers (VAMP8, LC3B, RAB26, GABARAP and GABARAPL1). We observed a quantitative difference in co-localization with 16 out of 20 intra cellular markers where the co-localization Pearson correlation coefficient (PCC) is significantly higher for FL-FVIII. While at LC3B and RAB26 we observed higher PCC for BDD-FVIII albeit the PCC values are low for both FL- and BDD-FVIII. However, at PDI and Furin we have equal PCC; this is largely due to the two markers being spread over large compartments in the cell (ER, Golgi, and post Golgi), having low compartment specificity. Therefore, these co-localization data show clear higher presence of FL-FVIII in the cells when compared to BDD-FVIII **(Figure 14)** and this goes in line with the higher total intra-cellular content **(Figure 13D)**. We excluded two confounding factors that could interfere with the results. First, the use of only one clone each corresponding to a FL- or a BDD-FVIII that could be associated with different level of expression and specific secretion level of FVIII. Therefore, we repeated the co-localization analysis of FVIII with three markers

(MCFD2, LAMPI and Rab7) in all five BDD- and all five FL-FVIII clones. bWe didn't observe significant inter-group (within FL- or BDD-FVIII clones) difference between the clones **(Figure 15)** while the observed above differences between BDD- and FL-FVIII was retained.

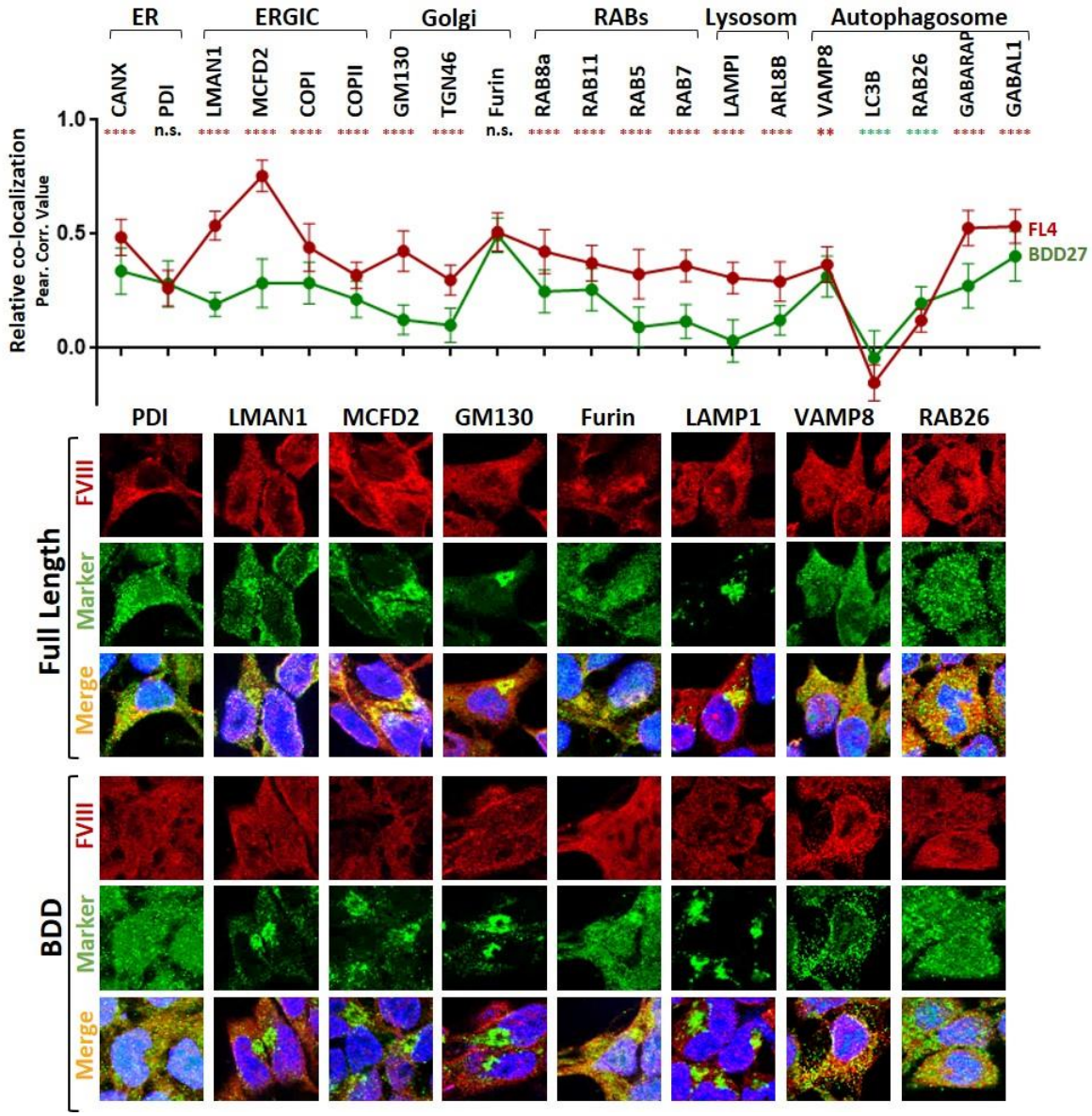

Figure 14. Co-localization of FL- and BDD-FVIII with selected intracellular markers.
Upper panel: Dot plot representing average Pearson Correlation values of either FL-FVIII (FL4) (filled red circles connected with red lines) or BDD-FVIII (BDD27) (filled green circles connected with green lines) with individual cellular markers. P values of t-test statistical significance is depicted as stars below the markers name (ns: p>0.05; *: p≤0.05; **: p≤0.01; ***: p≤0.001; ****: p≤0.0001). **Lower panel:** Sample Co-localization immunofluorescence microscopy pictures for selected markers for both FL- and BDD-FVIII (Red, green and orange correspond to anti FVIII, anti- intracellular marker and merged signals respectively).

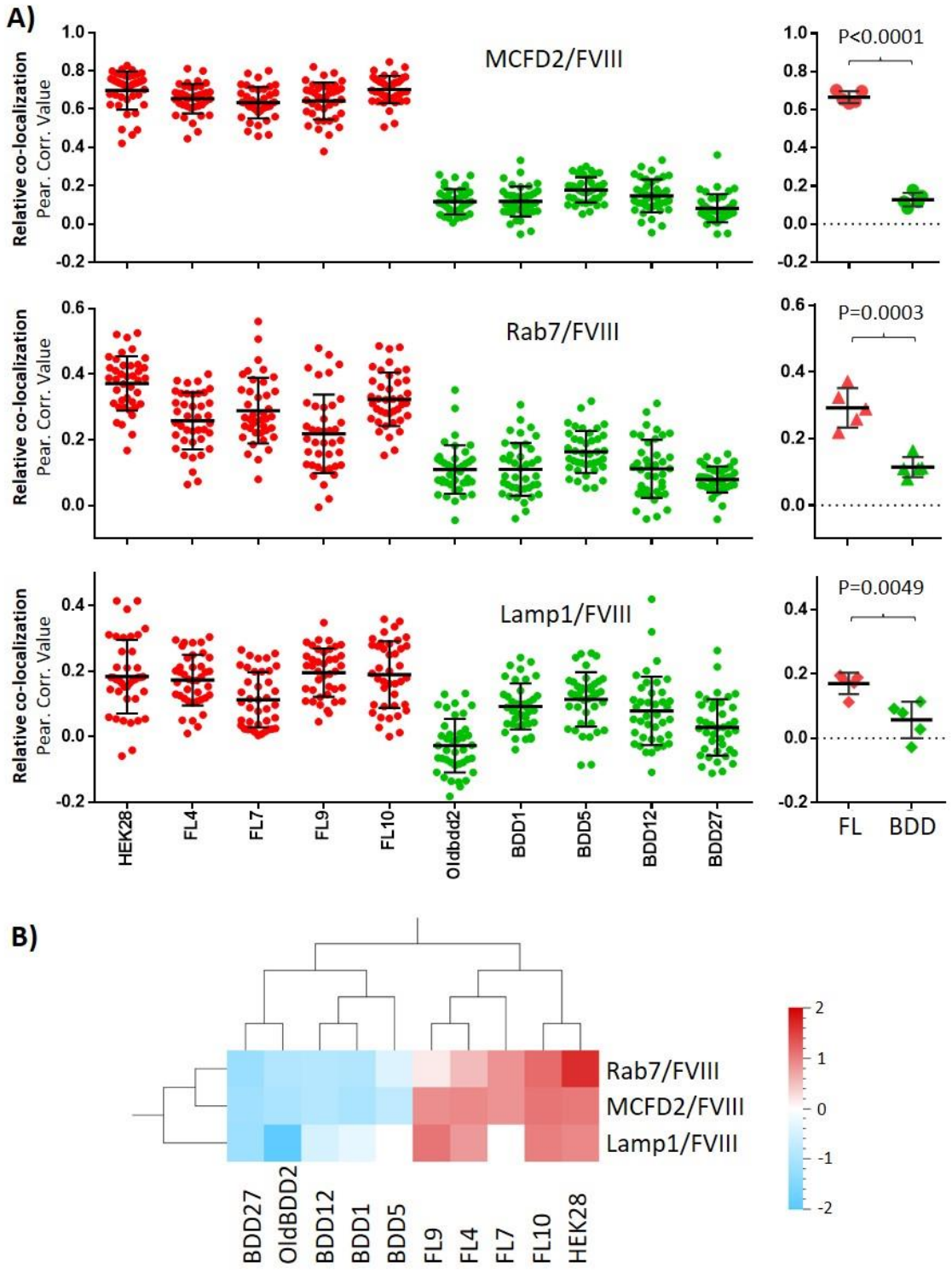

Figure 15. Co-localization analysis of FVIII (detected with Polyclonal antibody) with MCFD2, RAB7 and LAMP1 in 5 clones each from FL- and BDD-FVIII secreting cells.

A- Dot plots showing individual co-localization values for each pair of antibodies; right panel shows dot plot of average co-localization of each clone, t-test p values above each plot show the significance when comparing the two groups of FL- and BDD-FVIII clones. **B-** Heat map of hierarchical clustering of all clones and the three pairs of co-localization values shows complete separation of the two groups of FL- and BDD-FVIII. Second, bias in detecting FL- and BDD-FVIII with the polyclonal anti-FVIII antibody. In

order to exclude this, we transfected HEK293 parental cells (that do not express FVIII) with Alfa-tagged-FL-FVIII or Alfa-tagged-BDD-FVIII. This allows the detection of both variants using the same antibody without bias related to specificity of antibody.

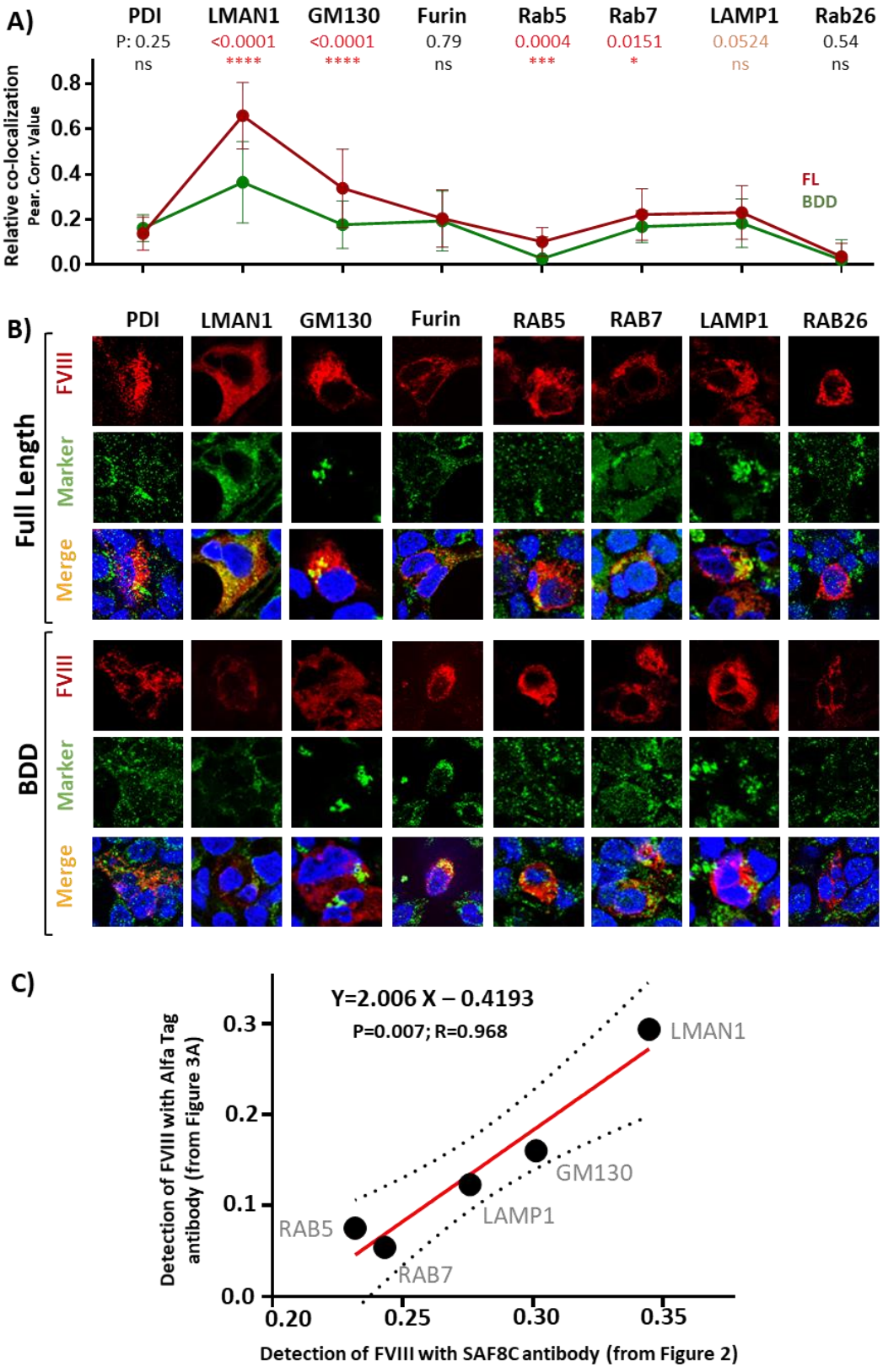

Figure 16. Co-localization of Alfa tagged FL-FVIII and Alfa tagged BDD-FVIII with 8 selected intracellular markers.

A- Dot plot representing average Pearson co-localizations values of either Alfa-FL-FVIII (filled red circles connected with red lines) or Alfa-BDD-FVIII (filled green circles connected with green lines) with individual cellular markers. Degree of t-test statistical significance is shown and depicted as values and stars above the figure (ns: p>0.05; *: p≤0.05; **: p≤0.01; ***: p≤0.001; ****: p≤0.0001). **B-** Samples Co-localization microscopy pictures for used intracellular markers for both FL- and BDD-FVIII (Red, green and orange correspond to anti-Alfa, anti-intracellular marker and merged signals respectively). **C-** Correlation between difference of co-localization between FL-FVIII and BDD-FVIII with a given intracellular marker using two FVIII antibodies SAF8C polyclonal antibody (on X axis) or anti-Alfa tag antibody (on Y axis) for FVIII detection (markers that show less than 0.01 differences are excluded).

Using this approach, we assessed co-localization for both alfa-tagged-BDD-FVIII and Alfa-tagged-FL-FVIII with each of PDI, LMAN1, GM130, Furin, RAB5, RAB7, LAMP1 and RAB26 intracellular markers **(Figure 16)**. We observed the same tendency of expected lower co-localizations of BDD-FVIII to LMAN1, GM130, RAB5, RAB7 and LAMP1, and the expected similar co-localization levels for PDI, Furin and RAB26 **(Figure 16A and B)**. Next, we calculated the differences in PCC between FL-FVIII and BDD-FVIII with the above markers for both antibody detection. We observed excellent correlation between both sets of data derived from both antibodies' detection (Pear. Corr. R=0.968, p=0.007) **(Figure 16C)**. This analysis excludes a bias due to a specific antibody detection.

IV- Perturbation of intracellular organelles and cytoplasmic vesicles differentially affects the secretion levels of FL- and BDD-FVIII

To explore the distinct intracellular trafficking, as we expect, for FL- and BDD-FVIII, we treated cells with various drugs and chemicals targeting specific cellular biofunction and compartments: Glucose starvation, Brefeldin A (BFA), Chloroquine, and Rab7 inhibitor were used to affect cellular metabolism, Golgi morphology/function, autophagy, and the endosomal system, respectively **(Figure 17A)**. We speculated that if both FL- and BDD-FVIII follow the same intracellular route(s), there should be no difference in their response to these cellular treatments. Glucose starvation led to a similar decrease in FVIII activity in both FL- and BDD-FVIII secreting cells, upon treatment FVIII activity decreased to about 50% in media for both FL- and BDD-FVIII compared to untreated cells (p=0.5691). BFA treatment, which disrupts Golgi-related trafficking, reduced FVIII activity similarly in both variants, with FVIII activity, in media, decreasing to about 80% in media of FL- and BDD-FVIII secreting cells, compared to untreated cells (p=0.0590). The above indicates a shared impact of Glucose starvation

and BFA treatment on synthesis and intracellular flow and secretion for both variants **(Figure 17B)**.

A)

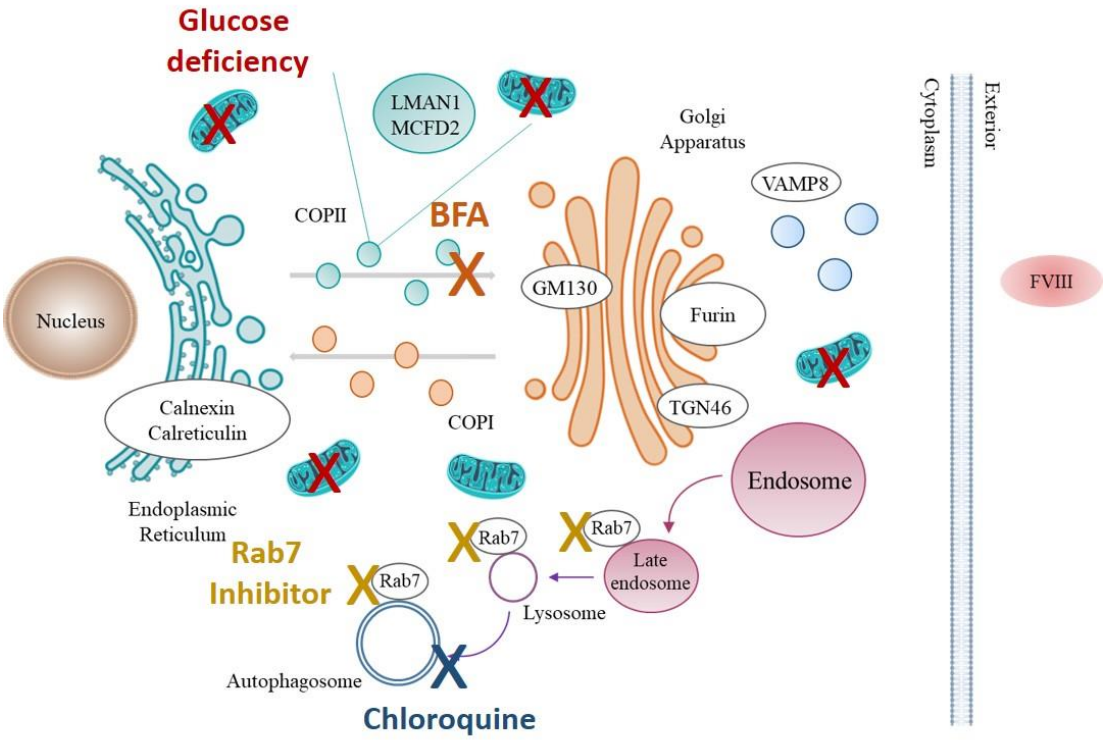

B)

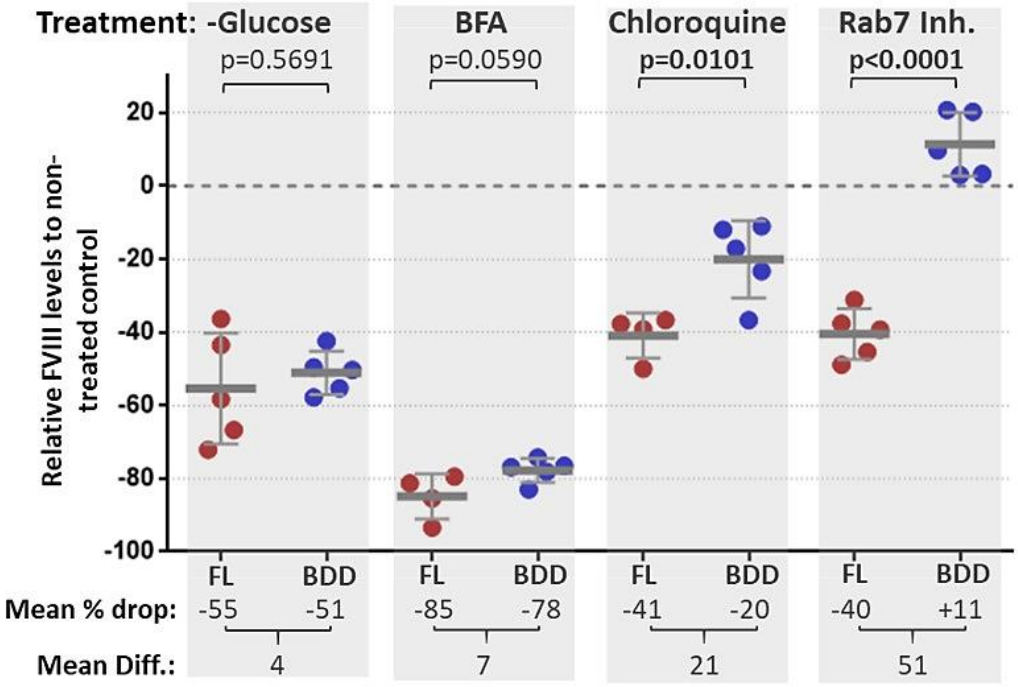

Figure 17. Effect of various chemical treatments on FL- and BDD-FVIII secretion.

A- Schematic representation of intracellular trafficking and the targeted sites of action for each treatment. *Created with BioRender.com*. **B-** Each dot represents the relative percentage FVIII activity compared to untreated cells, with the y-axis indicating the percentage change of FVIII activity in media and the x-axis representing the different chemical treatments. Red dots correspond to FL-FVIII clones, while blue dots represent BDD-FVIII. Mean % drop is shown below the graph as well as the mean difference between FL- and BDD-FVIII clones for a given treatment. T-test p value for significant difference between FL- and BDD-FVIII are shown at the top.

This was clearly accompanied by significant disturbance in FVIII co-localization to intracellular markers (COPII, GM130, TGN46, RAB7, LAMP1 and RAB8a) for both FL- and BDD-FVIII, albeit no clear pattern immerged **(Figure 18A)**.

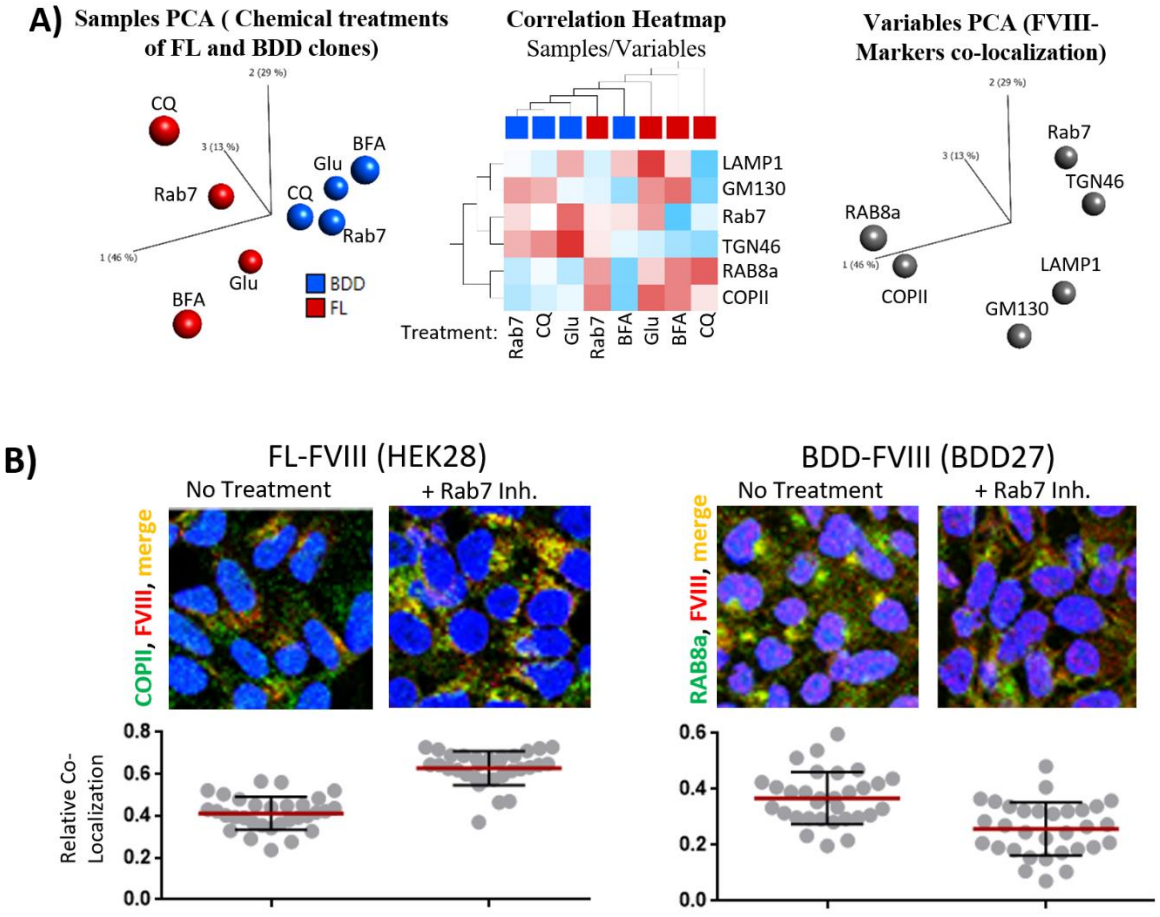

Figure 18. Effect of various chemical treatments on FL- and BDD-FVIII co-localization with intra-cellular markers.
A- Dot blot showing the values of Pearson coefficient correlation of co-localization of FVIII with one of six intracellular markers (COPII, GM130, TGN46, RAB7, LAMP1 and RAB8a). P-values corresponding to t-test of co-localization of FVIII before and after treatment with given marker are shown above each comparison. (Chloroquine, Rab7 Inh: Rab7 Inhibitor, Gluc. Starv : Glucose starvation, BFA: Brefeldin treatment) (red: FL clone HEK28 after treatment, blue: BDD clone BDD27 after treatment, Black: Before treatment). **B-** Sample fluorescence immunostaining before and after treatment with

Rab7-Inhibitor of the co-localization of COPII, GM130 and RAB8a with FL-FVIII (left side) and BDD-FVIII (right side) (Green=marker, Red=FVIII, Yellow=merge).

On the other hand, Chloroquine treatment resulted in a more substantial and significant decrease in FVIII activity in FL-FVIII (-48%) secreting cells compared to BDD-FVIII (-20%) secreting cells ($p=0.01$), suggesting differential sensitivity to autophagy inhibition. Similarly, Rab7 inhibition led to a marked reduction in FVIII activity in the media for FL-FVIII-secreting cells, with activity decreasing by approximately 40% compared to untreated cells (similar to Chloroquine treatment). In contrast, a slight increase of 11% in FVIII activity was observed in BDD-FVIII-secreting cells. The difference between FL- and BDD-FVIII was statistically significant ($p<0.0001$) **(Figure 17)**. This was again here clearly accompanied by significant disturbance in FVIII co-localization to intracellular markers; however this was much seen for FL-FVIII clones in comparison to FL-FVIII clones **(Figure 18A)**. Particularly, the Rab7-Inhibitor treatment did not decrease FVIII secretion for BDD-FL clones and largely didn't change FVIII co-localization except at RAB8a marker. This is clearly seen by the Immuno-fluorescent staining at COPII, GM130 and RAB8a markers, where the first two are different after treatment for FL-FVIII but not for BDD-FVIII; the reverse is observed at the RAB8a **(Figure 18)**.

V- FL- vs. BDD-FVIII synthesis/secretion appear to induce differential co-localization of intra-cellular markers

The previous data showed us, first, significant differences in intracellular co-localization between FL- and BDD-FVIII and, second, a clear differential effect on secretion between FL- and BDD-FVIII after chemical disturbance of specific cellular compartments.

Therefore, we hypothesized that the synthesis and secretion of the two forms of FVIII (FL and BDD-FVIII) could follow not only common intracellular paths but also significantly induces differential "pressure" on specific routes and cytoplasmic vesicles. This, in turn, should manifest in differential interactions and co-localizations of proteins involved in vesicle formation and in the endosomal system.

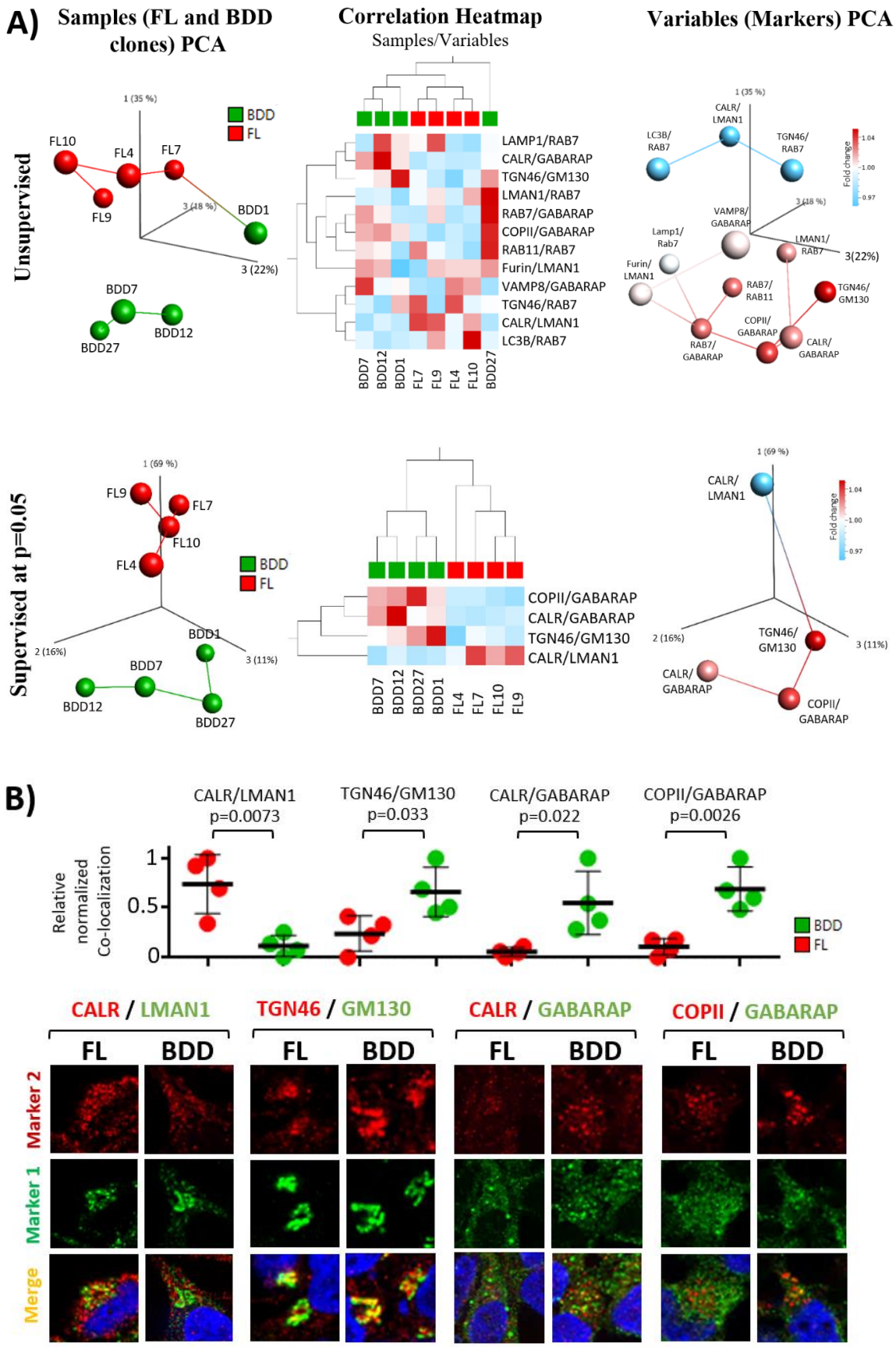

Figure 19. Pairwise intracellular markers co-localization.

A- Data on twelve pair of intra-cellular marker co-localization in BDD- and FL-FVIII secreting clones are shown as sample PCA plot (left panel), as correlation heat map of samples vs. variables and variables PCA plot (right panel). Upper part and lower part depict unsupervised and supervised data at $p<0.05$ (showing four significant differences in co-localization between FL- and BDD-FVIII secreting clones for 4 markers pairs) respectively. **B-** Dot plot showing individual cell clone data of significantly different ($p<0.05$) pairs markers co-localization between FL- and BDD-FVIII clones (data are normalized from 0 to 1 corresponding from lower to higher co-localization respectively). Lower part shows corresponding represented immunofluorescent staining of the significantly different co-localized markers between FL- and BDD-FVIII secreting clones.

To investigate this, we utilized immunofluorescence staining of intercellular markers (CALR, LMAN1, COPII, TGN46, GM130, Furin, RAB7, RAB11, VAMP8, LC3B, LAMP1 and GABARAP) to study pairwise co-localizations (LAMP1/RAB7, CALR/GABARAP, TGN46/GM130, LMAN1/RAB7, RAB7/GABARAP, COPII/GABARAP, RAB11/RAB7, Furin/LMAN1, VAMP8/GABARAP, TGN46/RAB7, CALR/LMAN1, LC3B/RAB7) and their relationship to the synthesis and secretion of FL-FVIII and BDD-FVIII. The results clearly separated the samples based on the pairwise co-localization data **(Figure 19)**. Most of pair-marker co-localization levels showed clear differences in the co-localization levels between FL- and BDD-FVIII secreting clones. At $p<0.05$, four of the pairs' co-localizations where significantly different between the two groups of clones **(Figure 19A lower panel and 19B)**. Specifically, CALR/LMAN1 pair had higher co-localization in FL-FVIII, while CALR/GABARAP, COPII/GABARAP, and GM130/TGN46 had higher co-localization in BDD-FVIII secreting clones.

VI- Impact of B-Domain Deletion on Proliferation of FVIII-Expressing Cells

To investigate and delve deeper on differential effect of BDD- and FL-FVIII expression/synthesis on the host cells, we studied the effects of B-Domain deletion on cell proliferation. Our thorough investigation revealed a significant finding: proliferation was downregulated in BDD-FVIII-expressing cells compared to their FL counterparts. Through a proliferation assay, we observed a significant disparity in proliferation rates, with BDD-FVIII-expressing cells showing significantly slower growth kinetics in contrast to FL-FVIII-expressing cells. Specifically, our analysis quantified the difference in proliferation rate between FL-HEK cells and BDD-HEK cells after approximately 72 hours and revealed a notable discrepancy with a difference of relative proliferation rate of 0.167 **(Figure 20B)**.

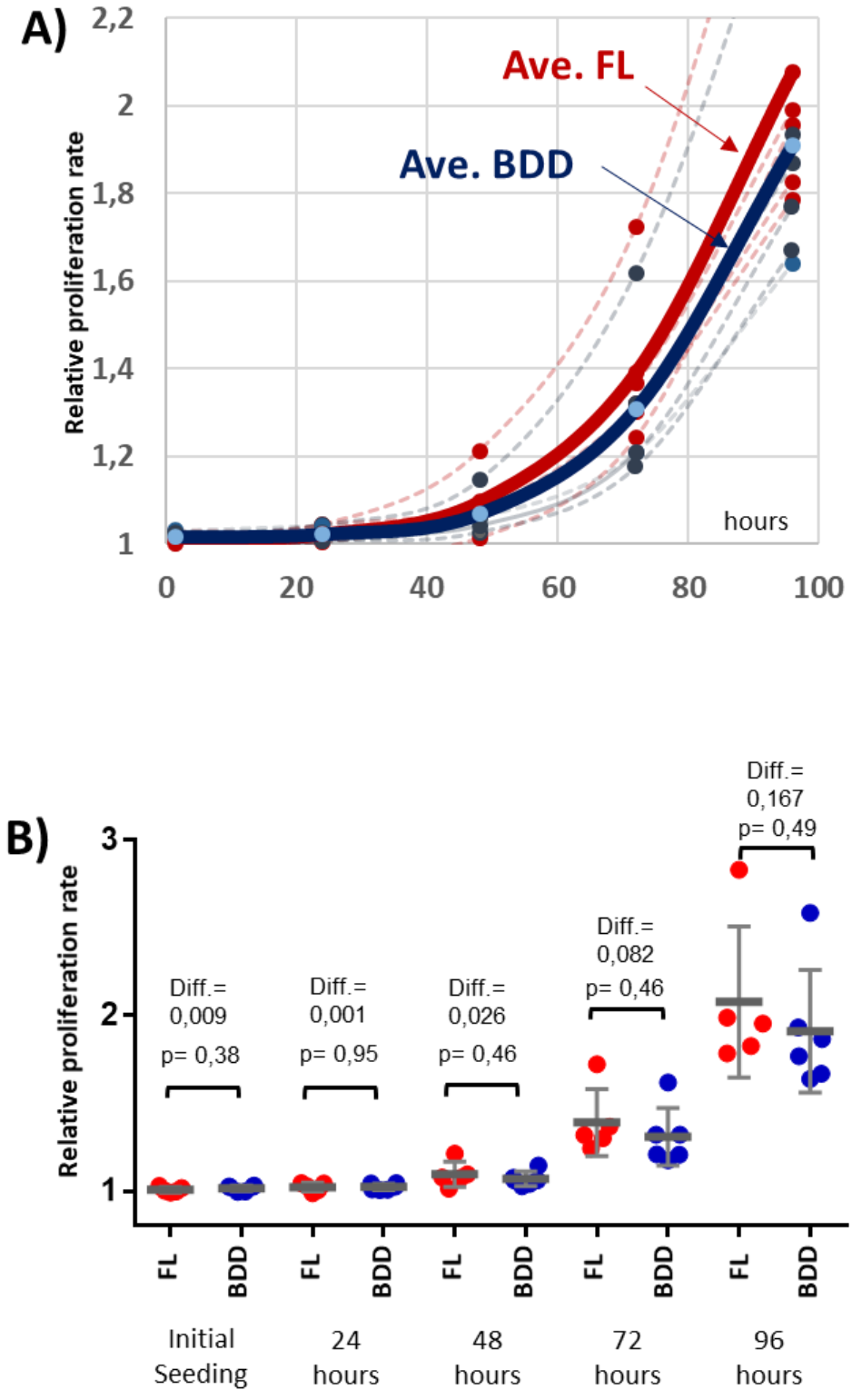

Figure 20. Single cells clone proliferation assay using the Agilent's xCELLigence assay.

A- Predicted individual proliferation curves for all clones. Thin dotted curves represent individual cell lines and thick plan curves represent the average. Red is for FL and Blue for BDD. **B-** Dot plot of proliferation intervals for the used clones, the statistical p value at specific time point is shown 24 hours intervals.

Moreover, our findings align with the differential expression markers identified by Laucard-Paulet et al., who reported 157 genes associated with cell proliferation. Impressively, 154 of these genes were detected in our dataset, reinforcing the robustness of our gene expression analysis.

Principal Component Analysis (PCA) of these 154 genes **(Figure 21A)** demonstrates a clear segregation between BDD-FVIII and FL-FVIII samples, indicating distinct transcriptomic profiles related to proliferative activity. BDD samples cluster separately from FL samples along the primary components, suggesting divergent regulation of proliferation-associated genes between the two conditions.

The hierarchical clustering heatmap **(Figure 21B)** further supports this separation, with the majority of FL-FVIII samples showing upregulated expression (red) in genes related to proliferation, while BDD-FVIII samples are dominated by downregulation (blue) of the same genes. Notably, the clustering accurately groups biological replicates within each condition and highlights statistically significant differential expression with q-values < 0.05, reinforcing the biological reproducibility and statistical robustness of our findings.

The volcano plot **(Figure 21C)** visually illustrates the magnitude and significance of differential expression across the 157 genes. Of the 122 genes more highly expressed in FL-FVIII samples, 69 reached statistical significance ($p < 0.05$), and are marked in green. Conversely, only 4 of the 32 genes upregulated in BDD-FVIII samples were significant ($p < 0.05$), highlighted in red. Genes such as CCNB1, CDC20, DDX20, PANBP1, and CSE1L were among the most upregulated in FL-FVIII, further emphasizing enhanced proliferative potential in these cells. These trends underscore a prominent shift towards a proliferative transcriptional landscape in FL-FVIII samples, consistent with previous literature and our own phenotypic observations.

Figure 21D presents Ingenuity Pathway Analysis (IPA) of the same gene set, identifying the top canonical pathways enriched in our dataset. The most significantly affected pathways include cell cycle checkpoints, synthesis of DNA, mitotic roles of polo-like kinases, and chromosomal replication control, and all critical drivers of cell proliferation. These pathways are enriched in FL-FVIII samples, as reflected by high -log (p-value) and strong z-scores predicting pathway activation. Conversely, a few pathways such as mitotic G1/S transition and sumoylation pathway appear

downregulated or inhibited in BDD-FVIII, suggesting suppressed cell cycling. The visualization also ranks pathways by significance and ratio, helping to prioritize those most affected in the dataset.

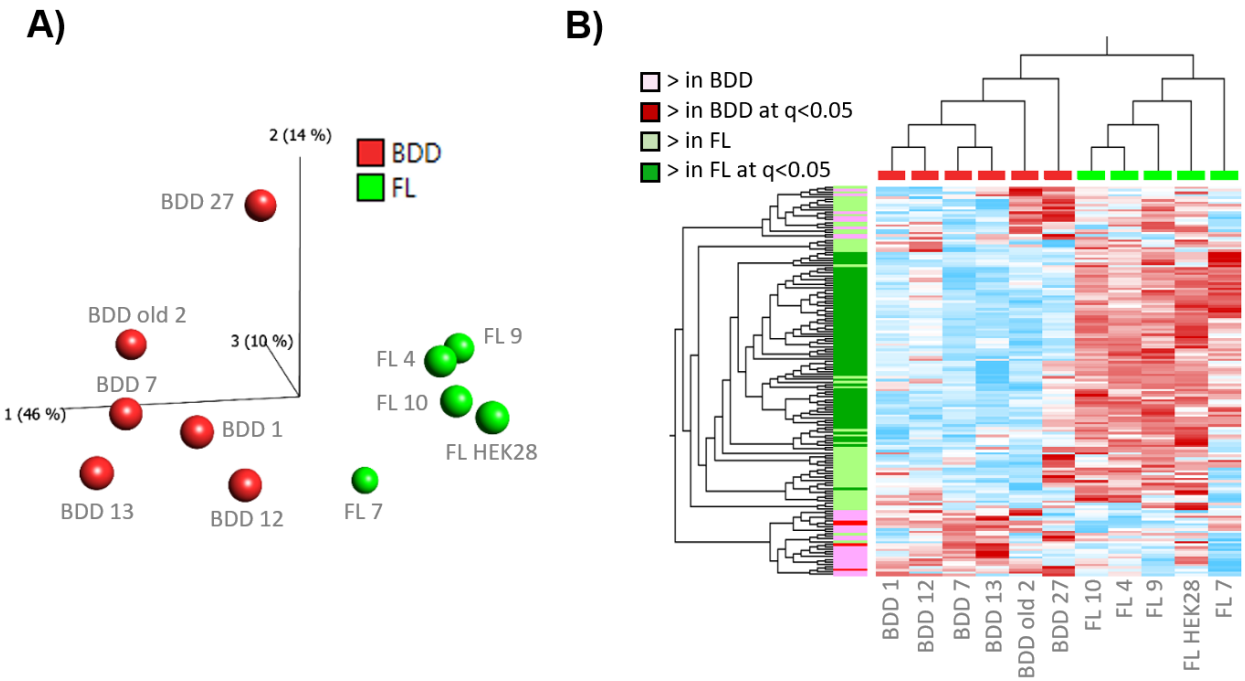

C)

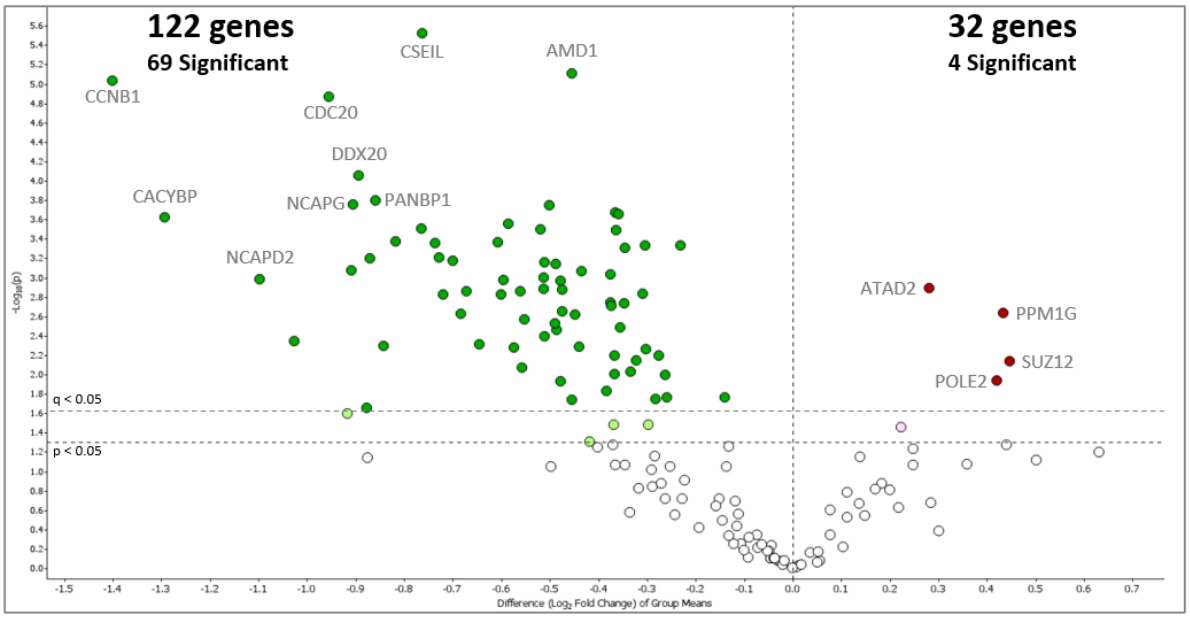

D)

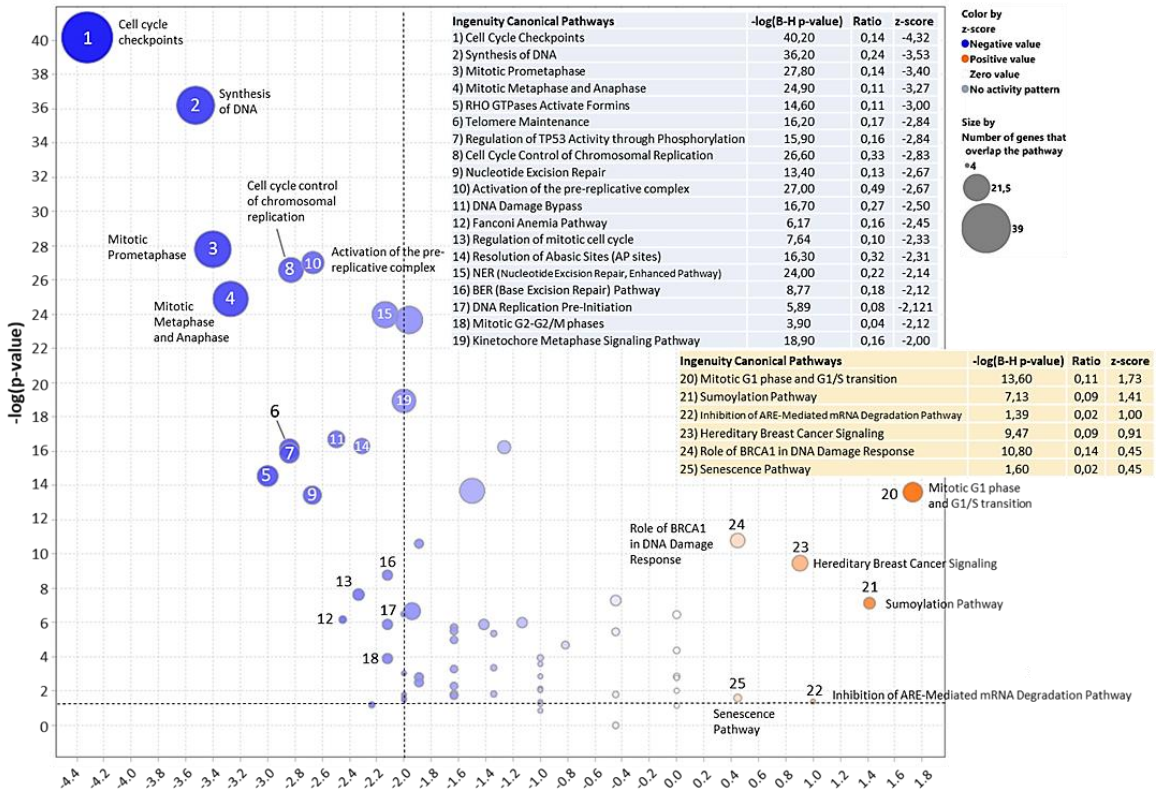

Figure 21. Unsupervised clustering and pathway analysis of 157 proliferation-related genes in BDD- and FL-FVIII secreting clones.

A- Principal Component Analysis (PCA) plot showing clustering of samples based on expression of 154 proliferation-related genes. Green spheres represent FL-FVIII samples; red spheres represent BDD-FVIII samples. **B-** Heatmap illustrating the normalized expression levels of the proliferation-related genes across BDD-FVIII and FL-FVIII clones. Red indicates higher expression; blue indicates lower expression. **C-** Volcano plot displaying log2 fold-change versus –log10 p-values for the differentially expressed proliferation-related genes between BDD-FVIII and FL-FVIII samples. Green dots represent genes upregulated in FL-FVIII; red dots represent genes upregulated in BDD-FVIII. **D-** Ingenuity Pathway Analysis (IPA) of the expressed proliferation-related genes, showing significantly enriched canonical pathways. Dot size corresponds to the number of genes in the pathway; color reflects predicted activation or inhibition.

VII- Residual cellular ATP and calculated Consumption in FVIII Synthesis: Comparing BDD and FL Variants

We investigated the cellular energy dynamics associated with the BDD- and FL-FVIII cells expressing variants. Inspired by the work of Gutierrez, Jahir M. et al., who recognized the critical role of energy in factor VIII synthesis, we calculated the required

ATP associated with FVIII production[128]. Notably, our calculations based only on FVIII size (no post translation modification is added) yielded an expected observation: BDD-FVIII production requires about 37% less ATP compared to FL-FVIII, suggesting potential energy-saving benefits brought by the BDD variant **(Figure 22)**.

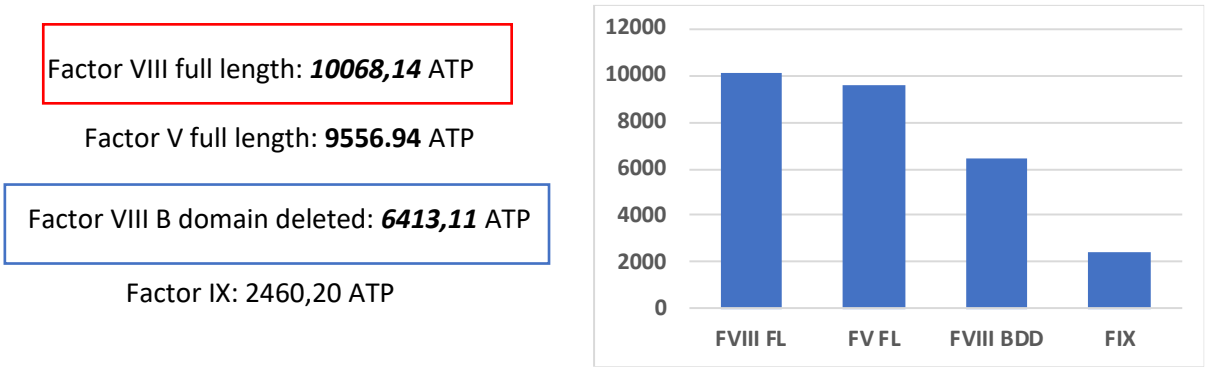

Figure 22. Estimated ATP Cost for the Secretion of FVIII FL, FV FL, FVIII BDD, and FIX.
Bar chart illustrating the calculated ATP cost for synthesizing and secreting full-length FVIII (FVIII FL), full-length FV (FV FL), B-domain-deleted FVIII (FVIII BDD), and Factor IX (FIX). The calculations were performed using the "Estimation of protein secretion cost" method as described in Gutierrez, Jahir M., et al.

The above prompted us to examine the residual levels of ATP in our cells. Notably, our investigation revealed that BDD-expressing cells had higher residual ATP levels (Av. = 0.87μM) compared to FL counterparts (Av. = 0.78 μM) **(Figure 23A)**, suggesting lower ATP consumption during FVIII synthesis with the BDD variant. This observation not only highlights the energy-efficient nature of BDD-FVIII production but also suggests possible differences in cellular energy dynamics between the two expressed/translated variants.

Furthermore, we sought to elucidate the relationship between FVIII secretion and ATP levels. Our analysis revealed a positive correlation between FVIII secretion and ATP levels in both FL (Pear R^2 = 0.6922) and BDD-FVIII-expressing cells (Pear R^2 = 0.4528), indicating the crucial role of ATP in supporting the secretion process for both variants. However, the dependence of FL-FVIII on ATP levels was significantly more pronounced, highlighting the higher energy requirement for efficient FVIII secretion **(Figure 23B)**.

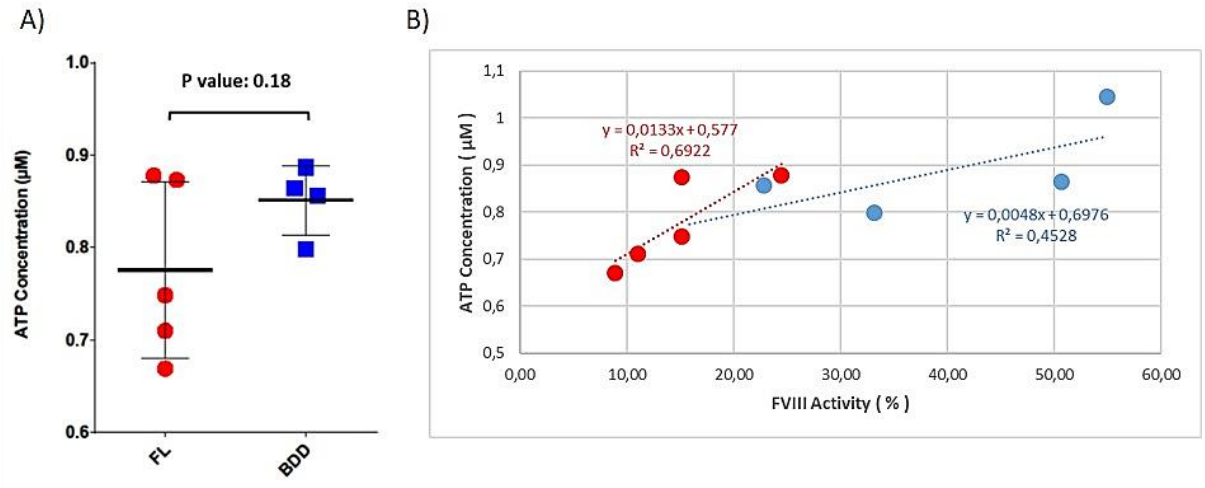

Figure 23. Measurement of residual cellular ATP levels.
BDD-FVIII showed a higher residual ATP level compared to FL-FVIII. **A-** Dot blot showing individual ATP value for different cell clone. **B-** Correlation between ATP levels and FVIII activity. One BDD sample was excluded as an outlier based on GraphPad Prism's ROUT method (Q = 1%).

VIII- Mitochondrial Respiration of BDD- and FL- FVIII Expressing Cells

The Seahorse XF Mito Stress Test was used to assess mitochondrial respiration in FL-FVIII and BDD-FVIII expressing cells, providing insights into the metabolic differences associated with FVIII processing and secretion. **Figure 24A** illustrates the experimental approach, where oxygen consumption rate (OCR) was measured in response to sequential metabolic inhibitors to evaluate key mitochondrial parameters. Basal respiration was measured before any treatment, followed by oligomycin injection to inhibit ATP synthase and reveal ATP-linked respiration. The addition of FCCP (Carbonyl cyanide-4-(trifluoromethoxy)phenylhydrazone), a mitochondrial uncoupler that collapses the proton gradient across the inner mitochondrial membrane, allowed for the measurement of maximal respiration. Rotenone and antimycin A were then used to inhibit mitochondrial complexes I and III, reducing OCR to non-mitochondrial levels. The spare respiratory capacity was determined by calculating the difference between maximal and basal respiration. This approach enables the evaluation of mitochondrial energy production, stress, and adaptability in FL-FVIII (red) and BDD-FVIII (blue) expressing cells.

The mitochondrial respiration profile over time (**Figure 24B)** reveals that FL-FVIII cells exhibit consistently higher OCR than BDD-FVIII cells. Baseline OCR levels were approximately 180 pmol/min in FL-FVIII and 150 pmol/min in BDD-FVIII, indicating that

FL-FVIII cells have higher mitochondrial energy consumption under normal conditions, possibly due to the more complex processing demands of full-length FVIII. Following oligomycin injection, OCR dropped to around 50 pmol/min in both groups, but FL-FVIII cells showed greater ATP-linked respiration (~100 pmol/min) compared to BDD-FVIII (~70 pmol/min). This suggests that FL-FVIII cells rely more on oxidative phosphorylation for ATP production, likely due to their higher intracellular burden for FVIII synthesis and trafficking. After FCCP injection, which uncouples oxidative phosphorylation and forces maximal electron transport chain activity, OCR increased to ~220 pmol/min in FL-FVIII and ~180 pmol/min in BDD-FVIII, demonstrating that FL-FVIII cells possess a greater spare respiratory capacity (~100 pmol/min) compared to BDD-FVIII (~70 pmol/min). The final injection of rotenone and antimycin A reduced OCR to ~50 pmol/min in both groups, confirming that non-mitochondrial respiration was similar in both conditions. These results indicate that FL-FVIII cells have higher overall mitochondrial respiration, suggesting that FVIII synthesis, folding, and trafficking impose a greater metabolic demand on cells expressing full-length FVIII compared to those expressing BDD-FVIII.

The quantification of basal respiration and spare respiratory capacity **(Figure 24C)** further supports these observations. Basal respiration was approximately 120 pmol/min in FL-FVIII and 90 pmol/min in BDD-FVIII, indicating that cells expressing FL-FVIII require more mitochondrial ATP production to support FVIII processing and secretion. The spare respiratory capacity, which reflects the ability of mitochondria to increase energy production in response to stress, was higher in FL-FVIII cells (~40 pmol/min) than in BDD-FVIII (~30 pmol/min). This suggests that FL-FVIII cells have a higher capacity to respond to increased energy demands, possibly to accommodate periods of increased FVIII synthesis and secretion.

Figure 24D highlights the differences in proton leak and ATP production between the two cell types. Proton leak, which reflects mitochondrial inefficiency or stress, was higher in FL-FVIII (~30 pmol/min) compared to BDD-FVIII (~10 pmol/min). This suggests that FL-FVIII cells experience greater mitochondrial uncoupling, which could be related to increased protein folding demands in the endoplasmic reticulum (ER), leading to higher oxidative stress and mitochondrial compensation mechanisms. The ATP-linked respiration was also higher in FL-FVIII (~100 pmol/min) than in BDD-FVIII (~70 pmol/min), confirming that FL-FVIII expression requires greater ATP generation through oxidative phosphorylation. The increased ATP demand in FL-FVIII cells aligns

with the greater complexity of processing the full-length FVIII protein, which includes the B-domain that undergoes extensive post-translational modifications and trafficking. In contrast, BDD-FVIII cells demonstrate a more energy-efficient mitochondrial profile, likely because they bypass many of the processing steps associated with the B-domain, reducing the burden on cellular energy systems.

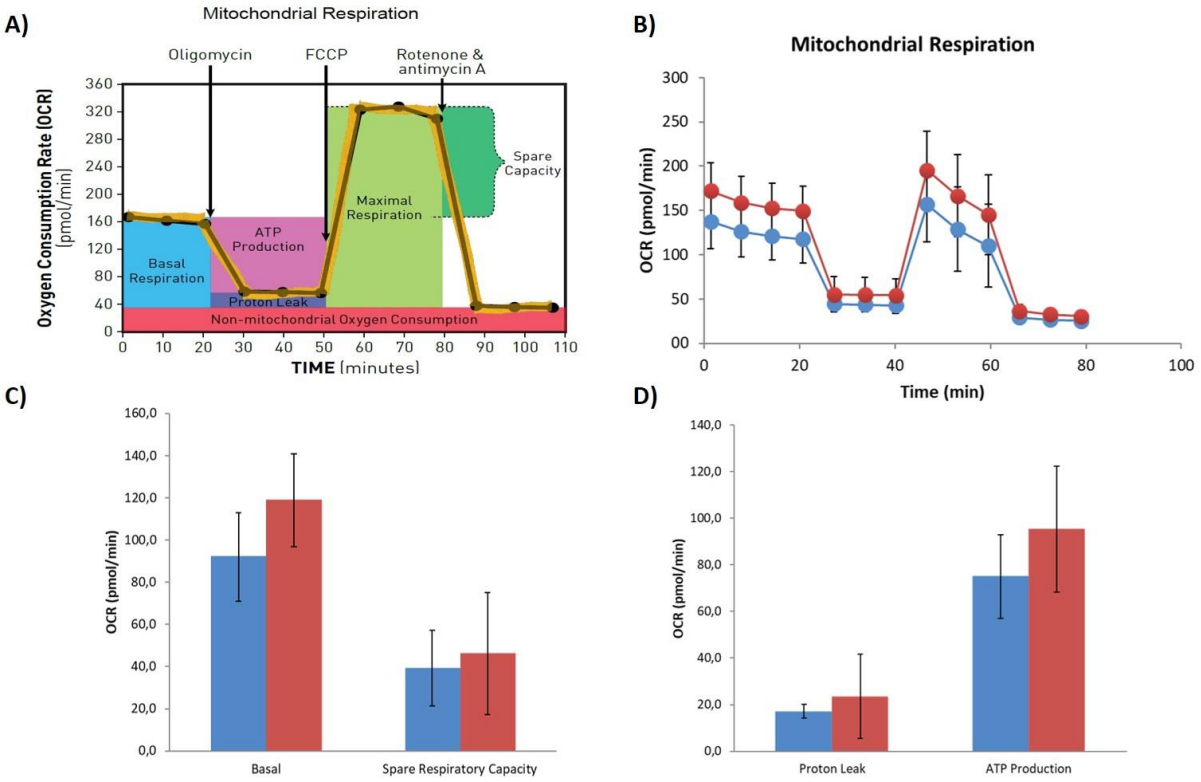

Figure 24. Mitochondrial Respiration, ATP Production, and Spare Respiratory Capacity in BDD-FVIII and FL-FVIII Expressing Cells.
A- Seahorse XF Mito Stress Test Profile: Schematic representation of mitochondrial respiration, illustrating the sequential injections of oligomycin (ATP synthase inhibitor), FCCP (uncoupler for maximal respiration), and rotenone/antimycin A (complex I and III inhibitors) to assess key mitochondrial parameters. **B-** OCR Profile Over Time: Line graph displaying oxygen consumption rate (OCR) in BDD-FVIII and FL-FVIII expressing cells throughout the Seahorse assay. **C-** Basal Respiration and Spare Respiratory Capacity: Bar graph quantifying basal respiration and spare respiratory capacity, with spare capacity calculated as the difference between maximal and basal respiration. **D-** Proton Leak and ATP Production: Bar graph summarizing proton leak and ATP-linked respiration, where ATP production was derived from the OCR decrease after oligomycin injection. Error bars represent standard deviation, with red indicating FL-FVIII and blue representing BDD-FVIII.

To further explore the relationship between mitochondrial activity and overall cellular energy status, we analyzed the correlation between ATP production (as measured by the Seahorse XF assay) and total intracellular ATP levels. Interestingly, distinct patterns emerged between the two FVIII-expressing cell lines **(Figure 25)**.

Both FL-FVIII and BDD-FVIII cells demonstrate a positive correlation between Seahorse-derived ATP production and retained cellular ATP levels (R^2 = 0.51), suggesting that increased mitochondrial activity corresponds with greater energy availability.

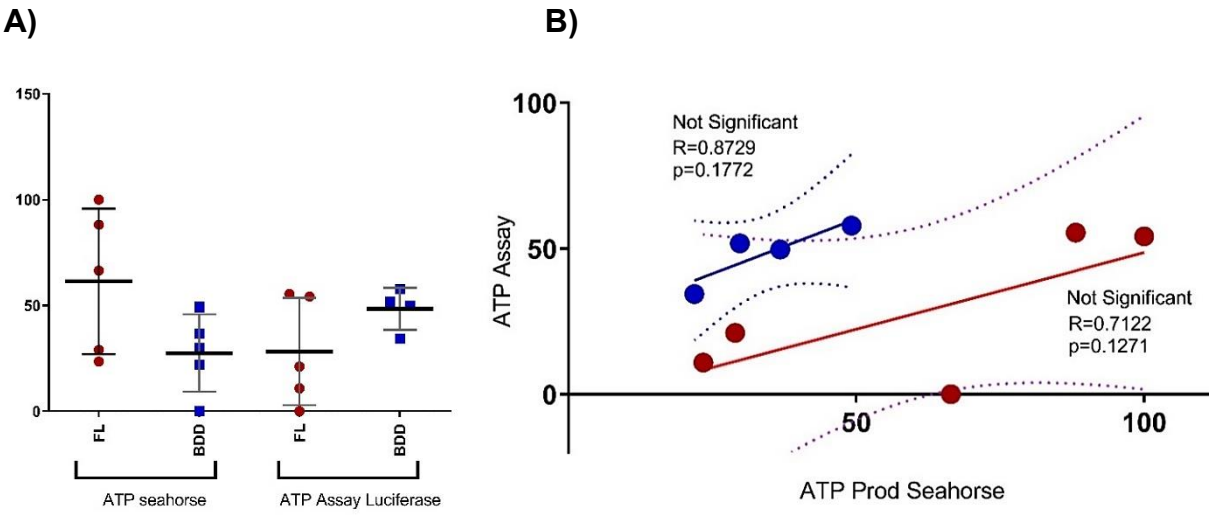

Figure 25. Comparison and correlation of ATP levels in FL-FVIII and BDD-FVIII expressing HEK293 clones.
A- Bar graph showing normalized ATP production measured by Seahorse XF Analyzer and normalized total ATP content measured by a luciferase-based endpoint ATP assay. Values were normalized to account for differing units across the two assays to enable direct comparison. Each dot represents an individual clone; red indicates FL-FVIII clones and blue indicates BDD-FVIII clones. **B-** Scatter plot showing the correlation between raw ATP production (Seahorse XF Analyzer, x-axis; pmol/min) and total ATP concentration (ATP assay, y-axis; µM). Each point represents a clone. Linear regression lines are shown for FL-FVIII (red) and BDD-FVIII (blue) groups, along with Pearson correlation coefficients (R) and p-values. One BDD sample was excluded as an outlier based on GraphPad Prism's ROUT method (Q = 1%).

IX- Transcriptomic Profiling Reveals Distinct Gene Expression Signatures between Full-Length and B-domain-deleted Factor VIII Expressing Clones

The observed disparities in intracellular trafficking between FL-FVIII and BDD-FVIII highlight distinct intracellular distributions and interactions with cellular markers. FL-FVIII exhibits significantly higher co-localization with 16 out of 20 intracellular markers, reflecting its greater intracellular presence, while BDD-FVIII shows slightly elevated co-localization with LC3B and RAB26. Furthermore, differential responses to chemical perturbations indicate that FL-FVIII is more sensitive to autophagy inhibition (Chloroquine) and Rab7 inhibition, whereas BDD-FVIII appears to be less affected. These findings suggest that FL-FVIII and BDD-FVIII not only follow distinct intracellular

pathways but also exert different influences on cellular trafficking and secretion dynamics. However, the precise molecular mechanisms driving these distinctions remain unclear.

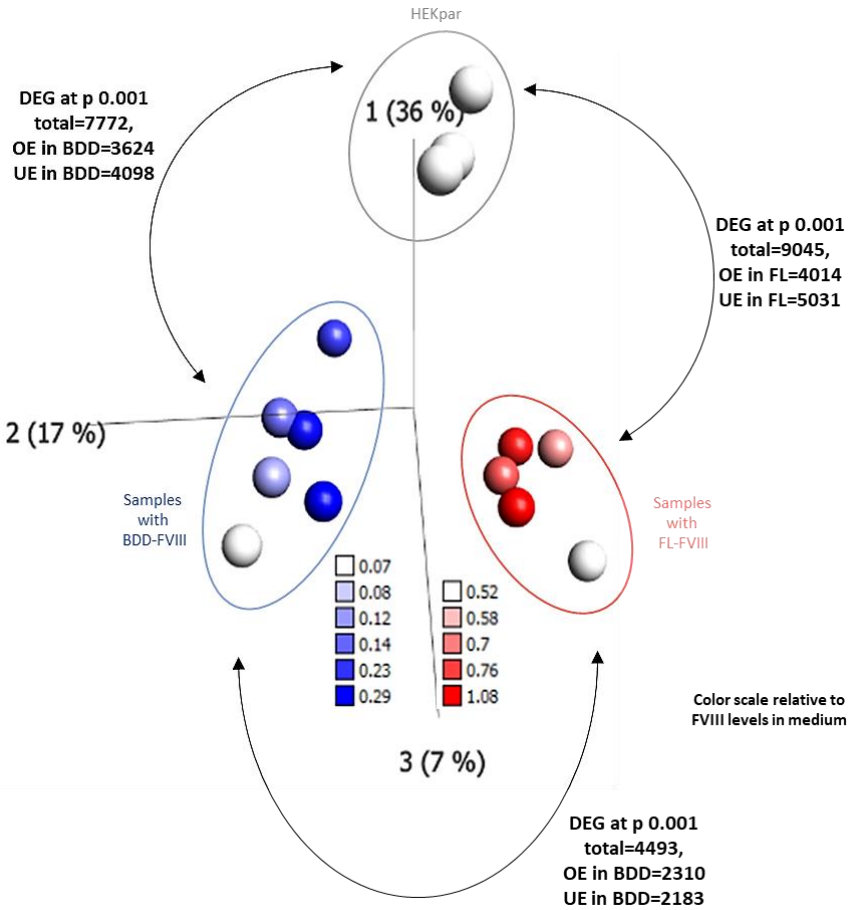

Figure 26. Gene Expression Profiles in HEK Cells Expressing Full-Length and B-Domain Deleted Factor VIII.
3D-PCA Plot: illustrating differentially expressed genes between HEK293 (white dots), HEK cells stably expressing Full-Length FVIII (FL-FVIII, red dots), and B-domain-deleted FVIII (BDD-FVIII, blue dots) at a significance level of p = 0.001. The scale of red and blue color indicates the level of FVIII secretion in each clone, with lighter shades representing lower secretion levels and darker shades indicating higher secretion levels.

To delve deeper into understanding the molecular basis of these differences and to verify the existence of underlying reasons reflected on the expression profiling, we turned to RNA profiling through 3'RNAseq analysis. This approach aims to elucidate the transcriptional landscape and identify potential regulatory elements or signaling pathways that contribute to the observed differential behavior of FL- and BDD-FVIII variants. Our RNA sequencing data revealed significant differences in gene expression between FL- and BDD- FVIII expressing clones. Utilizing various visualization

techniques such as Heatmaps, Volcano plots, and PCA (Principal Component Analysis), we observed clear distinctions in the transcriptional profiles of HEK cells expressing BDD-FVIII and FL-FVIII. The PCA plot (at $p<0.001$) displayed distinct clustering, with HEK293 cells expressing BDD-FVIII and FL-FVIII positioned apart, indicating substantial differences in gene expression patterns among these groups. Further comparison of Differentially Expressed Genes (DEGs) between HEK293 cells expressing FL-FVIII and those expressing BDD-FVIII revealed 4493 DEGs at a significance level of $p < 0.001$. Of these, 2310 genes were over expressed in BDD cells, while 2183 were under expressed **(see Figure 26)**. These comparisons shed light on the unique transcriptional signatures induced by each FVIII variant, providing valuable insights into the molecular mechanisms underlying the differences between FL- and BDD-FVIII expressing clones.

- **IPA pathway analysis predicted differences, among others, related to energy Pathways, cytoplasmic organization and proliferation**

Integrative Pathway Analysis (QIAGEN Ingenuity Pathway Analysis IPA) was used to explore the canonical pathways, upstream regulators, and causal networks underlying the differential gene expression observed between Full-Length (FL) and B-domain-deleted (BDD) Factor VIII (FVIII) expressing HEK clones. The graphical summary of the enriched signaling pathways and upstream regulators provides a comprehensive overview of the differentially expressed genes (DEGs) between FL-FVIII and BDD-FVIII expressing and secreting clones. Pathways and upstream regulators highlighted in red indicate upregulation in BDD- compared to FL-FVIII expressing clones, while those in blue indicate downregulation. A key finding was the upregulation of the Sirtuin signaling pathway in BDD-FVIII clones, suggesting shifts in cellular metabolism and stress response **(Figure 27)**. Tumor proliferation and senescence are opposing processes; when senescence is upregulated, it suppresses tumor proliferation. In BDD-FVIII clones, markers associated with tumor proliferation were downregulated, while cellular senescence was upregulated, suggesting a potential shift in cell cycle regulation and DNA damage response pathways. This differential regulation indicates that BDD-FVIII expression may favor a more senescent cellular state, leading to a suppression of uncontrolled cell growth. The observed reduction in proliferation markers, coupled with the activation of key senescence regulators, highlights a distinct cellular adaptation in BDD-FVIII clones compared to FL-FVIII. Overall, the graphical summary provides valuable insights into the differential regulation of signaling

pathways and upstream regulators associated with FL and BDD-FVIII expression, shedding light on the underlying molecular mechanisms driving their distinct cellular phenotypes.

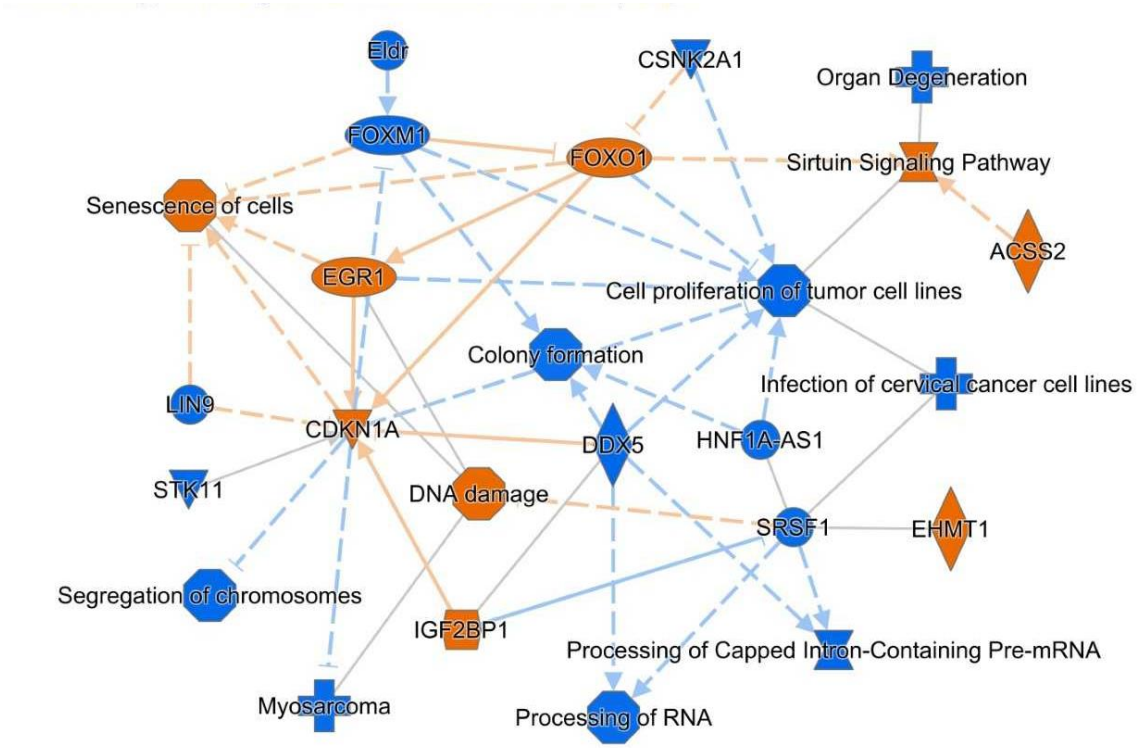

Figure 27. Gene Expression Profiles in HEK Cells Expressing Full-Length and B-Domain Deleted Factor VIII.
Graphical Summary of Enriched Pathways/Upstream Regulators: The graphical summary represents enriched pathways/upstream regulators representing Differentially Expressed Genes (DEGs) between FL-FVIII and BDD-FVIII expressing HEK clones. Pathways/upstream regulators highlighted in red are upregulated in BDD-FVIII compared to FL-FVIII, while those highlighted in blue indicate downregulated pathways/upstream regulators in BDD-FVIII compared to FL-FVIII.

In our investigation, we delved into the canonical pathways to discern potential differences between FL- and BDD- FVIII expression in HEK cells. The bubble chart **(Figure 28)** represents pathway enrichment analysis in FL-FVIII and BDD-FVIII expressing cells, highlighting key biological pathways affected by differential gene expression between the two groups. The x-axis likely represents pathway enrichment significance, while the y-axis corresponds to the Z-score, indicating the predicted activation or inhibition of each pathway. The size of the bubbles represents the number of genes overlapping with each pathway, while the color reflects the Z-score, with orange and red indicating activated pathways and blue representing inhibited pathways. Several pathways appear activated, including Sirtuin signaling, which is the

most significantly enriched pathway with 98 out of 293 genes involved, suggesting a strong modulation of cellular metabolism and protein regulation. Other pathways such as Androgen signaling, Granzyme A signaling, and the G2/M DNA damage checkpoint regulation pathway are also enriched, pointing to potential differences in cell cycle regulation, hormonal signaling, and proteostasis. The ERK/MAPK signaling pathway, which plays a key role in cell growth, differentiation, and intracellular signaling, is also upregulated. In contrast, pathways such as Oxidative Phosphorylation, Nucleotide Excision Repair, tRNA Charging, and Assembly of RNA Polymerase II Complex are inhibited. Oxidative phosphorylation shows the strongest downregulation, with 59 out of 111 genes involved, suggesting a shift in cellular energy metabolism. The inhibition of nucleotide excision repair suggests potential changes in DNA maintenance mechanisms, while downregulation of tRNA charging and RNA polymerase II complex assembly indicates modulation of translational and transcriptional activities.

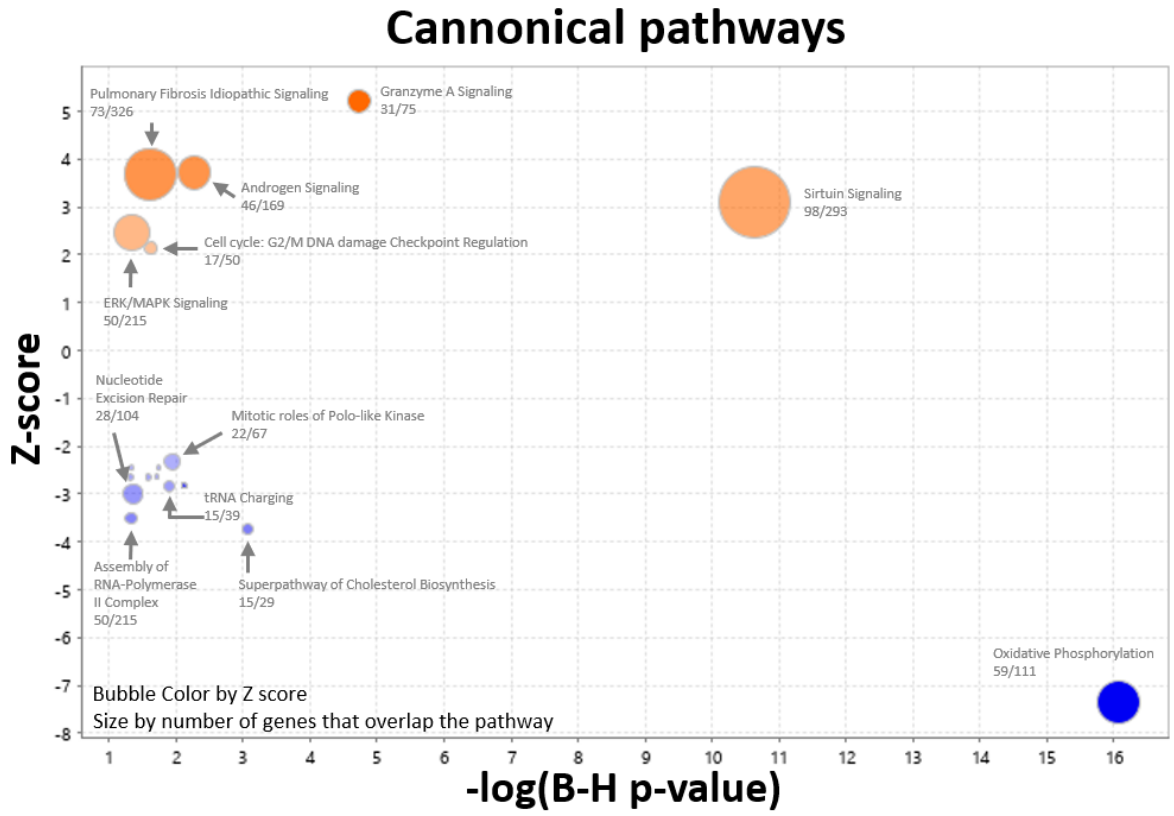

Figure 28. Bubble chart illustrates canonical pathways affected by the comparison between Full-Length (FL) FVIII HEK cells and B-Domain Deleted (BDD) FVIII HEK cells.
Red bubbles represent pathways that are upregulated in BDD-FVIII compared to FL-FVIII, while blue bubbles represent pathways that are downregulated in BDD-FVIII compared to FL-FVIII, based on the z-score. The size of each bubble corresponds to

the number of genes that overlap with the pathway, indicating the relative significance of gene enrichment within each pathway.

These results provide insight into the metabolic and cellular functional differences between FL-FVIII and BDD-FVIII cells. The upregulation of pathways related to cellular signaling and protein regulation in FL-FVIII cells suggests that they may have a higher demand for intracellular processing, likely due to the more complex folding and trafficking requirements of full-length FVIII. The downregulation of oxidative phosphorylation suggests that FL-FVIII cells may rely on alternative energy sources, which could be linked to their increased intracellular burden.

The inhibition of DNA repair and transcription-related pathways further suggests that FL-FVIII cells may experience differences in cellular maintenance processes compared to BDD-FVIII cells, which have a simplified secretion process and likely require less transcriptional and metabolic regulation. Overall, the pathway analysis indicates that FL-FVIII cells have a greater cellular processing and metabolic demand compared to BDD-FVIII cells, which may contribute to differences in FVIII secretion efficiency, intracellular trafficking, and overall cellular function. These findings provide insight into how FVIII structure influences cellular metabolism, secretion pathways, and energy utilization.

Upon examination of upstream regulators, including transcription factors, kinases, cytokines, and chemicals/drugs, to gain insights into the regulatory networks associated with FL- and BDD- Factor VIII (FVIII) expression in HEK cells, we observed intriguing differences between FL and BDD-FVIII expressing HEK cells. Transcription Factors and Signaling Regulators: CDKN1A (p21), TGFB1, and RICTOR are among the most significantly activated regulators, suggesting increased regulation of cell cycle arrest, growth factor signaling, and mTORC2-associated functions. The presence of MAP4K4 and CPT1B also suggests involvement in lipid metabolism and stress adaptation. Conversely, INSR (Insulin receptor), ESR2, and LIN9 are among the inhibited regulators, suggesting reduced insulin signaling, estrogen receptor-related transcriptional activity, and cell cycle-associated functions in BDD-FVIII cells **(Figure 29A)**.

Transcriptional Regulators Involved in Cell Cycle and Stress Response**: Figure 29B** represents transcriptional regulators related to cell cycle control and cellular stress

responses. TP53 (p53), HIF1A (Hypoxia-Inducible Factor 1-alpha), and FOXO3 are significantly activated in FL-FVIII cells, indicating a potential involvement in DNA damage response, hypoxic adaptation, and oxidative stress management. The activation of CDKN2A and let-7 suggests a role in senescence and differentiation control. In contrast, MYC, TEAD1, and RB1 are among the most inhibited regulators, suggesting a reduction in proliferative signaling and cell cycle progression in BDD-FVIII cells.

Chemical and Drug-Based Regulatory Influence: **Figure 29C** represents chemical compounds and drugs that influence gene expression patterns, highlighting molecules that either mimic or suppress the observed gene expression changes. Drugs such as 5-fluorouracil, doxorubicin, imatinib, and calcitriol are activated, suggesting their potential role in modulating pathways affected in FL-FVIII cells. The upregulation of compounds like GABA, GnRH-A, and ST1926 suggests involvement in neuroendocrine and apoptosis-related mechanisms. Conversely, metribolone, curcumin, and aflatoxin B1 are inhibited, which may indicate that hormonal signaling, anti-inflammatory, or detoxification pathways are suppressed. Building upon the broad chemical regulator analysis presented in **Figure 29C**, we next focused specifically on steroids, given their widespread use in gene therapy protocols for modulating inflammation and immune responses.

Among the differentially predicted steroids, Budesonide emerged as a key upstream regulator, showing significant inhibition in BDD-FVIII cells compared to FL-FVIII **(Figure 29D)**. This finding is particularly notable because Budesonide is commonly administered clinically following FVIII gene therapy. The strong downregulation of Budesonide-responsive gene networks in BDD cells suggests that the transcriptional impact of B-domain deletion overlaps with Budesonide's pharmacological effects. This reinforces our hypothesis that steroidal intervention may serve as a strategy to shift the cellular phenotype of BDD-FVIII closer to that of full-length FVIII, potentially improving therapeutic outcomes by restoring the expression of critical immune and stress-regulatory genes.

A)

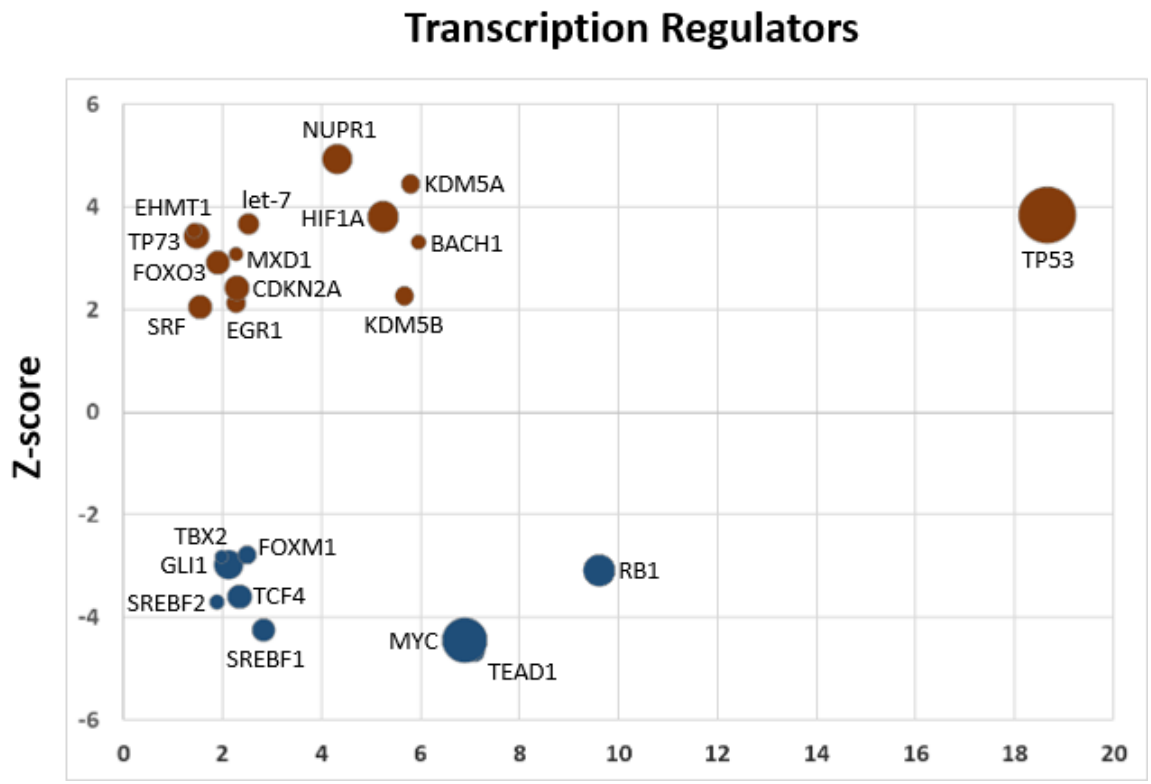
Transcription Regulators
Z-score
NUPR1
KDM5A
EHMT1
let-7
HIF1A
TP73
BACH1
MXD1
FOXO3
CDKN2A
SRF
EGR1
KDM5B
TP53
TBX2
FOXM1
GLI1
RB1
SREBF2
TCF4
SREBF1
MYC
TEAD1

B)

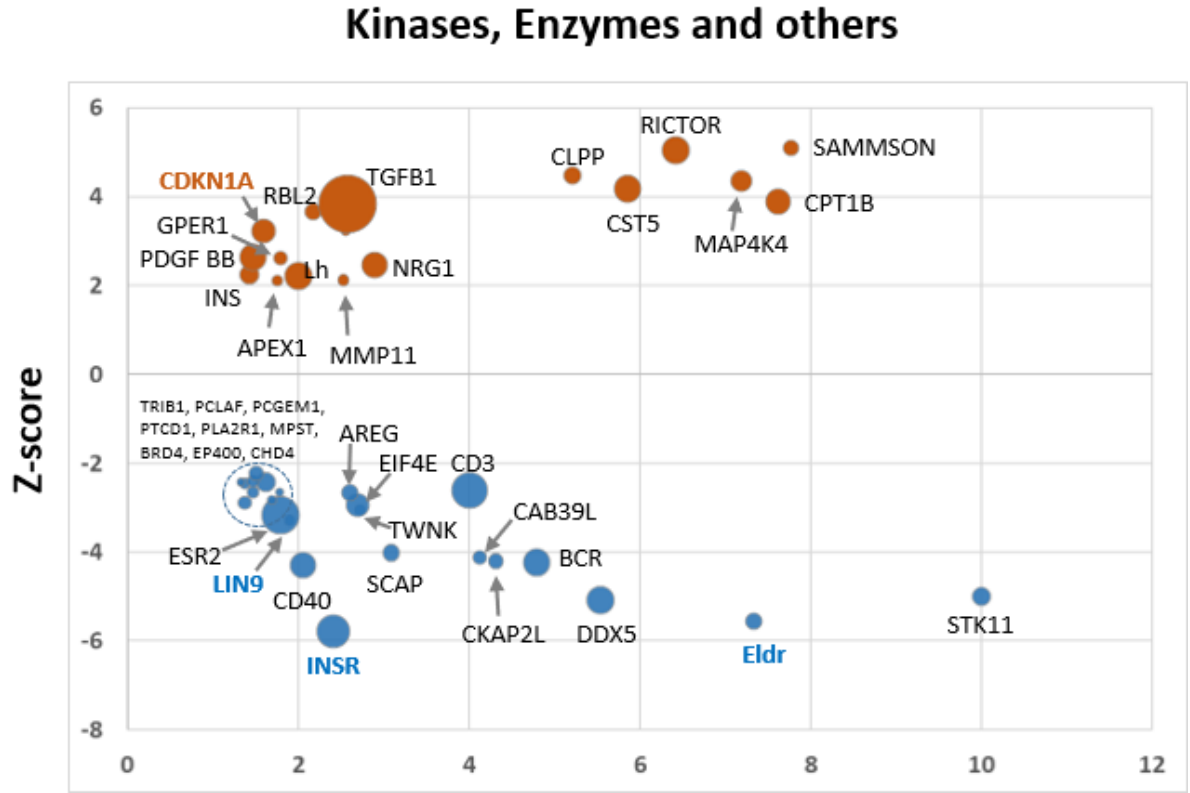
Kinases, Enzymes and others
Z-score
RICTOR
SAMMSON
CLPP
CDKN1A
TGFB1
RBL2
CPT1B
CST5
GPER1
MAP4K4
PDGF BB
Lh
NRG1
INS
APEX1
MMP11
TRIB1, PCLAF, PCGEM1, PTCD1, PLA2R1, MPST, BRD4, EP400, CHD4
AREG
EIF4E
CD3
CAB39L
TWNK
ESR2
BCR
LIN9
SCAP
CD40
CKAP2L
DDX5
STK11
INSR
Eldr

C)

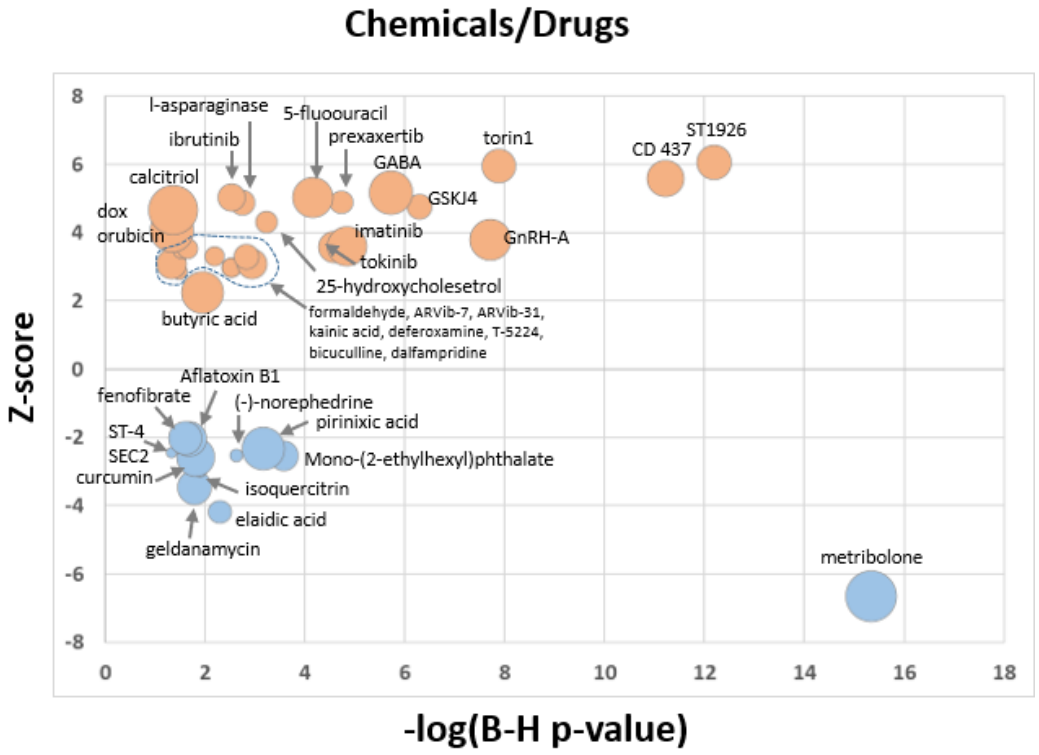

D)

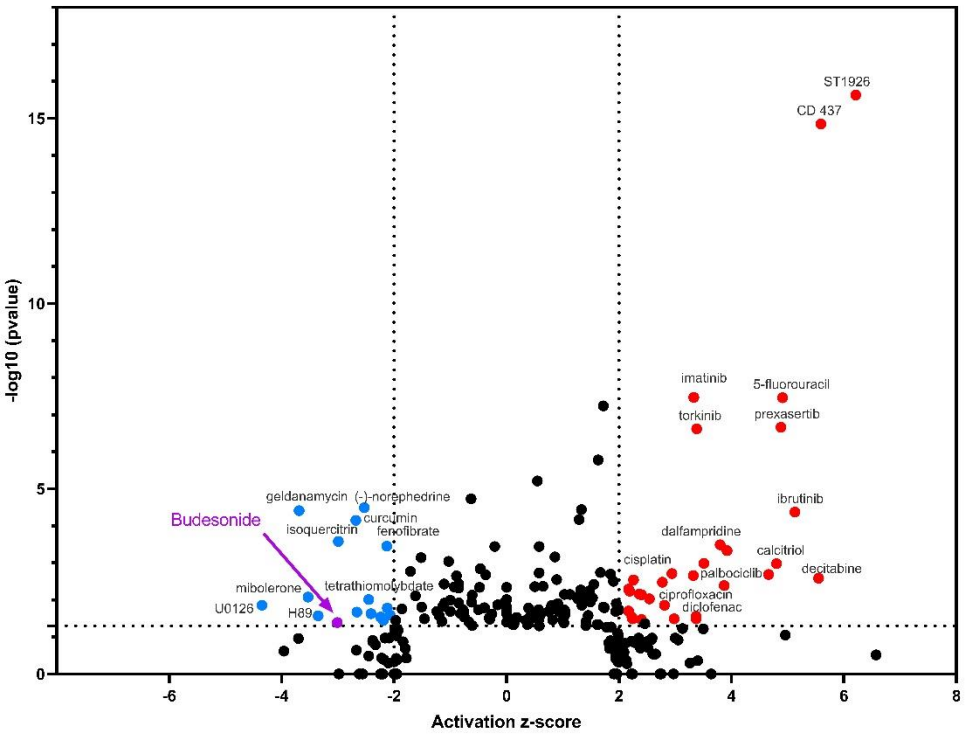

Figure 29. Upstream Regulator Analysis Reveals Differential Activation of Transcriptional Programs and Chemical Drugs in FL-FVIII vs. BDD-FVIII Expressing HEK293 Cells.

A-B-C: Bubble chart illustrating upstream regulators (transcription factors, kinases, cytokines, and chemical/drugs). Red bubbles represent pathways that are upregulated in BDD-FVIII compared to FL-FVIII, while blue bubbles represent pathways that are downregulated in BDD-FVIII compared to FL-FVIII, based on the z-score. The size of each bubble corresponds to the number of genes that overlap with the pathway, indicating the relative significance of gene enrichment within each pathway. **D-** Volcano plot displaying the predicted activation or inhibition of upstream Chemical Drugs based on differential gene expression between HEK293 cells expressing FL-FVIII and BDD-FVIII. The x-axis represents the Activation Z-score (positive values indicate predicted activation in FL-FVIII; negative values indicate predicted activation in BDD-FVIII). The y-axis shows the statistical significance of the prediction (−log10(p-value)). Each point represents a Chemical Drug as defined in IPA, with red and blue dots highlighting those significantly predicted to be activated or inhibited, respectively.

Further investigation into stress-related pathways revealed intriguing differences between the two FVIII variants.

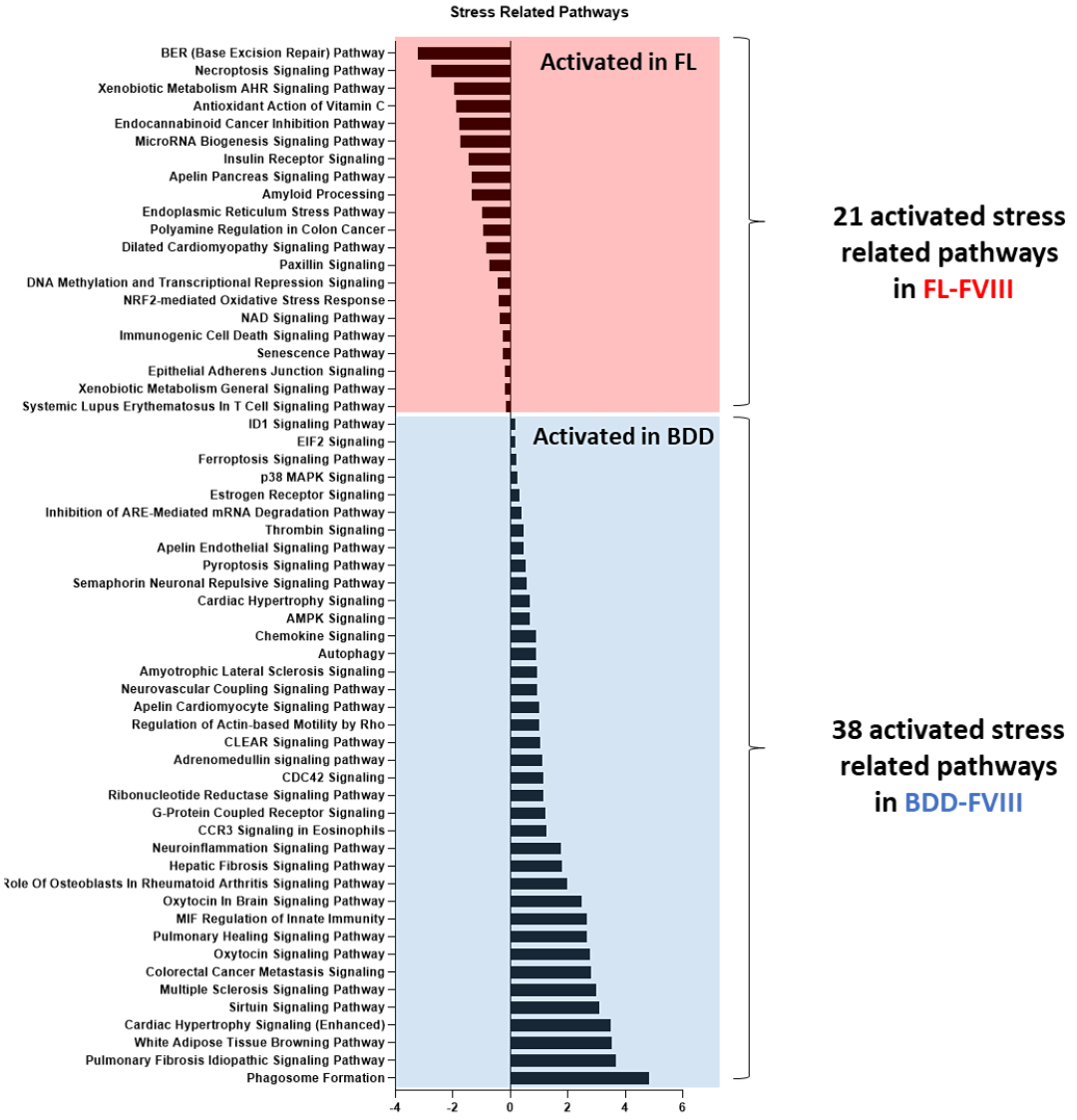

Figure 30. Selected stress-related pathways.

Red bubbles represent stress-related pathways activated in FL-FVIII HEK cells, while blue bubbles represent stress-related pathways activated in BDD-FVIII HEK cells compared to FL-FVIII.

Specifically, we found that 38 stress-related pathways were activated in BDD-FVIII expressing HEK cells, whereas only 21 were activated in FL-FVIII expressing HEK cells **(Figure 30).** This disparity underscores the potential role of stress response mechanisms in modulating the cellular phenotype associated with BDD-FVIII expression.

X- Comparative Analysis of transient siRNA Knockdown and Stable Knockout of Key proteins in HEK Cells stably expressing FL-FVIII and BDD-FVIII.

- **Transient siRNA Knockdown**

In order to further show the differences in internal trafficking and cellular processing between FL- and BDD-FVIII, we conducted both transient siRNA knockdown and stable knockout experiments of ER chaperones and ERGIC compartment proteins in HEK cells stably expressing either FL-FVIII or BDD-FVIII. By targeting the ER chaperones Calnexin (CNX) and Calreticulin (CALR), as well as the ERGIC proteins LMAN1 and MCFD2, we aimed to evaluate their individual contributions to the secretion dynamics of each FVIII variant. Additionally, and according to earlier studies using a yeast two-hybrid screen, GABARAP was shown to be a particular interactor with Factor VIII's B-Domain. Given its binding specificity to an area supposed to be important in FVIII trafficking and secretion, this interaction suggested that GABARAP has a special function in modulating FVIII processing. Thus, in our HEK cell models producing FL-FVIII and BDD-FVIII, we expanded our study to include GABARAP. This gave us a thorough grasp of their effects on both FVIII forms by allowing us to investigate how the lack of these proteins impacts FVIII secretion dynamics and evaluate their more general regulatory function in FVIII intracellular pathways. The following results compare the effects of siRNA knockdown on FVIII secretion for FL-FVIII and BDD-FVIII. We used siRNA targeting CNX, CALR, LMAN1, MCFD2, and GABARAP to transfect stable, secreting FL- or BDD-FVIII single-cell clones (5 from each) in order to examine the impact of different proteins on FVIII secretion. Media samples were taken 24, 48, and 72 hours after transfection to track FVIII secretion; the effects peaked around 48 hours later **(Figure 31)**.

CNX: FVIII secretion increased as a result of CNX knockdown, with FL clones showing a much greater impact than BDD clones (p = 0.0001). FL clones showed an average 22% increase in FVIII secretion, whereas BDD clones showed an average 5% increase.

CALR: FVIII secretion decreased when CALR was knocked down; this impact was more noticeable in FL clones than in BDD clones (p = 0.0363). For FL clones, the average reduction in FVIII secretion was 50%, whereas for BDD clones, it was 25%. Regardless of the baseline secretion levels, the BDD clones showed superior consistency among single-cell clones.

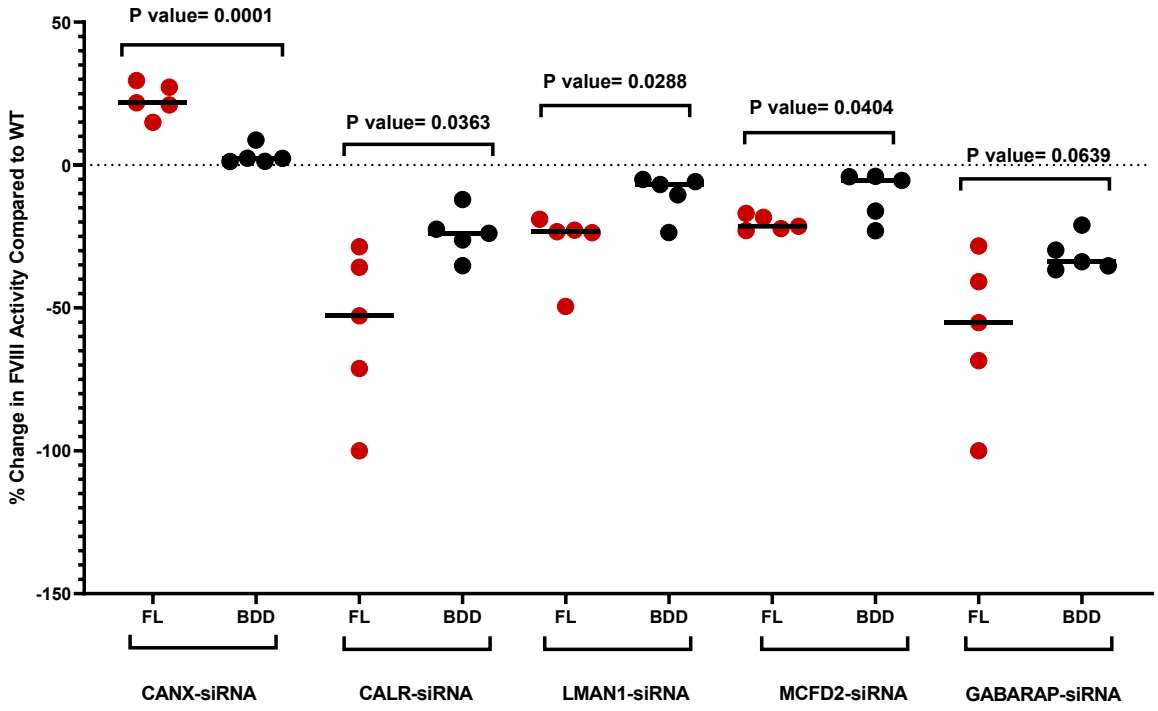

Figure 31. Effect of siRNA Knockdown on FVIII Secretion in FL and BDD Clones. This figure represents the impact of siRNA-mediated knockdown of intracellular trafficking and chaperone proteins on FVIII secretion in Full-Length (FL, red) and B-domain-deleted (BDD, black) expressing clones. Each condition consists of five different FL or BDD clones, which were previously characterized and generated in earlier experiments. The % change in FVIII activity is shown relative to wild-type (WT) levels. The siRNAs target CNX, CALR, LMAN1, MCFD2, and GABARAP. Statistical significance between FL and BDD groups for each siRNA treatment is indicated by the respective p-values, with horizontal bars showing group comparisons. The dotted line represents the 0% change in FVIII activity, corresponding to WT levels.

LMAN1: FVIII secretion decreased as a result of siRNA-mediated LMAN1 knockdown, with FL clones showing a larger drop than BDD clones (p = 0.0288). FL clones showed

an average drop in FVIII secretion of 55%, whereas BDD clones showed an average decrease of 33%. Once again, BDD clones showed superior consistency across clones.

MCFD2: FVIII secretion was shown to expectantly decrease with MCFD2 knockdown, with the impact being more noticeable in FL clones ($p = 0.0404$). For FL clones, the average reduction in FVIII secretion was 22%, whereas for BDD clones, it was 5%.

GABARAP: FL clones showed a higher reduction in FVIII secretion than BDD clones for GABARAP knockdown ($p = 0.0639$), with average decreases of 55% and 33%, respectively. In terms of secretion levels, BDD clones showed more uniformity between clones. The treatment with siRNA had expected and surprising effects on FVIII secretion in FL-secreting cells. Treatment with siRNA resulted in the expected decrease in FVIII secretion for the ERGIC proteins LMAN1 and MCFD2. However, FVIII secretion increased when siRNA targeted CNX, but FVIII secretion reduced when CALR was knocked down. Regardless of the baseline secretion levels, knockdowns for BDD-secreting cells often demonstrated a lower decrease in FVIII secretion than FL clones, with improved consistency between individual clones.

- **Stable Knockout**

Next, we produced stable knockouts of CNX, CALR, LMAN1, MCFD2, and GABARAP in one stable FL-FVIII clone (HEK28) and one BDD-FVIII clone (HEKBDD27) in order to validate these findings. The role of these proteins in the control of FVIII secretion was supported by the findings of stable knockout tests, which were in agreement with the siRNA-mediated knockdowns.

Such stable knockouts would allow the detailed characterization of specific knockouts effects on FVIII intracellular trafficking and cellular distribution. To verify the gene knockouts, We 1) sequenced the targeted locus, 2) performed western blots using specific antibodies against the knocked-out proteins, 3) performed fluorescence immunostaining of wild-type and knockouts cell lines. Sequencing revealed non-frame insertions or deletions **(Figure 32A)**.

We also determined the knockout effect on protein availability by both immunostaining and western blot (when specific antibody is available and compared to wild type

HEK28) **(Figure 32 B and D)**. These two approaches prove the absence of all targeted knocked out corresponding proteins.

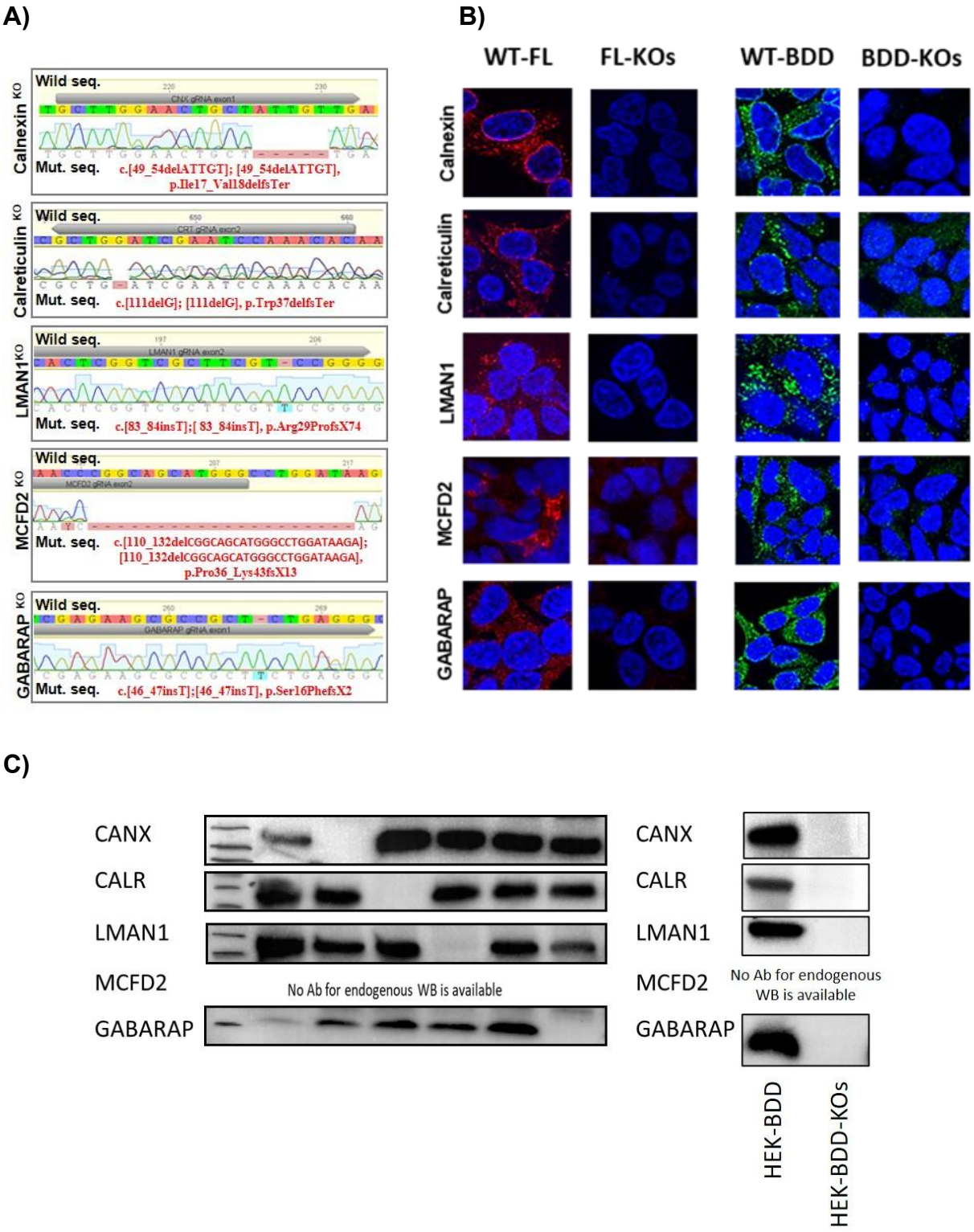

Figure 32. Characteristic and proof of knockouts cell line status.

A- DNA sequences of the mutations created by CRISPR, the altered sequence, type of mutation and nomenclature are indicated for each knockout cell line. **B-**

Immunofluorescent staining of the proteins corresponding to the gene knockouts in the knockout and wild type cells. **C-** Western blots of all corresponding knockouts genes from all cell lines.

Ultimately, to further prove the specific effect of the CRISPR/Cas9 KOs we rescued the phenotype by transient transfection with the normal gene product corresponding to the knocked-out gene **(Figure 32).**

The rescue process worked efficiently for ER (CNX and CALR), ERGIC specific gene knockouts (LMAN1 and MCFD2) and GABARAP as seen with the return of the FVIII activity values toward the wild type/mock levels (green curved arrows **in Figure 33A**).

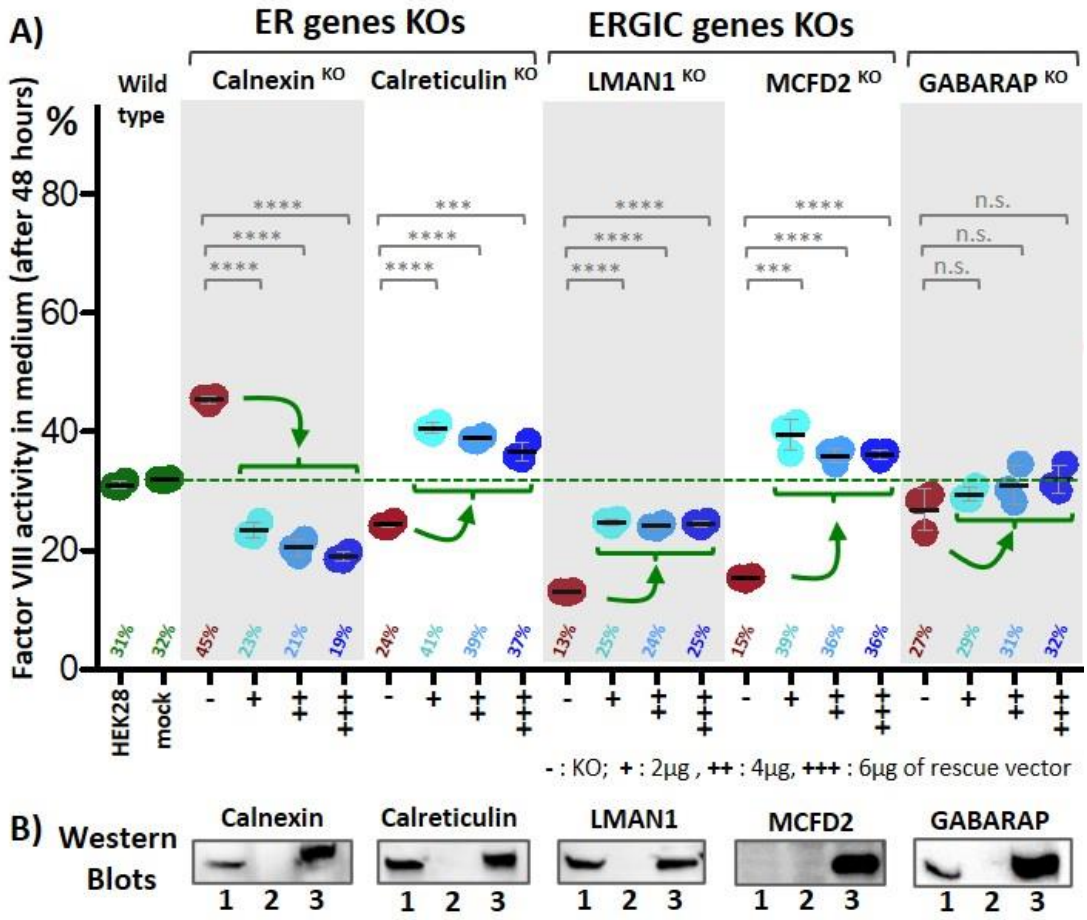

Figure 33. Genetic rescue of the CRISPR based knockouts.
A- Dot diagram showing the FVIII secretion potentials (as depicted from factor VIII activity in the medium at 48 hours) before rescue (in red) and after rescue with 2 µg (in cyan), or 4 µg (in light blue), or 6 µg of vectors carrying the rescued gene (n.s.: non-significant; *: p <0.05; **: p <0.01; ***: p <0.001; ****: p <0.0001). **B-** Detection of corresponding gene rescue protein by western blots; for every gene category the wild type, the knockout and the rescued knockout samples are shown.

Quantitatively, the FVIII activity in the medium was significantly reduced in all knockout conditions, with baseline activity dropping to approximately 23% in Calnexin KO, 25% in Calreticulin KO, 25% in LMAN1 KO, 28% in MCFD2 KO, and 38% in GABARAP KO. Upon genetic rescue via transient transfection of the respective wild-type gene, FVIII activity levels showed a dose-dependent recovery. Specifically, for CNX, CALR, LMAN1, and MCFD2 KO, the FVIII secretion increased to approximately 33%–35% (2 µg), 37%–38% (4 µg), and 39%–40% (6 µg), approaching wild-type levels. Notably, the restoration of FVIII secretion in GABARAP KO was not statistically significant across different rescue doses (n.s.), indicating a limited role of this gene in FVIII secretion. Western blot validation **(Figure 33B)** confirmed the successful expression of the rescued genes, with reappearance of the corresponding proteins in the rescued knockout samples.

These findings collectively confirm that the observed FVIII secretion defects were directly caused by the loss of the targeted genes, and the rescue experiments provide strong evidence for their specific roles in FVIII secretion. After confirming the knockouts, we measured the FVIII secretion in the media of different knockout cells (after 48 h) and observed the same trend as for the siRNA. i.e.: Our analysis showed that the gene knockouts had consistent impacts on FVIII activity in both FL- and BDD-FVIII cell lines, with differences primarily in the magnitude of the change. The Calnexin knockout led to an increase in FVIII secretion in both cell lines, with a more pronounced effect in FL-FVIII cells (p-value=0,0018).

Conversely, the Calreticulin knockout resulted in a significant decrease in FVIII activity, approximately 25% in FL cells and around 15% in BDD cells (p-value=0,0017). Knockouts of LMAN1 and MCFD2, essential ER-Golgi intermediate compartment (ERGIC) proteins, led to decreased FVIII secretion in both cell types, with reductions more substantial in FL cells (average decrease of 50-60%) compared to BDD cells (average decrease of 15-20%), supported by p-values < 0.0001. The GABARAP knockout similarly decreased FVIII activity in both cell lines, with no significant difference between both cell lines (approximately 25% reduction, p-value=0.112).

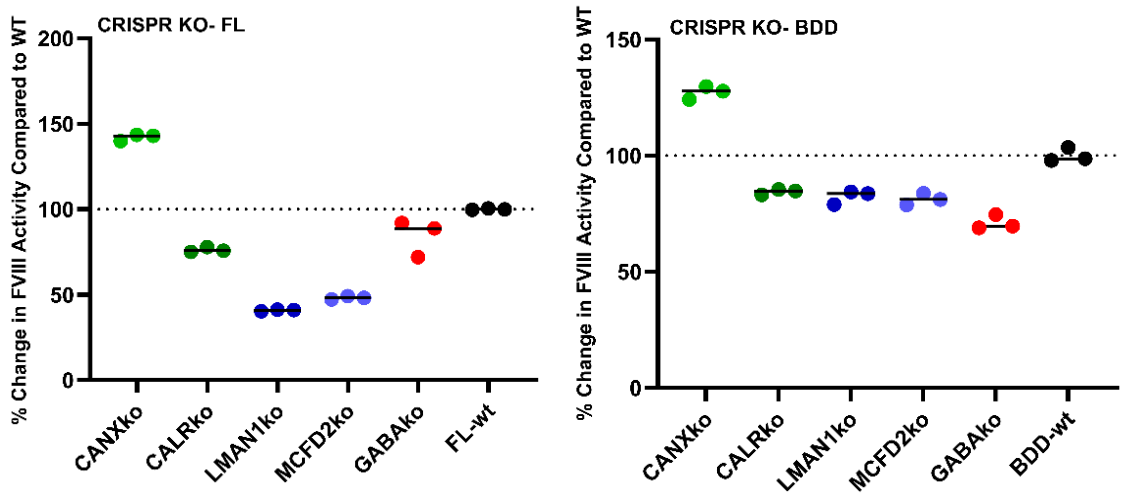

Figure 34. CRISPR based stable knockouts effect on FVIII activity.

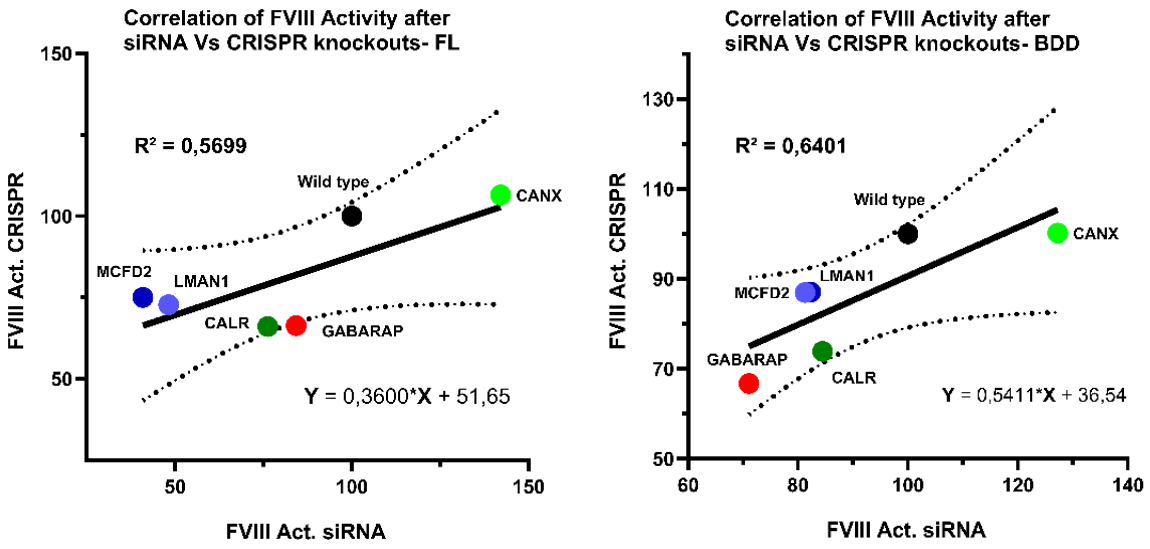

Figure 35. Correlation between the factor VIII activity in mediums from the siRNA and CRISPR based knockout cells.

Discussion

Gene therapy represents a groundbreaking advancement in the treatment of Hemophilia A and B, offering the potential for long-term endogenous expression of clotting factors and reducing reliance on prophylactic replacement therapy. AAV-mediated gene therapies have demonstrated significant efficacy in clinical trials, substantially reducing annualized bleeding rates (ABR) and exogenous factor administration. However, despite these promising outcomes, a key challenge remains: the durability of transgene expression varies significantly between Hemophilia A and Hemophilia B, influencing long-term treatment efficacy.

Several clinical trials have reported notable differences in FVIII and FIX expression levels over time. The most recent findings indicate that Valoctocogene Roxaparvovec (Roctavian) for Hemophilia A achieves mean Factor VIII activity levels of 42.9 IU/dL at first year, which decline to 24 IU/dL at second years, marking a 44% reduction with expression lasting approximately two to three years before significant decline [129,130].

Etranacogene Dezaparvovec (Hemgenix) for Hemophilia B has shown consistent Factor IX expression over four years, with average levels of 41.5 IU/dL in the first year, 36.7 IU/dL in the second year, 38.6 IU/dL in the third year, and 37.4 IU/dL in the fourth year after infusion [122]. Importantly, 94% of patients did not need to keep taking continuous prophylaxis treatment at year four, and none of the patients went back to prophylaxis between years three and four [122].

These findings highlight a clear difference in the durability of expression between Hemophilia A and B gene therapies, with FIX therapies demonstrating longer-lasting effects than FVIII therapies.

A fundamental difference between Hemophilia A and B lies in the properties of Factor VIII and Factor IX. FVIII (~235 kDa) is a large, multi-domain glycoprotein with extensive post-translational modifications, whereas FIX (~57 kDa) is a small, single-chain serine protease that requires less complex processing [131]. Their natural expression sites also differ, with FVIII synthesized in liver sinusoidal endothelial cells (LSECs) [132], whereas FIX is synthesized in hepatocytes. Current AAV gene therapies target hepatocytes [133], making FIX gene therapy more efficient and durable, whereas FVIII gene therapy must adapt to an unnatural expression environment in hepatocytes.

Gene therapy for Hemophilia A and B relies on adeno-associated virus (AAV) vectors, which can trigger immune responses affecting treatment efficacy [134]. Both FVIII and FIX gene therapies share common immunological challenges related to AAV vector recognition and the mode of administration [135]. When AAV vectors are infused intravenously, the innate immune system detects viral capsid proteins, leading to activation of toll-like receptors (TLRs), interferon signaling, and recruitment of antigen-presenting cells (APCs) [136,137]. These responses can stimulate adaptive immunity, resulting in cytotoxic T-cell responses targeting transduced hepatocytes, potentially leading to loss of transgene expression [138] [139]. Additionally, pre-existing neutralizing antibodies (NAbs) against AAV serotypes can block vector uptake and reduce transduction efficiency, further limiting gene therapy success [140] ,[141]. However, while these immune mechanisms are common to both FVIII and FIX gene therapies, the degree of immune activation varies between FVIII and FIX gene therapy, with FVIII being more immunogenic[31]. FVIII gene therapy faces greater immune challenges than FIX gene therapy due to the higher prevalence of pre-existing inhibitors (~30% in severe Hemophilia A vs. ~3-5% in Hemophilia B)[142–144]. The immune clearance risk is higher for FVIII, as it has more immunogenic epitopes and undergoes B-domain deletion (BDD) modifications, whereas FIX has fewer immunogenic sites and remains closer to its natural form. Another key difference is immune tolerance in hepatocytes, FVIII is naturally produced in liver sinusoidal endothelial cells (LSECs)[132,145], making hepatocyte-targeted gene therapy an unnatural expression site, whereas FIX is naturally produced in hepatocytes [133,146], leading to better immune acceptance. These differences impact treatment durability, with FVIII transgene expression declining faster due to immune clearance, while FIX gene therapy maintains stable expression for years[147]. Steroid administration before or after gene therapy has also been shown to influence the durability of transgene expression. The timing of steroid administration is a key factor influencing therapeutic durability, with prophylactic use in Hemophilia B correlating with improved outcomes, unlike the reactive use commonly applied in Hemophilia A, which may be insufficient to mitigate early immune responses. In Hemophilia B trials such as HOPE-B for Etranacogene Dezaparvovec, steroids were given proactively [148], helping sustain FIX expression for years, while in Hemophilia A trials such as Valoctocogene Roxaparvovec, steroids were often given reactively after ALT elevations, which may be less effective [149]. By suppressing cytotoxic T-cell activation, reducing hepatic inflammation, and minimizing transgene clearance,

steroids help prolong gene therapy durability. However, the timing and dosage of corticosteroid administration play a crucial role in determining the overall effectiveness of immune modulation strategies.

A major limitation in current gene therapy for Hemophilia A is the reliance on B-domain-deleted Factor VIII (BDD-FVIII) rather than full-length FVIII (FL-FVIII). The deletion of the B-Domain is necessary to allow efficient packaging within AAV vectors, but this modification could have significant consequences on FVIII's intracellular processing, trafficking, secretion, and stability. Given the stark contrast in durability between Hemophilia A and Hemophilia B gene therapies, it is plausible that the structural modifications imposed on FVIII, particularly the B-domain deletion, may contribute to its reduced long-term expression compared to FIX, which is naturally smaller and remains largely unmodified, except for one amino acid, in gene therapy applications. The potential impact of FVIII truncation on protein stability, trafficking pathways, and cellular stress responses is not yet fully understood, making it a critical area for investigation in optimizing gene therapy efficacy. It is not known how the intracellular effects of expressed therapeutic proteins contribute to limitation of gene therapy.

To address this, our study explores the intracellular fate of FL-FVIII and BDD-FVIII, comparing their expression, trafficking, stability, and secretion profiles in HEK293 clones stably expressing each variant. This work investigates the impact of cellular stress reactions and energy metabolism on FVIII activity. Understanding how the removal of the B-Domain alters FVIII's intracellular behavior is essential for determining whether truncation-related secretion advantages come at the expense of long-term stability, potentially influencing the well-being of the host cells and durability of Hemophilia A gene therapy.

This study provides a comprehensive analysis of the expression, secretion, and stability profiles of FL- and BDD- FVIII in single-cell HEK293 clones, highlighting their distinct intracellular behaviors and production dynamics.

I- Distinct Intracellular Behaviors of FL- and BDD-FVIII

Our results confirmed a strong positive correlation between *F8* copy number and expression levels for both constructs, with BDD-FVIII exhibiting a steeper correlation slope **(Figure 13A)**. This suggests higher relative expression per gene copy for BDD-FVIII, likely due to the shorter transcript and reduced transcriptional or translational

demands compared to FL-FVIII. This observation aligns with findings from Chiaromonte et al. (2003), who demonstrated that gene length negatively correlates with expression levels across the genome, with shorter genes typically exhibiting higher expression efficiency, possibly due to faster transcription and simpler regulatory constraints [150]. The initial breakthrough in the development of higher expression recombinant FVIII molecules came with the discovery that removal of the entire B-Domain resulted in up to a 20-fold increase in mRNA and primary translation product [151]. However, in their studies, only a 2- to 3-fold increase in secreted FVIII was observed [111]. However, we were able to demonstrate in our study that BDD-FVIII clones demonstrated smoother trafficking and secretion, with less antigen retained intracellularly than FL-FVIII **(Figure 13B and D)**. This efficient release of BDD-FVIII from the ER to the Golgi is likely facilitated by the absence of the B-Domain, which reduces folding constraints, intracellular retention, and trafficking bottlenecks.

Interestingly, this secretory behavior contrasts with Factor V (FV), another homologous coagulation factor, which is transported efficiently from the ER to the secretory pathway with minimal retention. FV and FVIII share structural similarities, yet they exhibit striking differences in their intracellular processing and trafficking mechanisms [152]. In contrast to FV, which is efficiently transported from the ER to secretion, FVIII experiences prolonged ER retention, suggesting that the two homologous proteins differ in their folding efficiency and interaction with ER chaperones. It is well established that FVIII remains in the ER for a longer duration compared to FV, a difference attributed to its more complex folding process and differential interaction with ER chaperones. Unlike FV, which progresses efficiently through the secretory pathway, FVIII exhibits extensive interaction with calnexin (CNX), a critical ER chaperone involved in glycoprotein quality control. This prolonged retention is mediated by CNX binding, which plays a pivotal role in ensuring only properly folded proteins proceed to the secretory pathway. Notably, the interaction of FVIII with CNX is facilitated through its B-Domain, explaining why B-domain-deleted FVIII (BDD-FVIII) exhibits improved secretion efficiency and reduced intracellular retention compared to full-length FVIII. The absence of the B-Domain in BDD-FVIII disrupts this prolonged CNX interaction, thereby accelerating its ER exit and subsequent transport to the Golgi.

Importantly, both constructs demonstrated robust correlations between antigen and activity levels in the medium, validating the reliability of antigen measurements in

estimating FVIII activity **(Figure 13C)**. It is noteworthy that FVIII activity was assessed using a chromogenic assay, which measures the functional activation of the coagulation cascade by detecting the generation of activated Factor X in a two-step enzymatic reaction. In contrast, the antigen assay is based on an immunoassay format, where specific antibodies capture FVIII protein regardless of its functional state. The strong agreement between these two assays suggests that a substantial portion of the secreted FVIII is functionally active and highlights the stability of the expressed protein in both FL- and BDD-FVIII constructs. Although a proportion of BDD-FVIII may be misfolded or subject to intracellular degradation, its markedly higher secretion efficiency appears to compensate by allowing sufficient quantities of properly folded and active protein to accumulate in the culture medium. This is reflected in the chromogenic assay results, which selectively detect enzymatically competent FVIII, irrespective of its folding history or antigen content. Furthermore, the chromogenic assay specifically captures only the active fraction capable of initiating Factor X activation, whereas the antigen assay reflects total FVIII protein, including inactive or misfolded forms. This distinction further underscores the biological relevance of the observed antigen-activity correlation. While BDD-FVIII exhibits superior secretion efficiency, this gain may come at the cost of increased cellular stress and reduced proliferation, potentially compromising long-term transgene durability despite initial expression advantages.

II- Trafficking Pathways: Conventional vs. Alternative Routes

1. Mapping FVIII Trafficking: A Comparative Co-Localization Study

Building on the previous mentioned study regarding the role of CNX in mediating FVIII retention, we further explored the intracellular trafficking dynamics of BDD-FVIII and FL-FVIII. To this end, we performed a quantitative analysis of co-localization with 20 intracellular markers, including CNX. This analysis revealed that FL-FVIII exhibited higher co-localization with 16 markers, spanning compartments such as the endoplasmic reticulum (ER), Golgi, endosomes, and lysosomes **(Figure 14)**. Notably, FL-FVIII displayed greater association with CNX, further supporting the notion that its prolonged retention in the ER is mediated by CNX interaction. This increased co-localization aligns with the higher intracellular retention of FL-FVIII observed in antigen assays **(Figure 13D)**.

Additionally, FL-FVIII exhibited significantly higher co-localization with 15 key chaperones and intracellular markers, including LMAN1, COPI, COPII, GM130, and TGN46, suggesting that the B-Domain plays a crucial role in FVIII intracellular transport from the ER through the ERGIC to the Golgi and secretion. LMAN1, a cargo receptor in the ERGIC, specifically interacts with the B-Domain, regulating FVIII export from the ER, while COPII facilitates ER-to-Golgi transport and COPI mediates Golgi-to-ER retrieval, contributing to FL-FVIII's prolonged retention. Additionally, FL-FVIII showed higher co-localization with GM130, indicating extended residence in the early Golgi, and lower co-localization with TGN46, suggesting a delayed transition to the trans-Golgi and secretion. In line with these findings, FL-FVIII also exhibited higher co-localization with Rab GTPases, including Rab8a, Rab11, Rab5, and Rab7, which are involved in vesicular trafficking and intracellular sorting. Rab8a and Rab11 regulate post-Golgi transport and recycling, suggesting that FL-FVIII undergoes multiple rounds of intracellular sorting before secretion, leading to its prolonged retention. Similarly, Rab5 and Rab7, which are key regulators of early and late endosomal pathways, respectively, also displayed higher co-localization with FL-FVIII. This suggests that a fraction of FL-FVIII is trafficked through endosomal compartments before secretion or degradation, further contributing to its increased intracellular retention compared to BDD-FVIII. The lower co-localization of BDD-FVIII with these markers suggests a more streamlined secretion pathway that bypasses extensive retention, retrieval, and recycling processes. Although no direct interaction between the B-Domain and Rab GTPases has been demonstrated, its deletion likely alters FVIII's folding dynamics and how it engages ER quality control. These changes may in turn influence FVIII's access to Rab-dependent vesicular pathways, leading to the distinct trafficking behaviors observed.

Previous study, from our institute, identified eight FVIII B-Domain variations (p.Asp845Glu, p.Pro947Arg, p.Glu1057Lys, p.His1066Tyr, p.Arg1126Trp, p.Arg1329His, p.Leu1481Pro, and p.Ala1610Ser) that led to a decrease in FVIII:C values, indicating a mild Hemophilia A (HA) phenotype. These findings supported the functional roles of the B-Domain in FVIII trafficking and secretion, as most variants showed reduced relative secretion[72].

Additional evidence supporting the B-Domain role in intracellular processing of FVIII are seen from secretion studies of B-Domain variants. For example studies have

attempted to investigate whether adding partial sequences of the B-Domain to the BDD-FVIII will enhance FVIII expression [153]. Various FVIII expression cassettes with different B-Domain constructs, including SQ (first 14 amino acids), N6 (first 228 amino acids), and Fugu B (first 201 amino acids), were utilized [110,112,154] . From these codon-optimized sequences, significantly higher expression was observed for both SQ FVIII Fugu B (co) and SQ FVIII N6 (co) compared to SQ FVIII (co) [112].

These results also suggest that FVIII naturally follows two distinct trafficking pathways. One pathway, taken by FL-FVIII, appears to involve extensive interactions with chaperones, retrieval mechanisms, and recycling through the endosomal system, leading to prolonged intracellular retention. The second pathway, which becomes dominant when the B-Domain is deleted, bypasses many of these steps, allowing for a faster and more direct route to secretion.

A similar phenomenon has been observed in other proteins that adopt alternative secretion routes when trafficking marker interactions are altered. Some proteins, like GRP78 and APP, take unconventional secretion pathways when their ER-Golgi transport dynamics are disrupted. For example, GRP78, which is normally retained in the ER, can be rerouted to the cell surface via endosomal transport when ER stress disrupts retrograde Golgi transport, a process mediated by Rab GTPases (Rab4, Rab11, and Rab15), SNARE proteins (BET1 and Syntaxin 13), and PERK-AKT-mTOR signaling. Similarly, APP has been shown to utilize alternative intracellular trafficking routes when it’s normal processing through the Golgi and endosomal compartments is altered, impacting its secretion and cellular distribution. In an analogous manner, the deletion of the B-Domain in FVIII appears to prevent its extensive interaction with chaperones and trafficking regulators, shifting its transport from the conventional secretion pathway to an alternative route. Just as GRP78 and APP reroute their trafficking in response to cellular conditions, BDD-FVIII likely adopts a faster, more direct secretion pathway by bypassing the prolonged retention mechanisms that govern FL-FVIII trafficking. Interestingly, co-localization with PDI and Furin was comparable for both variants, highlighting their shared utilization of general protein-processing machinery.

The robustness of these findings was confirmed through two approaches. First, repeating co-localization analyses with different FVIII clones showed consistent differences between FL- and BDD-FVIII while excluding clone-specific variability

(Figure 15). Second, using α-tagged FVIII constructs eliminated detection biases associated with polyclonal antibodies. The high correlation of results between α-tagged constructs and polyclonal antibody-based detection methods further validated the findings **(Figure 16)**. This was particularly important given that polyclonal antibodies recognize multiple epitopes, some of which may reside within or near the B-domain. Since B-domain deletion can alter the structural conformation of FVIII and potentially mask or remove native epitopes [70], consistent results across both detection strategies indicate that the observed differences were not due to epitope accessibility or structural rearrangements but reflected true biological variance between FL- and BDD-FVIII.

To dissect more the intracellular trafficking dynamics of FL- and BDD-FVIII, we employed a panel of cellular chemical treatments targeting specific organelles and pathways involved in protein synthesis, trafficking, and degradation. These included glucose starvation (metabolic stress), brefeldin A (BFA, ER-to-Golgi trafficking blockade)[155], chloroquine (CQ, autophagy inhibition)[156], and a Rab7-specific inhibitor (endolysosomal disruption)[157]. The rationale behind this approach was simple: if both FVIII variants share the same trafficking routes, we would expect similar secretion responses to each treatment. However, if their responses diverge, it would indicate different intracellular processing mechanisms. As expected, both glucose starvation and BFA significantly reduced FVIII secretion in both FL- and BDD-expressing cells (by approximately 50% and 80%, respectively). This suggests that early secretory processes, like entry into the ER and transit through the Golgi, are equally essential for both variants. Supporting this, co-localization studies with early secretory markers (COPII and GM130) showed disrupted trafficking in both forms, confirming shared dependence on the ER-Golgi pathway. In contrast, the effects of autophagy inhibition and endosomal disruption were notably different. Chloroquine treatment reduced FL-FVIII secretion by about 48%, but only reduced BDD-FVIII secretion by 20% ($p = 0.01$). This indicates that FL-FVIII is more reliant on autophagy-related degradation, possibly due to a higher burden of misfolded or excess protein.

The divergence became even more striking with Rab7 inhibition. While FL-FVIII secretion dropped by ~40%, BDD-FVIII secretion actually increased by 11% ($p < 0.0001$). This suggests that FL-FVIII is actively processed through late endosomal-lysosomal pathways, perhaps due to retention or quality control mechanisms. On the other hand, BDD-FVIII seems to avoid these pathways entirely, resulting in improved

secretion. These functional differences were confirmed by co-localization analysis **(Figure 18A)**. Rab7 inhibition disrupted FL-FVIII's association with early secretory markers (COPII and GM130), suggesting that endosomal pathways might provide feedback that affects early trafficking steps. BDD-FVIII, in contrast, showed little change in marker association and only minor effects on RAB8a co-localization. Fluorescence microscopy **(Figure 18B)** visually supported these observations: FL-FVIII displayed altered intracellular distribution after treatment, while BDD-FVIII maintained its typical spatial organization.

Together, these findings suggest that BDD-FVIII follows a more direct and degradation-resistant trafficking route compared to FL-FVIII. One possible explanation is structural: the absence of the B-domain in BDD-FVIII may reduce its interaction with chaperones or quality control machinery, allowing it to bypass degradative checkpoints like autophagy and the lysosome. In conclusion, although both FVIII variants depend on the early secretory pathway, only FL-FVIII is significantly affected by disruptions in autophagy and endosomal trafficking. This highlights a key difference in how each form is processed inside the cell, and provides insight into why BDD-FVIII exhibits improved secretion and therapeutic performance.

To further understand the intracellular dynamics of FL- and BDD-FVIII, we examined how the expression and secretion of each variant modulate the organization and interaction of key vesicle-trafficking proteins. Building on earlier observations of differential sensitivity to chemical perturbation and trafficking pathway reliance, we hypothesized that the two FVIII forms could not only follow partially distinct intracellular routes but might also impose differential "pressure" or demand on specific trafficking pathways. If true, this should be reflected in distinct co-localization patterns between intracellular markers associated with secretion and degradation vesicle systems.

To test this, we used a systematic pairwise immunofluorescence staining approach across 12 key intracellular marker pairs. These markers span critical checkpoints in the secretory pathway (e.g., CALR, LMAN1, COPII, TGN46, and GM130), Golgi maturation (Furin), and degradative/autophagic pathways (RAB7, LC3B, GABARAP, LAMP1, VAMP8, and RAB11). The goal was to assess whether FL- and BDD-FVIII expression differentially influenced the spatial proximity, and thereby the functional engagement, of these markers within the cell. The results **(Figure 19A)** show that

pairwise co-localization patterns strongly separate FL- and BDD-FVIII clones, both in unsupervised and supervised principal component analyses. Importantly, four marker pairs exhibited statistically significant differences ($p < 0.05$) between the two groups **(Figure 19B)**. Specifically:

CALR/LMAN1 co-localization was higher in FL-FVIII clones, suggesting enhanced reliance on ER chaperoning and cargo loading machinery, consistent with the known folding complexity and ER retention of FL-FVIII.

In contrast, CALR/GABARAP, COPII/GABARAP, and GM130/TGN46 co-localization were higher in BDD-FVIII clones. These patterns suggest a modified intracellular handling strategy for BDD-FVIII, potentially involving:

- More efficient ER exit (COPII)

- Engagement with GABARAP-related autophagic or trafficking processes, possibly as a buffering or regulatory mechanism for secretory flow rather than degradation.

- Consistent with its delayed secretion, FL-FVIII shows lower co-localization with TGN46 alone, while BDD-FVIII shows enhanced co-localization between GM130 and TGN46, reinforcing a smoother Golgi maturation flow.

These findings align with the earlier data **(Figures 15 and 16)**, which demonstrated a reduced sensitivity of BDD-FVIII to autophagy and endosomal trafficking inhibition, in contrast to FL-FVIII. The higher CALR/LMAN1 co-localization in FL-FVIII clones likely reflects a greater dependency on ER-resident folding and quality control, leading to higher retention and rerouting to degradative systems when overwhelmed. The co-localization data also support the idea that BDD-FVIII expression favors a more streamlined, secretion-compatible intracellular organization, with minimal activation of quality control bottlenecks. The presence of elevated GABARAP interactions (with both CALR and COPII) in BDD-FVIII suggests the potential involvement of non-canonical trafficking routes or alternative vesicle scaffolding systems that facilitate secretion under high expression pressure. GABARAP is known to play roles in both autophagy and unconventional secretion[158]. In the context of BDD-FVIII, its co-localization with COPII and CALR may reflect a secretory buffering mechanism, rather than enhanced degradation, although concurrent association with LC3B/RAB26 **(Figure12)** suggests partial routing into degradative pathways as well.

These results are also reflected in the fluorescence microscopy data **(Figure 19, lower panel)**, where visibly distinct spatial overlap patterns between marker pairs could be observed between the two groups.

Co-localization analysis has been widely validated as a powerful approach to investigate intracellular trafficking routes, particularly for proteins whose structure or mutation alters their cellular routing. For example, in a study examining the recycling pathways of the membrane protein Tetherin, researchers used fluorescently tagged versions of Tetherin and various endosomal markers, including Vps35, Rab4, Rab11, and Arf6, to trace its post-endocytic trafficking. The findings showed that Tetherin predominantly recycled through the retromer-dependent pathway, with minor routing via Rab4- and Rab11-mediated recycling, while Rab5 co-localization was minimal, suggesting rapid sorting from early endosomes[159]. Importantly, this study confirmed that differential co-localization with compartment-specific markers can precisely identify which intracellular routes are favored or bypassed by a protein, especially when its trafficking is altered due to mutation, structural modification, or overexpression. This directly supports our approach of using co-localization to map and compare the distinct trafficking behaviors of FL- vs. BDD-FVIII, which differ not only in structure but also in how they engage the secretory and degradative networks within the cell.

The differences in folding and trafficking between FL-FVIII and BDD-FVIII are evident, and these differences must be considered due to their potential impact on cellular function and disease outcomes. The tumorigenic effect of expression of variant FVIII with different B-Domain constructs was recently investigated [114]. Specifically, the effect of two FVIII variants with different folding efficiencies in the ER upon expression in hepatocytes was investigated in mice: 1) complete B-Domain deletion; and 2) a short variant that retains 6 glycosylation sites (N6, which retains 226 amino acids) that does not significantly aggregate or cause hepatocyte apoptosis. Remarkably, 100% of mice that received the BDD vector developed hepatocellular carcinoma (HCC), whereas only 58% of mice that received N6 vector and none of the mice that received empty vector developed liver tumors [114].

These trafficking and folding differences are not unique to FVIII but have been observed in other cases where truncated proteins exhibit altered intracellular interactions compared to their full-length variant. Overexpression of a truncated protein with a point mutation or deletion of part of its sequence, can disrupt normal protein-

protein interactions within the cell. This disruption may lead to the dysregulation of signaling pathways, metabolic processes, or other cellular functions. For example, a truncated tumor suppressor protein like p14ARF can lose its interaction with MDM2, resulting in the abnormal retention of MDM2 in the nucleus [160]. The ΔF508 mutation in CFTR causes a deletion of phenylalanine at position 508, which also disrupts the folding of the CFTR protein. As a result, the protein fails to achieve its proper conformation and is retained in the endoplasmic reticulum (ER), where it is targeted for degradation by the ER-associated degradation (ERAD) pathway [161].

2. Knockout Studies Reveal Differential Dependencies in Trafficking

To further investigate the distinct trafficking pathways utilized by FL- and BDD-FVIII, we systematically disrupted key components of the ER and ERGIC machinery through both transient siRNA knockdown and stable CRISPR/Cas9 knockout (KO) approaches. These interventions targeted five functionally relevant proteins: Calnexin (CNX), Calreticulin (CALR), LMAN1, MCFD2, and GABARAP, each implicated in ER quality control, ER-to-Golgi transport, or vesicle-mediated trafficking.

A direct comparison of FVIII secretion changes between siRNA and CRISPR conditions revealed strong correlation for both FL-FVIII ($R^2 = 0.57$) and BDD-FVIII ($R^2 = 0.64$). This correlation validates the reproducibility of the observed phenotype and further confirms that the differences in sensitivity between FL and BDD forms are due to their intrinsic trafficking and folding properties, not off-target or stochastic effects of gene disruption **(Figure 35)**.

To definitively prove that the secretion deficits were due to loss of the targeted gene, we performed genetic rescue by transiently re-expressing the corresponding wild-type genes in the KO cells **(Figure 33)**.

- CNX, CALR, LMAN1, and MCFD2 rescues produced dose-dependent increases in FVIII secretion, with activity values approaching or recovering ~40% of wild-type levels ($p < 0.01$ to $p < 0.0001$).
- GABARAP rescue, however, did not significantly restore FVIII secretion (non-significant across all doses), suggesting a more indirect or supportive role that cannot be rescued by simple reintroduction, possibly due to altered cellular context or localization.

These rescue data reinforce that ER chaperones (CNX, CALR) and ERGIC cargo receptors (LMAN1, MCFD2) have direct, rate-limiting roles in FL-FVIII trafficking, while GABARAP plays a modulatory role, potentially influencing the vesicle pool or autophagic routing available for both variants.

Knocking out LMAN1 and MCFD2, components of the cargo receptor complex for ER-to-Golgi transport, resulted in a significant reduction in FVIII secretion, with FL-FVIII secretion decreasing by 50–60% and BDD-FVIII by only 15–20% ($p<0.0001$). This confirms FL-FVIII's strong reliance on receptor-mediated transport, while BDD-FVIII utilizes alternative pathways, reducing its dependence on this complex. Calnexin (CNX) knockout increased secretion of both FVIII variants, with FL-FVIII showing a more pronounced effect ($p=0.0018$), suggesting that CNX-mediated quality control contributes to FVIII retention in the ER. In contrast, calreticulin (CALR) knockout reduced FVIII secretion (~25% in FL-FVIII and ~15% in BDD-FVIII, $p=0.0017$), reflecting its role in maintaining ER Ca^{2+} levels essential for secretion, with FL-FVIII being more dependent on this regulation. Knockout of GABARAP, a vesicular trafficking protein, reduced FVIII secretion by ~25% in both variants, suggesting a shared role in facilitating FVIII transport. However, BDD-FVIII remains more reliant on vesicle-mediated pathways overall. These results align with previous co-localization studies, further confirming FL-FVIII's reliance on chaperone-mediated ER quality control and receptor-dependent secretion, while BDD-FVIII preferentially follows vesicle-driven pathways.

Together, these data support the notion that FL-FVIII is heavily reliant on canonical ER folding, quality control, and receptor-mediated export mechanisms, while BDD-FVIII bypasses many of these checkpoints and follows a more efficient, less regulated secretory pathway.

III- Cellular Homeostasis, Metabolic Adaptations, and Therapeutic Implications of B-Domain Deletion in FVIII

Beyond evaluating expression and secretion levels, which represent the endpoints of FVIII overexpression, it is essential to examine the cellular homeostasis and metabolic impact of B-domain deletion.

1. Cellular Stress and Proliferation Dynamics

Overexpression of any protein imposes a burden on intracellular processes, particularly affecting energy metabolism, organelle function, and stress responses. Given that the B-Domain modulates FVIII folding, trafficking, and intracellular retention, its deletion may not only alter secretion efficiency but also affect broader cellular pathways, including proliferation, energy demands, and stress responses.

RNA sequencing (RNA-seq) data revealed significant downregulation of proliferation markers and upregulation of senescence markers in BDD-FVIII-expressing cells, suggesting a cellular stress response. This was experimentally validated using proliferation assays, where BDD-FVIII-expressing cells proliferated more slowly than FL-FVIII cells, confirming the RNA-seq findings. Heatmap analysis of proliferation-related genes, based on the dataset from Laucard-Paulet et al., [162] demonstrated that 154 out of 157 proliferation-related genes showed differential expression between FL- and BDD-FVIII samples **(Figure 21)**. The reduced proliferation rate in BDD-FVIII cells suggests that intracellular signaling and resource allocation are altered, potentially prioritizing protein production and secretion over cell division.

Moreover, BDD-FVIII-expressing cells exhibited activation of 38 stress-related pathways, compared to only 21 in FL-FVIII cells **(Figure 30)**, reinforcing the hypothesis that BDD-FVIII induces a stronger cellular stress response. This highlights the protective role of the B-Domain in mitigating stress, likely through its interactions with chaperones and folding machinery.

These observations of altered proliferation and heightened stress signaling in BDD-FVIII-expressing cells raised important questions about how these phenotypic changes intersect with cellular energy metabolism. Since stress responses and protein biosynthesis are tightly coupled to mitochondrial function and ATP availability, we next sought to investigate whether the metabolic landscape was also differentially affected by the presence or absence of the B-Domain. To this end, we performed a comprehensive analysis of mitochondrial activity, ATP dynamics, and transcriptomic signatures related to energy regulation.

2. Mitochondrial Function

Expression of different variants of Factor VIII (FVIII) in HEK293 cells reveals distinct cellular metabolic responses that are tightly linked to protein structure and folding burden. In this study, we compared cells expressing full-length FVIII to those expressing a B-domain-deleted (BDD) version, using ATP assays, Seahorse assay, and transcriptome (RNA-seq) analysis. HEK293 cells expressing full-length FVIII showed high ATP production in Seahorse assays but low residual ATP levels as measured by endpoint assays. This suggests an increase in mitochondrial activity aimed at compensating for significant ATP consumption, likely due to intense ER folding stress imposed by the structurally complex full-length FVIII protein. A positive correlation between Seahorse ATP and residual ATP supports this compensatory mechanism, though the residual ATP balance remains low, indicating energy exhaustion. In contrast, BDD-FVIII cells maintained higher levels of residual ATP while showing lower Seahorse-derived ATP production. This suggests that BDD-FVIII imposes less bioenergetic strain, which is consistent with its simpler folding and trafficking profile.

RNA-seq analysis further clarified the metabolic reprogramming between the two cell types. In BDD-FVIII cells, we observed upregulation of the Sirtuin signaling pathway, known to promote energy efficiency, and mitochondrial health, and downregulation of oxidative phosphorylation genes, indicating reduced reliance on mitochondrial respiration. These transcriptomic features align well with the low metabolic output and high energy conservation observed in BDD-expressing cells. Conversely, full-length FVIII cells demonstrated the opposite trend, increased oxidative phosphorylation gene expression and reduced sirtuin signaling, further supporting a state of elevated mitochondrial demand. These findings suggest that full-length FVIII imposes a heavy metabolic load that activates mitochondrial respiration but drains cellular ATP reserves. These results align with the findings presented in **Figure 22**, which show that BDD-FVIII synthesis is less energy demanding, requiring less ATP consumption, compared to FL-FVIII, due to its shorter protein length and reduced processing burden.

3. Upstream Regulatory Networks and Pharmacological Targets

To further explore the regulatory landscape, we examined upstream regulators influencing differentially expressed genes (DEGs). Notably, CDKN1A kinase was

predicted to be upregulated in BDD-FVIII cells. Given its role in cell cycle regulation and stress responses, CDKN1A may serve as an internal stress signal or a mediator of cellular stress induced by B-domain deletion. Targeting CDKN1A kinase could provide a strategy to reduce stress responses and restore BDD-FVIII cell behavior closer to FL-FVIII-expressing cells.

Beyond CDKN1A, several other key regulators were identified like:

TP53 was significantly upregulated, suggesting an activation of stress-related pathways. Given TP53's role in DNA damage response and apoptosis, its elevated levels in BDD-FVIII cells may indicate increased cellular stress or a compensatory response to altered intracellular trafficking.

RB1 (Retinoblastoma protein), a crucial regulator of cell cycle progression, was found to be downregulated in BDD-FVIII cells. This reduction in RB1 levels aligns with the observed decrease in proliferation rates, supporting the idea that BDD-FVIII cells may prioritize protein processing and secretion over cell division.

These upstream regulators are embedded within a broader regulatory network that reinforces key biological themes relevant to the BDD-FVIII phenotype. AI-assisted network analysis identified five dominant axes: (1) cell proliferation regulation, prominently featuring CDKN1A and FOXM1 as central nodes; (2) cellular senescence, supported by upregulation of genes like AGT, FOXO1, and the Sirtuin signaling pathway; (3) DNA damage response, in which genes like AGT and EGR1 contribute to senescence via increased genomic instability; (4) Sirtuin signaling, shown to regulate stress resistance and energy homeostasis via FOXO1 and ACSS2; and (5) tumor suppression, characterized by interconnections between CDKN1A, EGR1, FOXM1, and FOXO1, which collectively promote senescence, inhibit proliferation, and block transformation. Together, this network supports the interpretation that BDD-FVIII expression pushes cells into a low-proliferation, high-stress, metabolically conserved state.

Furthermore, steroid-related pathways were differentially regulated between FL- and BDD-FVIII, including metribolone. This led us to investigate Budesonide, a steroid currently used in post-gene therapy to reduce inflammation and immune responses [163]. RNA-seq data indicated that genes and pathways affected by Budesonide were significantly downregulated in BDD-FVIII compared to FL-FVIII, suggesting that its

mechanism of action overlaps with pathways altered by B-domain deletion. These findings further confirm our hypothesis that modulating these pathways pharmacologically, such as administering Budesonide, could potentially shift the BDD phenotype to behave more like FL-FVIII, providing a potential intervention to optimize FVIII expression and function in gene therapy applications. Notably, similar approaches have been used successfully in Factor IX (F9) gene therapy, particularly with AAV5-based vectors. In a recent review by Castaman and Pinotti (2025), it was reported that up to 62% of patients receiving AAV5-mediated F9 gene therapy (etranacogene dezaparvovec) required glucocorticoid treatment to manage elevated liver enzymes or preempt immune responses that might compromise transgene expression. This practice of prophylactic or reactive corticosteroid use has been instrumental in preserving vector efficacy and ensuring sustained FIX production [164]. These clinical strategies highlight how immune modulation, even before or alongside gene therapy, can play a critical role in shaping cellular tolerance and transgene performance, further supporting our rationale for exploring steroid co-treatment in BDD-FVIII models.

However, further in vitro validation is required to experimentally confirm the role of CDKN1A, for example, or other cytokines, transcription factors (TFs), or signaling molecules that may contribute to the BDD-FVIII stress response and altered intracellular trafficking. Future studies should focus on targeted inhibition of CDKN1A, alongside testing the effects of Budesonide and other steroid modulators, to determine whether these interventions can effectively reduce cellular stress and improve BDD-FVIII secretion efficiency.

Conclusion and Limitations

Conclusion

Our results demonstrated the followings:

- BDD-FVIII, while more efficiently secreted and less retained intracellularly than FL-FVIII, induces elevated cellular stress and alters homeostatic balance.
- FL-FVIII expression depends heavily on classical ER-Golgi trafficking pathways, engaging ER-resident chaperones such as Calnexin and cargo receptors like LMAN1 and MCFD2. In contrast, it could be speculated that BDD-FVIII is taking alternative, vesicle-driven trafficking routes that are less reliant on these conventional mechanisms and remain incompletely understood. This divergence in intracellular processing was consistently observed through co-localization studies, gene knockdown/knockout experiments, and chemical treatment assays.
- Transcriptomic profiling reveals a clear divergence between FL- and BDD-FVIII in their interaction with the host cell machinery. BDD-FVIII-expressing cells showed upregulation of stress response genes, along with higher residual ATP levels and reduced mitochondrial respiration, indicating a shift toward an energy-conserving but stress-prone cellular state. Notably, both transcriptomic data and functional proliferation assays demonstrated that BDD-FVIII expression significantly impairs cell proliferation compared to FL-FVIII, underscoring the broader physiological impact of B-domain deletion on host cell growth and stability.

Limitations

Several important limitations of this study highlight opportunities for future investigation:

- All data were generated in a single human cell line (HEK293). While this model is widely used for mechanistic and recombinant protein studies, it lacks the specialized features of hepatocytes or liver sinusoidal endothelial cells (LSECs), which are the native expression sites for FIX and FVIII, respectively.

The absence of cell-type specificity may limit the physiological relevance of observed trafficking and stress responses.

- Another limitation is the lack of glycosylation and proteomic profile analysis. Though trafficking and retention were well-characterized, this study did not include mass spectrometry-based profiling to examine post-translational modifications such as glycosylation, disulfide bonding, or proteoform heterogeneity. These biochemical features are known to influence FVIII activity, stability, and immunogenicity and may differ between FL- and BDD-FVIII due to structural variation.
- Additionally, while this study presents extensive co-localization and trafficking data, the precise trafficking routes of FVIII, particularly distinguishing conventional from alternative secretion pathways, remain incompletely resolved. FVIII likely uses multiple parallel routes depending on its structural form, folding status, and cellular context. A more detailed spatiotemporal analysis using real-time live-cell imaging, tagged constructs, and vesicle profiling would help map these dynamic pathways with greater resolution.
- A related technical consideration is the antibody-based detection of FL- and BDD-FVIII. Although efforts were made to reduce bias using transiently expressed tagged constructs and anti-tag antibodies, transient systems inherently limit reproducibility and long-term analysis. Establishing stable cell lines expressing epitope-tagged FVIII variants would improve quantification and enable more consistent tracking of intracellular localization, secretion kinetics, and degradation patterns.
- In addition, while transcriptomic profiling revealed compelling shifts in metabolic, proliferative, and stress-response pathways, these changes remain correlative. Further functional validation through gene knockdown, overexpression, or pharmacologic perturbation of candidate regulators like CDKN1A is necessary to determine causality and therapeutic potential. Finally, although Budesonide and other steroid-responsive pathways emerged as promising pharmacologic leads, no drug-based modulation was performed in this study.

References

1. Bhopale GM, Nanda RK. Blood coagulation factor VIII: An overview. *Journal of biosciences*. 2003;28(6):783-789.
2. Thompson AR. Structure and function of the factor VIII gene and protein. *Seminars in thrombosis and hemostasis*. 2003;29(1):11-22.
3. Hayakawa M, Sakata A, Hayakawa H, et al. Characterization and visualization of murine coagulation factor VIII-producing cells in vivo. *Scientific Reports*. 2021;11(1):14824.
4. Samuelson Bannow B, Recht M, Négrier C, et al. Factor VIII: Long-established role in Hemophilia A and emerging evidence beyond haemostasis. *Blood Reviews*. 2019;35:43-50. Available at: https://www.sciencedirect.com/science/article/pii/S0268960X18301292.
5. Do H, Healey JF, Waller EK, Lollar P. Expression of factor VIII by murine liver sinusoidal endothelial cells. *The Journal of biological chemistry*. 1999;274(28):19587-19592.
6. Shetty S, Lalor PF, Adams DH. Liver sinusoidal endothelial cells — gatekeepers of hepatic immunity. *Nature Reviews Gastroenterology & Hepatology*. 2018;15(9):555-567.
7. Czyzynska-Cichon I, Kotlinowski J, Blacharczyk O, et al. Early and late phases of liver sinusoidal endothelial cell (LSEC) defenestration in mouse model of systemic inflammation. *Cellular & Molecular Biology Letters*. 2024;29(1):139.
8. Jamil MA, Singer H, Al-Rifai R, et al. Molecular Analysis of Fetal and Adult Primary Human Liver Sinusoidal Endothelial Cells: A Comparison to Other Endothelial Cells. *International journal of molecular sciences*. 2020;21(20).
9. Knolle PA. Liver Sinusoidal Endothelial Cells: Role in Immunity and Tolerance. In: Mackay IR, Rose NR, Diamond B, Davidson A, eds. *Encyclopedia of Medical Immunology: Autoimmune Diseases*. New York, NY: Springer New York; 2014:643-651.
10. Elvevold K, Smedsrød B, Martinez I. The liver sinusoidal endothelial cell: a cell type of controversial and confusing identity. *American journal of physiology. Gastrointestinal and liver physiology*. 2008;294(2):G391-400.
11. Tagliavacca L, Wang Q, Kaufman RJ. ATP-Dependent Dissociation of Non-Disulfide-Linked Aggregates of Coagulation Factor VIII Is a Rate-Limiting Step for Secretion. *Biochemistry*. 2000;39(8):1973-1981.
12. Dorner AJ, Kaufman RJ. The Levels of Endoplasmic Reticulum Proteins and ATP Affect Folding and Secretion of Selective Proteins. *Biologicals*. 1994;22(2):103-112. Available at: https://www.sciencedirect.com/science/article/pii/S1045105684710165.
13. Poothong J, Pottekat A, Siirin M, et al. Factor VIII exhibits chaperone-dependent and glucose-regulated reversible amyloid formation in the endoplasmic reticulum. *Blood*. 2020;135(21):1899-1911.
14. Morris JA, Dorner AJ, Edwards CA, Hendershot LM, Kaufman RJ. Immunoglobulin Binding Protein (BiP) Function Is Required to Protect Cells from Endoplasmic Reticulum Stress but Is Not Required for the Secretion of Selective Proteins *. *The Journal of biological chemistry*. 1997;272(7):4327-4334.

15. Schröder M, Kaufman RJ. ER stress and the unfolded protein response. *Mutation Research/Fundamental and Molecular Mechanisms of Mutagenesis*. 2005;569(1):29-63. Available at: https://www.sciencedirect.com/science/article/pii/S0027510704003719.
16. Tantawy AA. Molecular genetics of Hemophilia A: Clinical perspectives. *Egyptian Journal of Medical Human Genetics*. 2010;11(2):105-114. Available at: https://www.sciencedirect.com/science/article/pii/S1110863010000108.
17. Bulaklak K, Gersbach CA. The once and future gene therapy. *Nature Communications*. 2020;11(1):5820.
18. Wang J-H, Gessler DJ, Zhan W, Gallagher TL, Gao G. Adeno-associated virus as a delivery vector for gene therapy of human diseases. *Signal Transduction and Targeted Therapy*. 2024;9(1):78.
19. Savita Rangarajan, Liron Walsh, Will Lester, et al. AAV5–Factor VIII Gene Transfer in Severe Hemophilia A. *New England Journal of Medicine*. 2017;377(26):2519-2530. Available at: https://www.nejm.org/doi/full/10.1056/NEJMoa1708483.
20. George Lindsey A., Monahan Paul E., Eyster M. Elaine, et al. Multiyear Factor VIII Expression after AAV Gene Transfer for Hemophilia A. *New England Journal of Medicine*. 2021;385(21):1961-1973.
21. Kohn DB, Chen YY, Spencer MJ. Successes and challenges in clinical gene therapy. *Gene Therapy*. 2023;30(10):738-746.
22. Meier AF, Fraefel C, Seyffert M. The Interplay between Adeno-Associated Virus and its Helper Viruses. *Viruses*. 2020;12(6).
23. Riyad JM, Weber T. Intracellular trafficking of adeno-associated virus (AAV) vectors: challenges and future directions. *Gene Therapy*. 2021;28(12):683-696.
24. Tabebordbar M, Lagerborg KA, Stanton A, et al. Directed evolution of a family of AAV capsid variants enabling potent muscle-directed gene delivery across species. *Cell*. 2021;184(19):4919-4938.e22.
25. Marrone L, Marchi PM, Azzouz M. Circumventing the packaging limit of AAV-mediated gene replacement therapy for neurological disorders. *Expert opinion on biological therapy*. 2022;22(9):1163-1176.
26. Hashim HZ, Che Abdullah ST, Wan Sulaiman WA, Hoo FK, Basri H. Hunting for a cure: The therapeutic potential of gene therapy in Duchenne muscular dystrophy. *Tzu Chi Medical Journal*. 2014;26(1):5-9. Available at: https://www.sciencedirect.com/science/article/pii/S101631901400007X.
27. Duan D. Dystrophin Gene Replacement and Gene Repair Therapy for Duchenne Muscular Dystrophy in 2016: An Interview. *Human gene therapy. Clinical development*. 2016;27(1):9-18.
28. Zhou Y, Zhang C, Xiao W, Herzog RW, Han R. Systemic delivery of full-length dystrophin in Duchenne muscular dystrophy mice. *Nature Communications*. 2024;15(1):6141.
29. Elangkovan N, Dickson G. Gene Therapy for Duchenne Muscular Dystrophy. *Journal of neuromuscular diseases*. 2021;8(s2):S303-S316.
30. Samelson-Jones BJ, George LA. Adeno-Associated Virus Gene Therapy for Hemophilia. *Annual review of medicine*. 2023;74:231-247.
31. Perrin GQ, Herzog RW, Markusic DM. Update on clinical gene therapy for Hemophilia. *Blood*. 2019;133(5):407-414.

32. Wolf D de, Singh K, Chuah MK, VandenDriessche T. Hemophilia Gene Therapy: The End of the Beginning? *Human gene therapy*. 2023;34(17-18):782-792.
33. Foley JH, Shehu E, Riddell A, et al. Differences in wild-type- and R338L-tenase complex formation are at the root of R338L-factor IX assay discrepancies. *Blood advances*. 2023;7(3):458-467.
34. Fu H, Liang Y, Zhong X, et al. Codon optimization with deep learning to enhance protein expression. *Scientific Reports*. 2020;10(1):17617.
35. El-Maarri O, Jamil MA, Oldenburg J. Molecular Profiling of Liver Sinusoidal Endothelial Cells in Comparison to Hepatocytes: Reflection on Which Cell Type Should Be the Target for Gene Therapy. *Hamostaseologie*. 2020;40(S 01):S26-S31.
36. Patel SR, Lundgren TS, Spencer HT, Doering CB. The Immune Response to the fVIII Gene Therapy in Preclinical Models. *Frontiers in immunology*. 2020;11:494.
37. Milani M, Canepari C, Liu T, et al. Liver-directed lentiviral gene therapy corrects Hemophilia A mice and achieves normal-range factor VIII activity in non-human primates. *Nature Communications*. 2022;13(1):2454.
38. Chen Z, Herzog RW, Kaufman RJ. Cellular stress and coagulation factor production: when more is not necessarily better. *Journal of Thrombosis and Haemostasis*. 2023;21(12):3329-3341. Available at: https://www.sciencedirect.com/science/article/pii/S1538783623007705.
39. Dorner AJ, Wasley LC, Kaufman RJ. Increased synthesis of secreted proteins induces expression of glucose-regulated proteins in butyrate-treated Chinese hamster ovary cells*. *The Journal of biological chemistry*. 1989;264(34):20602-20607. Available at: https://www.sciencedirect.com/science/article/pii/S0021925819471056.
40. Hetz C, Zhang K, Kaufman RJ. Mechanisms, regulation and functions of the unfolded protein response. *Nature Reviews Molecular Cell Biology*. 2020;21(8):421-438.
41. Butterfield JS, Yamada K, Bertolini TB, et al. IL-15 blockade and rapamycin rescue multifactorial loss of factor VIII from AAV-transduced hepatocytes in Hemophilia A mice. *Molecular Therapy*. 2022;30(12):3552-3569. Available at: https://www.sciencedirect.com/science/article/pii/S1525001622004269.
42. Swaroop M, Moussalli M, Pipe SW, Kaufman RJ. Mutagenesis of a Potential Immunoglobulin-binding Protein-binding Site Enhances Secretion of Coagulation Factor VIII*. *The Journal of biological chemistry*. 1997;272(39):24121-24124. Available at: https://www.sciencedirect.com/science/article/pii/S0021925819635696.
43. Poothong J, Jang I, Kaufman RJ. Defects in Protein Folding and/or Quality Control Cause Protein Aggregation in the Endoplasmic Reticulum. *Progress in molecular and subcellular biology*. 2021;59:115-143.
44. Moriya H. Quantitative nature of overexpression experiments. *Molecular Biology of the Cell*. 2015;26(22):3932-3939.
45. Shen R, Wang B, Giribaldi MG, Ayres J, Thomas JB, Montminy M. Neuronal energy-sensing pathway promotes energy balance by modulating disease tolerance. *Proceedings of the National Academy of Sciences of the United States of America*. 2016;113(23):E3307-14.

46. Drummond DA, Wilke CO. Mistranslation-induced protein misfolding as a dominant constraint on coding-sequence evolution. *Cell*. 2008;134(2):341-352.
47. Walsh IM, Bowman MA, Soto Santarriaga IF, Rodriguez A, Clark PL. Synonymous codon substitutions perturb cotranslational protein folding in vivo and impair cell fitness. *Proceedings of the National Academy of Sciences of the United States of America*. 2020;117(7):3528-3534.
48. Makrides SC. Strategies for achieving high-level expression of genes in Escherichia coli. *Microbiological reviews*. 1996;60(3):512-538.
49. Cutting GR. Cystic fibrosis genetics: from molecular understanding to clinical application. *Nature reviews. Genetics*. 2015;16(1):45-56.
50. Ntimbane T, Comte B, Mailhot G, et al. Cystic fibrosis-related diabetes: from CFTR dysfunction to oxidative stress. *The Clinical biochemist. Reviews*. 2009;30(4):153-177.
51. Yadegari H, Oldenburg J. The Current Understanding of Molecular Pathogenesis of Quantitative von Willebrand Disease, Types 1 and 3. *Hamostaseologie*. 2020;40(1):105-118.
52. Park S-Y, Ye H, Steiner DF, Bell GI. Mutant proinsulin proteins associated with neonatal diabetes are retained in the endoplasmic reticulum and not efficiently secreted. *Biochemical and Biophysical Research Communications*. 2010;391(3):1449-1454. Available at: https://www.sciencedirect.com/science/article/pii/S0006291X09024632.
53. Støy J, Franco E de, Ye H, Park S-Y, Bell GI, Hattersley AT. In celebration of a century with insulin – Update of insulin gene mutations in diabetes. *Molecular Metabolism*. 2021;52:101280. Available at: https://www.sciencedirect.com/science/article/pii/S2212877821001253.
54. Liessi N, Pedemonte N, Armirotti A, Braccia C. Proteomics and Metabolomics for Cystic Fibrosis Research. *International journal of molecular sciences*. 2020;21(15).
55. Sarmiento Doncel S, Díaz Mosquera GA, Cortes JM, Agudelo Rico C, Meza Cadavid FJ, Peláez RG. Hemophilia A: A Review of Clinical Manifestations, Treatment, Mutations, and the Development of Inhibitors. *Hematology reports*. 2023;15(1):130-150.
56. Bolton-Maggs PHB, Pasi KJ. Hemophilias A and B. *Lancet (London, England)*. 2003;361(9371):1801-1809.
57. Wong T, Recht M. Current options and new developments in the treatment of Hemophilia. *Drugs*. 2011;71(3):305-320.
58. Nathwani AC. Gene therapy for Hemophilia. *Hematology Am Soc Hematol Educ Program*. 2019;2019(1):1-8.
59. Daya S, Berns KI. Gene therapy using adeno-associated virus vectors. *Clinical microbiology reviews*. 2008;21(4):583-593.
60. Mazurkiewicz-Pisarek A, Płucienniczak G, Ciach T, Płucienniczak A. The factor VIII protein and its function. *Acta biochimica Polonica*. 2016;63(1):11-16.
61. Rosen S, Tiefenbacher S, Robinson M, et al. Activity of transgene-produced B-domain-deleted factor VIII in human plasma following AAV5 gene therapy. *Blood*. 2020;136(22):2524-2534.
62. Pipe SW, Miao HZ, Kucab PF, McVey JH, Kaufman RJ. The Secretion Efficiency of Factor VIII Can Be Regulated by the Size and Oligosaccharide Content of the B Domain. *Blood*. 2005;106(11):687.

63. Toole JJ, Knopf JL, Wozney JM, et al. Molecular cloning of a cDNA encoding human antihaemophilic factor. *Nature*. 1984;312(5992):342-347.
64. Roberts SA, Dong B, Firrman JA, Moore AR, Sang N, Xiao W. Engineering Factor Viii for Hemophilia Gene Therapy. *Journal of genetic syndromes & gene therapy*. 2011;1.
65. van Dieijen G, Tans G, Rosing J, Hemker HC. The role of phospholipid and factor VIIIa in the activation of bovine factor X. *The Journal of biological chemistry*. 1981;256(7):3433-3442. Available at: https://www.sciencedirect.com/science/article/pii/S0021925819696274.
66. Childers KC, Peters SC, Spiegel Jr PC. Structural insights into blood coagulation factor VIII: Procoagulant complexes, membrane binding, and antibody inhibition. *J Thromb Haemost*. 2022;20(9):1957-1970.
67. Vehar GA, Keyt B, Eaton D, et al. Structure of human factor VIII. *Nature*. 1984;312(5992):337-342.
68. Pipe SW. Functional roles of the factor VIII B domain. *Hemophilia : the official journal of the World Federation of Hemophilia*. 2009;15(6):1187-1196.
69. Fay PJ. Factor VIII structure and function. *International journal of hematology*. 2006;83(2):103-108.
70. Childers KC, Peters SC, Spiegel PC. Structural insights into blood coagulation factor VIII: Procoagulant complexes, membrane binding, and antibody inhibition. *Journal of Thrombosis and Haemostasis*. 2022;20(9):1957-1970. Available at: https://www.sciencedirect.com/science/article/pii/S1538783622021067.
71. Anzengruber J, Feichtinger M, Bärnthaler P, et al. How Full-Length FVIII Benefits from Its Heterogeneity - Insights into the Role of the B-Domain. *Pharmaceutical research*. 2019;36(5):77.
72. Pahl S, Pavlova A, Driesen J, Oldenburg J. Effect of F8 B domain gene variants on synthesis, secretion, activity and stability of factor VIII protein. *Thrombosis and haemostasis*. 2014;111(1):58-66.
73. Couture F, Kwiatkowska A, Dory YL, Day R. Therapeutic uses of furin and its inhibitors: a patent review. *Expert opinion on therapeutic patents*. 2015;25(4):379-396.
74. Newell JL, Fay PJ. Proteolysis at Arg740 facilitates subsequent bond cleavages during thrombin-catalyzed activation of factor VIII. *The Journal of biological chemistry*. 2007;282(35):25367-25375.
75. Myles T, Yun TH, Leung LLK. Structural requirements for the activation of human factor VIII by thrombin. *Blood*. 2002;100(8):2820-2826.
76. Siner JI, Samelson-Jones BJ, Crudele JM, et al. Circumventing furin enhances factor VIII biological activity and ameliorates bleeding phenotypes in Hemophilia models. *JCI insight*. 2016;1(16):e89371.
77. Nguyen GN, George LA, Siner JI, et al. Novel factor VIII variants with a modified furin cleavage site improve the efficacy of gene therapy for Hemophilia A. *J Thromb Haemost*. 2017;15(1):110-121.
78. Adams BM, Canniff NP, Guay KP, Hebert DN. The Role of Endoplasmic Reticulum Chaperones in Protein Folding and Quality Control. *Progress in molecular and subcellular biology*. 2021;59:27-50.

79. Kleizen B, Braakman I. Protein folding and quality control in the endoplasmic reticulum. *Current Opinion in Cell Biology*. 2004;16(4):343-349. Available at: https://www.sciencedirect.com/science/article/pii/S095506740400081X.
80. Pipe SW, Morris JA, Shah J, Kaufman RJ. Differential interaction of coagulation factor VIII and factor V with protein chaperones calnexin and calreticulin. *The Journal of biological chemistry*. 1998;273(14):8537-8544.
81. Dorner AJ, Wasley LC, Kaufman RJ. Overexpression of GRP78 mitigates stress induction of glucose regulated proteins and blocks secretion of selective proteins in Chinese hamster ovary cells. *The EMBO journal*. 1992;11(4):1563-1571.
82. Ellgaard L, Helenius A. Quality control in the endoplasmic reticulum. *Nature reviews. Molecular cell biology*. 2003;4(3):181-191.
83. Williams DB. Beyond lectins: the calnexin/calreticulin chaperone system of the endoplasmic reticulum. *Journal of cell science*. 2006;119(Pt 4):615-623.
84. Sitia R, Braakman I. Quality control in the endoplasmic reticulum protein factory. *Nature*. 2003;426(6968):891-894.
85. Christianson JC, Jarosch E, Sommer T. Mechanisms of substrate processing during ER-associated protein degradation. *Nature Reviews Molecular Cell Biology*. 2023;24(11):777-796.
86. Zhang Y, Liu Z, Zhang B. Separate roles of LMAN1 and MCFD2 in ER-to-Golgi trafficking of FV and FVIII. *Blood advances*. 2023;7(7):1286-1296.
87. Zhang B, Ginsburg D. Familial multiple coagulation factor deficiencies: new biologic insight from rare genetic bleeding disorders. *Journal of Thrombosis and Haemostasis*. 2004;2(9):1564-1572. Available at: https://www.sciencedirect.com/science/article/pii/S1538783622180517.
88. Zheng C, Page RC, Das V, et al. Structural characterization of carbohydrate binding by LMAN1 protein provides new insight into the endoplasmic reticulum export of factors V (FV) and VIII (FVIII). *The Journal of biological chemistry*. 2013;288(28):20499-20509.
89. Zheng C, Zhang B. Combined deficiency of coagulation factors V and VIII: an update. *Seminars in thrombosis and hemostasis*. 2013;39(6):613-620.
90. Spreafico M, Peyvandi F. Combined Factor V and Factor VIII Deficiency. *Seminars in thrombosis and hemostasis*. 2009;35(4):390-399.
91. Nichols WC, Ginsburg D. From the ER to the golgi: insights from the study of combined factors V and VIII deficiency. *American journal of human genetics*. 1999;64(6):1493-1498.
92. Zhang B, McGee B, Yamaoka JS, et al. Combined deficiency of factor V and factor VIII is due to mutations in either LMAN1 or MCFD2. *Blood*. 2006;107(5):1903-1907.
93. Zheng C, Liu H-H, Yuan S, Zhou J, Zhang B. Molecular basis of LMAN1 in coordinating LMAN1-MCFD2 cargo receptor formation and ER-to-Golgi transport of FV/FVIII. *Blood*. 2010;116(25):5698-5706.
94. Zhang Y, Zhu M, Zheng C, Wei W, Emmer BT, Zhang B. LMAN1-MCFD2 complex is a cargo receptor for the ER-Golgi transport of α1-antitrypsin. *The Biochemical journal*. 2022;479(7):839-855.
95. Stenmark H. Rab GTPases as coordinators of vesicle traffic. *Nature Reviews Molecular Cell Biology*. 2009;10(8):513-525.

96. Wandinger-Ness A, Zerial M. Rab proteins and the compartmentalization of the endosomal system. *Cold Spring Harbor perspectives in biology*. 2014;6(11):a022616.
97. Corbeel L, Freson K. Rab proteins and Rab-associated proteins: major actors in the mechanism of protein-trafficking disorders. *European journal of pediatrics*. 2008;167(7):723-729.
98. Chen P-I, Kong C, Su X, Stahl PD. Rab5 isoforms differentially regulate the trafficking and degradation of epidermal growth factor receptors. *The Journal of biological chemistry*. 2009;284(44):30328-30338.
99. Wang T, Ming Z, Xiaochun W, Hong W. Rab7: Role of its protein interaction cascades in endo-lysosomal traffic. *Cellular Signalling*. 2011;23(3):516-521. Available at: https://www.sciencedirect.com/science/article/pii/S0898656810002688.
100. Takahashi S, Kubo K, Waguri S, et al. Rab11 regulates exocytosis of recycling vesicles at the plasma membrane. *Journal of cell science*. 2012;125(Pt 17):4049-4057.
101. Luo L, Wall AA, Yeo JC, et al. Rab8a interacts directly with PI3Kγ to modulate TLR4-driven PI3K and mTOR signalling. *Nature Communications*. 2014;5(1):4407.
102. Binotti B, Pavlos NJ, Riedel D, et al. The GTPase Rab26 links synaptic vesicles to the autophagy pathway. *eLife*. 2015;4:e05597.
103. Guinto ER, Esmon CT, Mann KG, MacGillivray RT. The complete cDNA sequence of bovine coagulation factor V. *The Journal of biological chemistry*. 1992;267(5):2971-2978. Available at: https://www.sciencedirect.com/science/article/pii/S0021925819506822.
104. Esmail S, Manolson MF. Advances in understanding N-glycosylation structure, function, and regulation in health and disease. *European Journal of Cell Biology*. 2021;100(7):151186. Available at: https://www.sciencedirect.com/science/article/pii/S0171933521000376.
105. He M, Zhou X, Wang X. Glycosylation: mechanisms, biological functions and clinical implications. *Signal Transduction and Targeted Therapy*. 2024;9(1):194.
106. Wei W, Misra S, Cannon MV, et al. Molecular mechanisms of missense mutations that generate ectopic N-glycosylation sites in coagulation factor VIII. *The Biochemical journal*. 2018;475(5):873-886.
107. Pipe SW, Miao HZ, Kucab PF, McVey JH, Kaufman RJ. The Secretion Efficiency of Factor VIII Can Be Regulated by the Size and Oligosaccharide Content of the B Domain. *Blood*. 2005;106(11):687. Available at: https://www.sciencedirect.com/science/article/pii/S0006497119755773.
108. Zhou Q, Qiu H. The Mechanistic Impact of N-Glycosylation on Stability, Pharmacokinetics, and Immunogenicity of Therapeutic Proteins. *Journal of Pharmaceutical Sciences*. 2019;108(4):1366-1377. Available at: https://www.sciencedirect.com/science/article/pii/S0022354918307366.
109. Bangarh R, Khatana C, Kaur S, et al. Aberrant protein glycosylation: Implications on diagnosis and Immunotherapy. *Biotechnology advances*. 2023;66:108149.
110. Miao HZ, Sirachainan N, Palmer L, et al. Bioengineering of coagulation factor VIII for improved secretion. *Blood*. 2004;103(9):3412-3419.

111. Pittman DD, Marquette KA, Kaufman RJ. Role of the B Domain for Factor VIII and Factor V Expression and Function. *Blood*. 1994;84(12):4214-4225. Available at: https://www.sciencedirect.com/science/article/pii/S0006497120699840.
112. Ward NJ, Buckley SMK, Waddington SN, et al. Codon optimization of human factor VIII cDNAs leads to high-level expression. *Blood*. 2011;117(3):798-807.
113. Sandberg H, Almstedt A, Brandt J, et al. Structural and functional characteristics of the B-domain-deleted recombinant factor VIII protein, r-VIII SQ. *Thrombosis and haemostasis*. 2001;85(1):93-100.
114. Kapelanski-Lamoureux A, Chen Z, Gao Z-H, et al. Ectopic clotting factor VIII expression and misfolding in hepatocytes as a cause for hepatocellular carcinoma. *Molecular Therapy*. 2022;30(12):3542-3551.
115. Samelson-Jones BJ, Small JC, George LA. Roctavian gene therapy for Hemophilia A. *Blood advances*. 2024;8(19):5179-5189.
116. Margareth C. Ozelo, Johnny Mahlangu, K. John Pasi, et al. Valoctocogene Roxaparvovec Gene Therapy for Hemophilia A. *New England Journal of Medicine*. 2022;386(11):1013-1025. Available at: https://www.nejm.org/doi/full/10.1056/NEJMoa2113708.
117. Johnny Mahlangu, Radoslaw Kaczmarek, Annette von Drygalski, et al. Two-Year Outcomes of Valoctocogene Roxaparvovec Therapy for Hemophilia A. *New England Journal of Medicine*. 2023;388(8):694-705. Available at: https://www.nejm.org/doi/full/10.1056/NEJMoa2211075.
118. Symington E, Rangarajan S, Lester W, et al. Long-term safety and efficacy outcomes of valoctocogene roxaparvovec gene transfer up to 6 years post-treatment. *Hemophilia : the official journal of the World Federation of Hemophilia*. 2024;30(2):320-330.
119. George LA, Monahan PE, Eyster ME, et al. Multiyear Factor VIII Expression after AAV Gene Transfer for Hemophilia A. *The New England journal of medicine*. 2021;385(21):1961-1973.
120. Kenny Walter. Preliminary SPK-8016 Data Shows Promise Treating Hemophilia A. 2021. Available at: https://www.hcplive.com/view/preliminary-spk-8016-data-shows-promise-treating-Hemophilia-a.
121. Leavitt AD, Konkle BA, Stine KC, et al. Giroctocogene fitelparvovec gene therapy for severe Hemophilia A: 104-week analysis of the phase 1/2 Alta study. *Blood*. 2024;143(9):796-806.
122. CSL Behring. CSL Behring's Gene Therapy HEMGENIX® (etranacogene dezaparvovec-drlb): Four Years Post-Infusion Data Continue to Show Sustained Efficacy and Safety in Adults with Hemophilia B: CSL Newsroom. 2025. Available at: https://newsroom.csl.com/2025-02-07-CSL-Behrings-Gene-Therapy-HEMGENIX-R-etranacogene-dezaparvovec-drlb-Four-Years-Post-Infusion-Data-Continue-to-Show-Sustained-Efficacy-and-Safety-in-Adults-with-Hemophilia-B.
123. Pipe Steven W., Leebeek Frank W.G., Recht Michael, et al. Gene Therapy with Etranacogene Dezaparvovec for Hemophilia B. *New England Journal of Medicine*. 2023;388(8):706-718.
124. Dhillon S. Fidanacogene Elaparvovec: First Approval. *Drugs*. 2024;84(4):479-486.
125. Pfizer. FDA Accepts Pfizer's Application for Hemophilia B Gene Therapy Fidanacogene Elaparvovec. 2023. Available at:

https://www.pfizer.com/news/press-release/press-release-detail/fda-accepts-pfizers-application-Hemophilia-b-gene-therapy.
126. Chowdary P, Shapiro S, Makris M, et al. Phase 1-2 Trial of AAVS3 Gene Therapy in Patients with Hemophilia B. *The New England journal of medicine*. 2022;387(3):237-247. Available at: https://www.nejm.org/doi/pdf/10.1056/NEJMoa2119913?articleTools=true.
127. Türker Şener L, Albeniz G, Dinç B, Albeniz I. iCELLigence real-time cell analysis system for examining the cytotoxicity of drugs to cancer cell lines. *Experimental and therapeutic medicine*. 2017;14(3):1866-1870.
128. Gutierrez JM, Feizi A, Li S, et al. Genome-scale reconstructions of the mammalian secretory pathway predict metabolic costs and limitations of protein secretion. *Nature Communications*. 2020;11(1):68.
129. Ozelo MC, Mahlangu J, Pasi KJ, et al. Valoctocogene Roxaparvovec Gene Therapy for Hemophilia A. *The New England journal of medicine*. 2022;386(11):1013-1025.
130. Schutgens REG. Gene Therapy for Hemophilia A: How Long Will It Last? *HemaSphere*. 2022;6(6):e720.
131. Castaman G, Matino D. Hemophilia A and B: molecular and clinical similarities and differences. *Haematologica*. 2019;104(9):1702-1709.
132. Shahani T, Covens K, Lavend'homme R, et al. Human liver sinusoidal endothelial cells but not hepatocytes contain factor VIII. *J Thromb Haemost*. 2014;12(1):36-42.
133. Tatsumi K, Ohashi K, Mukobata S, et al. Hepatocyte Is a Sole Cell Type Responsible for the Production of Coagulation Factor IX In Vivo. *Cell medicine*. 2012;3(1-3):25-31.
134. Karakaya N. HEMOPHILIA: ADVANCES IN TREATMENTS. *Hematology, Transfusion and Cell Therapy*. 2024;46:S8-S9. Available at: https://www.sciencedirect.com/science/article/pii/S2531137924029419.
135. Chernyi N, Gavrilova D, Saruhanyan M, et al. Recent Advances in Gene Therapy for Hemophilia: Projecting the Perspectives. *Biomolecules*. 2024;14(7).
136. Di Cao, Byrne BJ, Jong YP de, et al. Innate Immune Sensing of Adeno-Associated Virus Vectors. *Human gene therapy*. 2024;35(13-14):451-463.
137. Kawai T, Akira S. Signaling to NF-κB by Toll-like receptors. *Trends in Molecular Medicine*. 2007;13(11):460-469. Available at: https://www.sciencedirect.com/science/article/pii/S1471491407001840.
138. Mingozzi F, High KA. Immune responses to AAV vectors: overcoming barriers to successful gene therapy. *Blood*. 2013;122(1):23-36.
139. Pei X, Earley LF, He Y, et al. Efficient Capsid Antigen Presentation From Adeno-Associated Virus Empty Virions In Vivo. *Frontiers in immunology*. 2018;9:844.
140. Mingozzi F, Anguela XM, Pavani G, et al. Overcoming preexisting humoral immunity to AAV using capsid decoys. *Science translational medicine*. 2013;5(194):194ra92.
141. Scallan CD, Jiang H, Liu T, et al. Human immunoglobulin inhibits liver transduction by AAV vectors at low AAV2 neutralizing titers in SCID mice. *Blood*. 2006;107(5):1810-1817.
142. Arruda VR, Samelson-Jones BJ. Gene therapy for immune tolerance induction in Hemophilia with inhibitors. *Journal of Thrombosis and Haemostasis*.

2016;14(6):1121-1134. Available at: https://www.sciencedirect.com/science/article/pii/S1538783622026010.
143. DiMichele D. Inhibitor development in Hemophilia B: an orphan disease in need of attention. *British Journal of Haematology*. 2007;138(3):305-315.
144. Eckhardt CL, van Velzen AS, Peters M, et al. Factor VIII gene (F8) mutation and risk of inhibitor development in nonsevere Hemophilia A. *Blood*. 2013;122(11):1954-1962. Available at: https://www.sciencedirect.com/science/article/pii/S0006497120529522.
145. Patterson P, Kaczmarek R, Herzog RW. Liver Sinusoidal Endothelial Cells but Not Hepatocytes Express a Fluorescent Reporter Under the Endogenous F8 Promoter in a New Hemophilia a Mouse Model. *Blood*. 2023;142(Supplement 1):2601.
146. Boost KA, Auth MKH, Woitaschek D, et al. Long-term production of major coagulation factors and inhibitors by primary human hepatocytes in vitro: perspectives for clinical application. *Liver international : official journal of the International Association for the Study of the Liver*. 2007;27(6):832-844.
147. Kaczmarek R, Miesbach W, Ozelo MC, Chowdary P. Current and emerging gene therapies for Hemophilia A and B. *Hemophilia : the official journal of the World Federation of Hemophilia*. 2024;30(S3):12-20.
148. Pipe SW, Leebeek FW, Recht M, et al. Adults with Severe or Moderately Severe Hemophilia B Receiving Etranacogene Dezaparvovec in the HOPE-B Phase 3 Clinical Trial Continue to Experience a Stable Increase in Mean Factor IX Activity Levels and Durable Hemostatic Protection after 24 Months' Follow-up. *Blood*. 2022;140(Supplement 1):4910-4912.
149. La Mura V, Cardinale V, Cristofaro R de, et al. Liver-related aspects of valoctocogene roxaparvovec gene therapy for Hemophilia A: expert guidance for clinical practice. *Blood advances*. 2024;8(22):5725-5734.
150. Chiaromonte F, Miller W, Bouhassira EE. Gene length and proximity to neighbors affect genome-wide expression levels. *Genome research*. 2003;13(12):2602-2608.
151. Pittman DD, Alderman EM, Tomkinson KN, Wang JH, Giles AR, Kaufman RJ. Biochemical, immunological, and in vivo functional characterization of B-domain-deleted factor VIII. *Blood*. 1993;81(11):2925-2935.
152. Bos MHA, Camire RM. Blood coagulation factors V and VIII: Molecular Mechanisms of Procofactor Activation. *Journal of coagulation disorders*. 2010;2(2):19-27.
153. Siner JI, Iacobelli NP, Sabatino DE, et al. Minimal modification in the factor VIII B-domain sequence ameliorates the murine Hemophilia A phenotype. *Blood*. 2013;121(21):4396-4403.
154. Brenner S, Elgar G, Sandford R, Macrae A, Venkatesh B, Aparicio S. Characterization of the pufferfish (Fugu) genome as a compact model vertebrate genome. *Nature*. 1993;366(6452):265-268.
155. Fujiwara T, Oda K, Yokota S, Takatsuki A, Ikehara Y. Brefeldin A causes disassembly of the Golgi complex and accumulation of secretory proteins in the endoplasmic reticulum. *The Journal of biological chemistry*. 1988;263(34):18545-18552.

156. Xu F, Tautenhahn H-M, Dirsch O, Dahmen U. Blocking autophagy with chloroquine aggravates lipid accumulation and reduces intracellular energy synthesis in hepatocellular carcinoma cells, both contributing to its anti-proliferative effect. *Journal of Cancer Research and Clinical Oncology*. 2022;148(12):3243-3256.
157. Vöing K, Michgehl U, Mertens ND, et al. Disruption of the Rab7-Dependent Final Common Pathway of Endosomal and Autophagic Processing Results in a Severe Podocytopathy. *Journal of the American Society of Nephrology : JASN*. 2023;34(7):1191-1206.
158. Chen J, Zhao H, Liu M, Chen L. A new perspective on the autophagic and non-autophagic functions of the GABARAP protein family: a potential therapeutic target for human diseases. *Molecular and Cellular Biochemistry*. 2024;479(6):1415-1441.
159. Ding Y, Li Y, Chhetri G, et al. Parkinson's Disease Causative Mutation in Vps35 Disturbs Tetherin Trafficking to Cell Surfaces and Facilitates Virus Spread. *Cells*. 2021;10(4).
160. Ruffalo M, Bar-Joseph Z. Protein interaction disruption in cancer. *BMC cancer*. 2019;19(1):370.
161. Thibodeau PH, Richardson JM3, Wang W, et al. The cystic fibrosis-causing mutation deltaF508 affects multiple steps in cystic fibrosis transmembrane conductance regulator biogenesis. *The Journal of biological chemistry*. 2010;285(46):35825-35835.
162. Locard-Paulet M, Palasca O, Jensen LJ. Identifying the genes impacted by cell proliferation in proteomics and transcriptomics studies. *PLoS computational biology*. 2022;18(10):e1010604.
163. BioMarin Pharmaceutical Inc. Roctavian summary of product characteristics. 2023. Available at: https://www.ema.europa.eu/en/documents/product-information/roctavian-epar product-information_en.pdf. Accessed March 23, 2025.
164. Castaman G, and Pinotti M. Could targeted gene insertion of factor 9 be a potential durable treatment for Hemophilia B? *Expert Review of Hematology*. 2025;18(2):105-107.

List of Publications

❖ Published Papers

1. **Rawya Al-Rifai ‡**, Muhammad Ahmer Jamil **‡**, Nicole Nuesgen, Janine Altmüller, Johannes Oldenburg and Osman El-Maarri. “The role of microRNAs in defining LSECs cellular identity and in regulating *F8* gene expression”.
Front. Genet. 15:1302685. doi: 10.3389/fgene.2024.1302685.
‡ Equal contribution as a first author.

2. Muhammad Ahmer Jamil ‡, Heike Singer ‡, **Rawya Al-Rifai**, Nicole Nüsgen, Melanie Rath, Sascha Strauss, Ioanna Andreou, Johannes Oldenburg, Osman El-Maarri. “Molecular Analysis of Fetal and Adult Primary Human Liver Sinusoidal Endothelial Cells: A Comparison to Other Endothelial Cells”.
Int. J. Mol. Sci. 2020, 21, 7776; doi:10.3390/ijms21207776.

❖ Manuscripts in Submission

3. **Rawya Al-Rifai**, Salime El-Hazzouri, Mira Ibrahim, Nicole Nüsgen, Johannes Oldenburg, and Osman El-Maarri. “B-domain-deleted Factor VIII exhibits significant differences in intracellular processing and localization when compared to full length Factor VIII”.
In submission to Blood.

4. Osman El-Maarri **‡**, Heike Singer **‡**, **Rawya Al-Rifai ‡**, Salime El-Hazzouri ‡, Mira Ibrahim ‡, Behnaz Pezeshkpoor, Nasim Shahidi Hamedani, Muhammad Ahmer Jamil, Nicole Nüsgen, Ursula Schreck, Melanie Rath, Judith Junen, Jens Müller, Johannes Oldenburg. “GABARAPs proteins modulation of FVIII secretion is molecule-specific and acts via cellular energy”.
‡ Equal contribution as a first author.
In submission to Nature Communication Journal.

5. Salime El-Hazzouri, **Rawya Al-Rifai**, Nicole Nüsgen, Melanie Rath, Heike Singer, Johannes Oldenburg, and Osman El-Maarri. “Investigation of FVIII Trafficking Dynamics in ER, ERGIC, Golgi and cytoplasmic vesicles using single and double gene CRISPR/Cas9 gene Knockout”.
In submission to Multi-Journal Cell.

6. Heike Singer ‡, Payal Chawla ‡, Katrin J. Czogalla-Nitsche, Pujan Engels, Francesco Forin, Muhammad Jamil, Melanie Rath, Jens Müller, **Rawya Al-Rifai**, Osman El-Maarri, Johannes Oldenburg. “Stability and Proteasomal Targeting of FVIII PTC variants in the Light Chain: Insights into Hemophilia A Immunogenicity”.
Submitted to Blood Journal.

Conference Contributions

- **Session Moderator**, ISTH Congress 2022, London, UK. Moderated a scientific Oral Communication session at the 30th Congress of the International Society on Thrombosis and Haemostasis (ISTH).

- **Oral Presentation**, ISTH Congress 2023, Montréal, Canada. "B-domain-deleted Factor VIII shows clear differences in intracellular processing and cellular responses when compared to full-length Factor VIII."

- **Oral Presentation**, ISTH Congress 2022, London, UK. "Whole genome expression analysis resolves the correlation between genetic knockouts of single genes and the obtained phenotype in relation to FVIII secretion. “

- **Poster Presentation,** GTH Congress 2024, Wien, Austria. "The miRNAs present in LSECs play pivotal role in defining their cellular identity and have an impact on the regulation of F8 gene expression"
  Hamostaseologie 44 DOI: 10.1055/s-0044-1779138

- **Poster Presentation,** GTH Congress 2023, Frankfurt, Germany. "Intrinsic difference in cellular response between full-length and B-domain-deleted FVIII HEK293 secreting cells: implication for gene therapy"
  Hamostaseologie 43 DOI: 10.1055/s-0042-1760540

- **Poster Presentation,** GTH Congress 2022, Leipzig, Germany. "In Contrast to Full-Length Factor VIII, the Calnexin (ER Chaperone) and LMAN1 (ERGIC transporter) Knockouts Have Minimal Effect on the Secretion of B-Domain-Deleted Factor VIII: Implication for Gene Therapy"
  Hamostaseologie 42 DOI: 10.1055/s-0042-1748631

- **Poster Presentation,** DGTI Congress 2022, Mannheim, Germany. "Whole genome expression analysis resolves the correlation between genetic knockout of single genes and the obtained phenotype in relation to FVIII secretion."

- **Poster Presentation,** Hämophilie Symposion 2022, Hamburg, Germany "Intrinsic difference in cellular response between full-length and B-domain-deleted FVIII HEK293 secreting cells: implication for gene therapy"

- **Poster Presentation,** GTH Congress 2020, Bremen, Germany. "Over Expression of Specific Transcription Factors to Boost FVIII Expression"
  Hamostaseologie 40 DOI: 10.1055/s-0040-1721598.

Awards

- **CNRS-L funding program:** Half-scholarship. National Center for Scientific Research CNRS August 2019- August 2022.

- **Best Poster Award**, GTH 68th Annual Meeting, Vienna, Austria (Feb 2024). "The Role of microRNAs in Defining LSECs Cellular Identity and in Regulating *F8* Gene Expression."

- **Best Poster Award**, GTH 67th Annual Meeting, Frankfurt, Germany (Feb 2023). "Intrinsic difference in cellular response between full-length and B-domain-deleted FVIII in HEK cells: Implication for gene therapy. “

- **Best Poster Award**, Hämophilie Symposion, Hamburg, Germany (Nov 13–14, 2021). "In contrast to full-length factor VIII, the Calnexin (ER chaperone) and LMAN1 (ERGIC transporter) knockouts have minimal effect on the secretion of B-domain-deleted factor VIII: Implication for gene therapy.

Acknowledgement

This achievement would not have been possible without the support and encouragement of many people, to whom I am deeply grateful.

Above all, I thank **God** for granting me the strength, patience, and perseverance to navigate this path. His guidance sustained me through every obstacle and moment of doubt.

I am sincerely grateful to **Prof. Johannes Oldenburg**, head of the institute, for the opportunity to work in such a supportive and stimulating environment.

My deepest gratitude goes to **Priv. Doz. Dr. Osman El-Maarri**, my first supervisor, for his dedicated guidance, constant support, and insightful feedback throughout my PhD journey.

I also sincerely thank my second supervisor, **Prof. Dr. Diana Imhof**, for her valuable input and motivation, which helped shape the direction and quality of this work.

A very special thank you to **Dr. Heike Singer**, who supported me from my master's internship through the early years of my PhD. Her mentorship laid the foundation of my scientific journey, and I will always be grateful for everything she shared with me.

I am also incredibly thankful to **Dr. Mohammad Ahmer Jamil** for handling the bioinformatics part of my research with dedication and clarity and for his patience in guiding me through complex analyses.

My warmest thanks to **Nicole**, our dedicated technician, for her invaluable help, steady support, and kind presence.

I am fortunate to have worked alongside such wonderful colleagues and friends at the institute, **my IHT family**. Your companionship and daily support have made this place feel like a second home.

A heartfelt thanks to **Mira**, **Samhitha**, and **Ann-Kathrin.** Your presence in my life has been a gift beyond measure. Through every chapter, your laughter has brought light, your friendship has brought comfort, and your unwavering support has carried me through challenges with grace.

And a special thanks to **Soulayma**, for all the moments we've shared over these years.

I truly couldn't have done it without you. I also want to thank my dear friends **Mirna** and **Ali** for their continuous encouragement and emotional support throughout my PhD. Your kindness, understanding, and motivation meant the world to me.

To my dearest **Mom**,
You are the heart of our home and the soul of my strength. Your unconditional love, gentle wisdom, and constant prayers have carried me through every high and low. Thank you for every silent sacrifice, every warm embrace, and every word of encouragement. Your love is a blessing I cherish more than anything in this world.

To my amazing **Dad**,
You've been my role model, my protector, and my greatest teacher. Your quiet strength, hard work, and unwavering belief in me have shaped the person I am today. Thank you for always standing tall for our family, and for showing me what resilience, honor, and love truly mean. I carry your values with me in all that I do.

In loving memory of my dear **Grandfather**,
You were the first to believe in my dream, even before I fully understood it myself. Your faith gave me strength, and your words still echo in my heart. I wish you were here to see this moment. I hope I've made you proud.

To my incredible siblings, **Bilal**, **Hilal**, **Haysam**, **Roukaya**, **Safaa**, and **Berna**, thank you for being my unwavering support system. Each of you brings a unique light into my life, and your constant encouragement, love, and laughter have made this journey richer and more meaningful. No matter the distance or the challenges, you've always been there with open hearts and steady hands.

And to my sweet **nieces** and **nephews**, you bring so much joy into my life! Your smiles, hugs, and pure love brighten my days in ways I can't describe. A big kiss to all of you, I love you more than words can say!

A special nod to my kittens, **Simba** and **Luna**, whose comforting presence brought light to many long nights of writing.

Lastly, to **my quiet strength**, thank you for always being there, offering comfort, perspective, and joy when I needed it most. I am truly grateful to share this journey with you.